Cardiff
Catalysis Institute

Sefydliad Catalysis
Caerdydd

Photocatalytic Reforming for Hydrogen Production using metal/TiO_2

Julia Kennedy

May 2016

Thesis submitted in accordance with the requirements of Cardiff University for the degree of Doctor of Philosophy

I would like to dedicate this thesis to my late father

Professor Paul Joseph Kennedy

A great advocate for women in science.

He is truly missed.

Abstract

The aim of this study was to develop photocatalysts which are active for the production of hydrogen from water and to further understanding of the factors involved in promoting the reaction. Different metals were loaded onto titania and used as photocatalysts for photocatalytic methanol reforming for hydrogen production. The catalysts were characterised using XPS and TPR to understand what produced highly active catalyst. The main factors influencing the catalysts were found to be the ease of reducibility and the work function of the metal used. Pt/TiO_2 was the most active of the catalysts tested for photocatalytic methanol reforming. This was attributed to the fact that platinum oxide is easily reduced to platinum metal. Platinum also has a high work function and it was concluded that this property allows better charge transfer and longer charge separation due to a Schottky barrier.

Different sacrificial agents with varying numbers of hydroxyl species were tested for photocatalytic hydrogen production. Alcohols, polyols, cyclo-alcohols and carboxylic acids were investigated. A relationship between the number of hydroxyl groups and hydrogen yield was established. The formula suggested for this was $2n+1$ = number of moles of hydrogen, where n = number of C-OH groups. The best sacrificial agent was found to be xylitol as it has five C-OH groups and it fully decomposes to carbon dioxide and hydrogen.

TiO_2 was synthesised using a sol-gel preparation method in an attempt to produce active photocatalysts for photocatalytic methanol reforming for hydrogen production. The phases of TiO_2 produced via this method were found to be anatase and brookite. The catalysts with more brookite were found to be more active. The study also highlighted the importance of crystallinity and surface area. The Turkevich method of producing gold nanoparticles was used to produce Au/TiO_2. This method produced a more active catalyst than the incipient wetness Au/TiO_2 and also emphasized the importance of removal of stabilising agents.

Acknowledgements

Firstly I would like to thank the EPSRC and my project supervisors Prof Michael Bowker and Prof Phil Davies for giving me the opportunity to study at the Cardiff Catalysis Institute. I greatly appreciate the time they have both given me to discuss and develop my work. I have always enjoyed my meetings with Mike and listening to his advice and opinions on academic matters and others, and Phil's never ending enthusiasm is something that I admire.

I would also like to extend my thanks to Dr Hasliza Bahruji, my post-doctoral supervisor whose dry and witty sense of humour kept me on track during a few difficult days.

I am grateful to the brilliant people also studying at the Cardiff Catalysis Institute for bringing a sense of fun to the department, especially Emir Bouleghlimat for the many cups of tea.

Finally I would like thank my parents, my brother and Mark for their endless support and love.

Chapter 1

Chapter 2

Chapter 3

Chapter 4

Chapter 5

Chapter 1

1.1 Fossil Fuels

In the 21st century there is a constant demand for energy to satisfy the needs of current lifestyles. The energy resource that is supplying this demand is primarily from fossil fuels. Fossil fuels are hydrocarbons that were formed millions of years ago from the decomposition and compression of dead organisms and include coal, petroleum and natural gas. It is believed that coal was formed from plants whereas natural gas and petroleum is thought to be formed from plankton. Using fossil fuels as an energy resource began during the industrial revolution in the late 18th and early 19th centuries and since then the use of fossil fuels has increased exponentially. The advantages of fossil fuels are that they are high in energy, readily available, relatively cheap and easy to transport. The effects of burning fossil fuels however are concerning for the Earth and coming generations. Firstly burning fossil fuels in air produces large amounts of CO_2. Over 300 million years ago during the carboniferous period, the level of CO_2 in the atmosphere was reduced from 5000 to 280 ppm, burning fossil fuels is releasing it back into the atmosphere as can be seen in Figure 1.1.

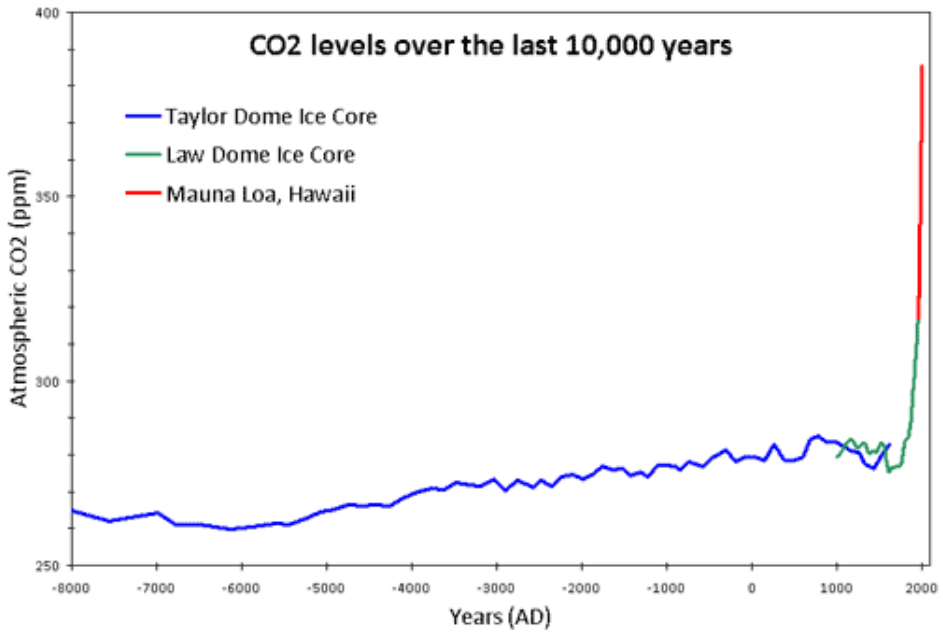

Figure 1.1. The level of CO_2 in the atmosphere over the last 10000 years

It can be seen in Figure 1.1 that the level of CO_2 was fairly constant from 8000 BC until the industrial revolution in the 18th century. Since then the level of CO_2 can be seen to increase by ~30%. The average level of CO_2 in the atmosphere in 2015 was ~401 ppm. CO_2 is considered a greenhouse gas along with methane, nitrous oxide and ozone. A greenhouse gas is a gas that absorbs heat energy that has been reflected by the Earth's surface from the sun which in turn makes the atmosphere warmer.[1] The effects of global warming would have devastating effects of the planet. The increase in global temperature could cause an increase in sea levels leading to loss of land and extinction of species. It is also likely there would be more droughts and extreme weather, affecting agriculture and causing famine. Burning fossil fuels also leads to air pollution affecting the environment and human health due to the release of harmful gases including carbon dioxide, carbon monoxide, nitrogen oxides, sulphur dioxide, and particulates. Finally fossil fuels are considered to be a non-renewable source of energy due to the time it takes for their formation. Therefore there is a need for an alternative energy resource.

1.2 Hydrogen as an alternative energy

There are a number of energy alternatives including solar power, wind, biomass, biofuels, geothermal and possibly most interestingly hydrogen. The only product from burning hydrogen is water (Equation 1.1). Therefore hydrogen is considered to be a clean fuel as it has zero carbon emissions and does not produce any other greenhouse or harmful gases. This makes hydrogen a very promising energy alternative.

Equation 1.1. Combustion of hydrogen

Hydrogen is considered to have the best energy to mass ratio when compared to other existing fuels such as natural gas or petroleum. The energy per unit mass of hydrogen and other fuels is shown in Table 1.1.[2]

Fuel	Energy per unit mass/ MJ kg^{-1}	Energy per unit volume/ MJ m^{-3}
Hydrogen	141.9	8520
Petroleum	46.7	31170
Methanol	23.3	16020
Natural gas	55.5	21250
Propane	48.9	23520
Ammonia	22.5	14350

Table 1.1. Fuels and energy content per mass and volume

It is clear from Table 1.1 that hydrogen has the best energy to mass ratio with 141.1 MJ kg^{-1} whereas the next best is propane with 48.9 MJ kg^{-1}. A disadvantage of hydrogen fuel is that it has a low energy to volume ratio. Hydrogen has 8520 MJ m^{-3} which is the lowest when compared to the other fuels. This means that the storage and transportation of hydrogen must be considered.

1.2.1 Hydrogen Storage

The main types of hydrogen storage available are high pressured tanks, condensation to liquid or even solid hydrogen and absorption of hydrogen in solids with high surface areas.[3] Gas cylinders can store hydrogen at up to 300 bar in steel cylinders and up to 600 bar in cylinders made of carbon fibre and hydrogen inert aluminium. The disadvantages of this type of storage is the need for additional pressure and that high pressured cylinders pose a safety risk. Condensation of hydrogen is an attractive option in that this would

increase the energy to volume ratio. Due to heat transfer from the container some hydrogen storage would be lost due to evaporation of the liquid hydrogen. An area of research gaining a lot of attention is the use of high surface area solids to store hydrogen.[4] It is possible for hydrogen to reversibly adsorb to the surface of the solid via physisorption using Van der Waals interactions. A significant amount of research is going into the use of carbon nanotubes for hydrogen storage with promising results.[5]

1.2.2 Hydrogen Production

Another problem with hydrogen fuel is that that even though hydrogen is most abundant element in the universe, it is usually present a compound. For example on Earth it is tied up in water or methane. Current methods of obtaining hydrogen come from the extraction from natural gas (48%), oil (30%), coal (18%) and electrolysis (4%).

1.2.2.1 Steam reforming

The most popular current method of producing hydrogen is steam reforming.[6] Steam reforming is the cheapest method of producing hydrogen. It involves heating methane in the presence of steam and a Ni catalyst at high temperatures of around 700-1100 °C (Equation 1.2).[7]

Equation 1.2. Steam reforming of methane

This is then followed using the CO produced in the water gas shift reaction to produce more hydrogen and also CO_2 (Equation 1.3).

Equation 1.3. Water gas shift reaction with CO

Hydrogen production from oil and coal involves partially oxidising the hydrocarbons using oxygen and high temperatures.

These processes, although economical, uses methane, oil and coal (non-renewable resources) and also produce CO_2 (a greenhouse gas) and so an alternative method to produce hydrogen is desired.

1.2.2.2 Electrolysis

Electrolysis to produce hydrogen uses electricity to split water into hydrogen and oxygen. Electrodes usually Pt, Ir or stainless steel are placed into water. A potential is applied between the electrodes and hydrogen is produced at the cathode and oxygen at the anode. The equations for the reactions are shown in Equation 1.4, Equation 1.5 and Equation 1.6.

Equation 1.4. Reaction at the cathode, HER ($E°_{red}$ = 0.00 V)

Equation 1.5. Reaction at the anode, OER ($E°_{ox}$ = - 1.23 V)

Equation 1.6. Electrolysis of water

Using the standard electrode potentials for the reduction and oxidation reactions occurring, the overall potential for splitting water is equal to -1.23 V. This means that a voltage of at least -1.23 V is required. Due to barriers such as activation energy and ion mobility, an over potential is usually needed for the production of hydrogen to proceed.

Electrolysis is not as economical as steam reforming and is therefore rarely used in industry however there is lot of interest in using solar electricity

1.2.2.3 Photoelectrolysis

The concept of photoelectrolysis is very similar to electrolysis in that water is split using electrical energy via HER and OER. Photoelectrolysis however uses a photoelectrode; a semi-conductor such a TiO_2, and a counter electrode usually a noble metal. Unlike electrolysis, the electrical energy is generated using sunlight. It is important to note that the energy band of the semi-conductor must overlap with the energy levels of the HER and OER. Fujishima *et al.* used a TiO_2 electrode and a Pt electrode for the electrochemical photolysis of water in 1972[8] using the set up shown in Figure 1.2. The photo-induced electrons reduce H_2O to H_2 and the holes left on the TiO_2 oxidise H_2O to O_2.

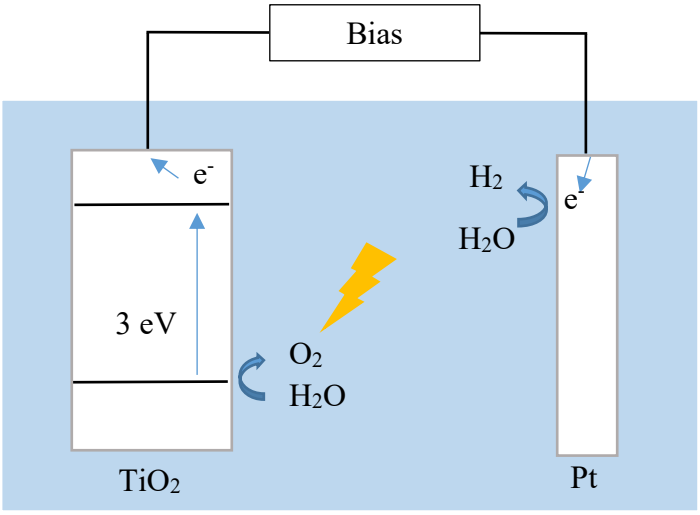

Figure 1.2. Photoelectrolysis

It was suggested that water could be split using visible light into hydrogen and oxygen and was the first study of its kind. The proposed mechanism is shown in Reaction schemes (1.1)-(1.4).

Excitation of TiO_2 by light…

$$TiO_2 + 2h\nu \rightarrow 2e^- \quad (1.1)$$

At the TiO_2 electrode…

$$2p^+ + H_2O \rightarrow -O_2 + 2H^+ \quad (1.2)$$

At the Pt electrode…

$$2e^- + 2H^+ \rightarrow H_2 \quad (1.3)$$

Overall…

$$H_2O + 2h\nu \rightarrow -O_2 + H_2 \quad (1.4)$$

The study by Fujishima *et al.* revealed the potential of using light energy to split water and sparked an interest in photocatalysis.

1.2.3 Catalysis and Photocatalysis

Catalysis is the increase in reaction due to the presence of a catalyst. A catalyst works by decreasing the activation energy required for a reaction to proceed. This is shown in Figure 1.3.

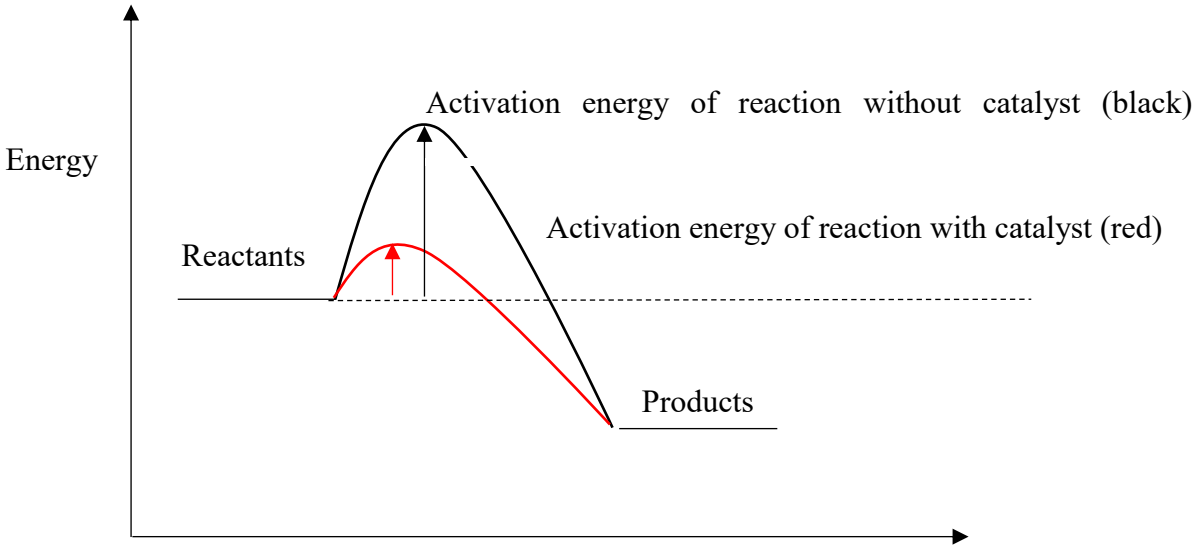

Figure 1.3. Energy profile of reaction with (red) and without (black) catalyst

1.2.4 General Principle of photocatalytic water splitting

Photocatalysis uses light energy to catalyse a reaction using a photocatalyst to harness the energy. The general water splitting process using a photocatalyst is as follows; the photocatalyst absorbs a photon which is greater in energy than the band gap of the semi-conductor. This generates an excited electron and an electron hole. The photoexcited carriers separate and migrate to the surface without recombining. The excited electron reduces the H_2O to H_2. The hole in the TiO_2 produced by the excitation of the electron can oxidise the H_2O to O_2 as seen in Figure 1.4. There are different types of semi-conductors with different properties. These will be discussed later in the chapter.

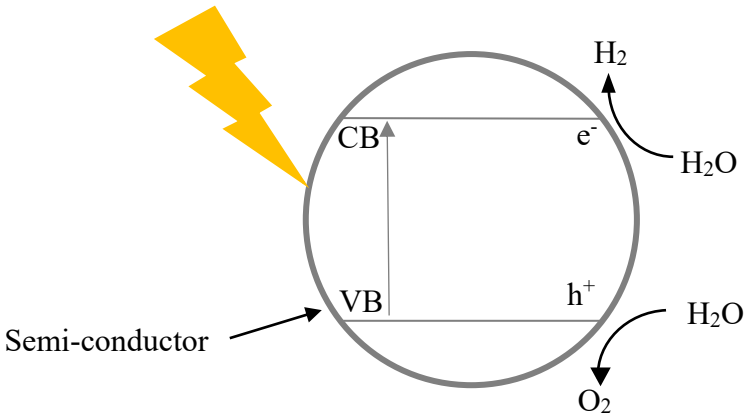

Figure 1.4. Principle of photocatalytic water splitting using a semiconductor

1.2.5 Difficulty of water splitting

To assess the difficulty of water splitting it is useful to look at the thermodynamics and the kinetics of the reaction. An energy diagram is shown below to illustrate the thermodynamics of splitting water into hydrogen and oxygen (Figure 1.5).

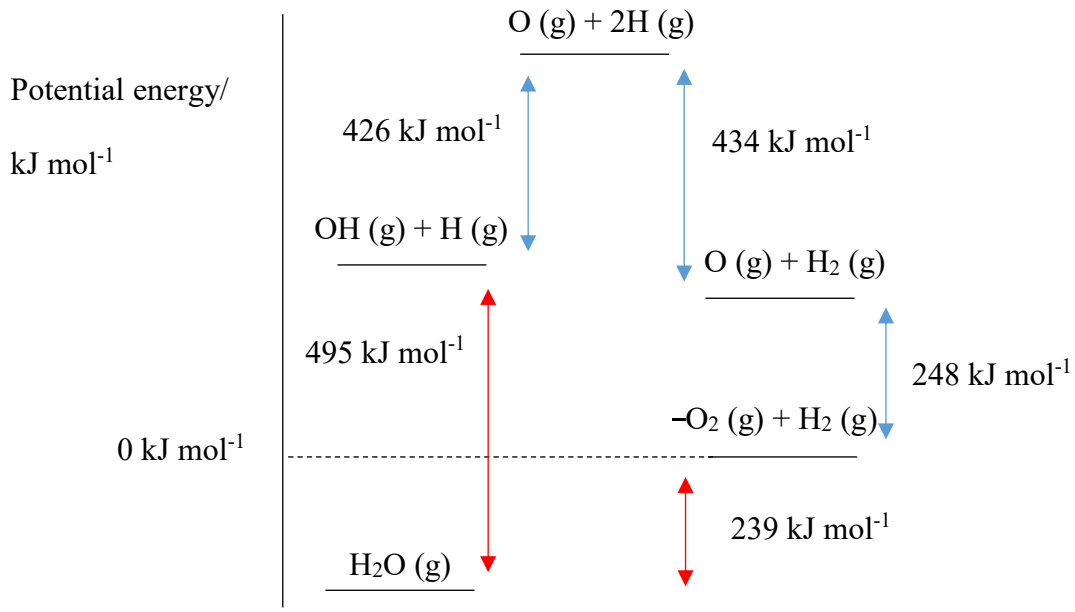

Figure 1.5. Energy diagram for water splitting

Figure 1.5 shows that the enthalpy for water splitting in the gas phase is 239 kJ mol^{-1}. Therefore, it is an endothermic reaction, which will not proceed without an energy input. 239 kJ mol^{-1} corresponds to light with a wavelength of around 500 nm. This wavelength of light is in the visible region (Figure 1.6) and reaches the Earth's surface. Luckily for us on Earth, the energy required to break the first O-H bond in water requires an energy of 495 kJ mol^{-1} (~250 nm) and such energy photons are not present at the Earth's surface. It is this kinetic barrier which makes water splitting difficult, and the use of a photocatalyst necessary. An important thing to note from Figure 1.5 is that it shows that

the backwards reaction is favourable. It is for this reason that there a sacrificial agent is employed to “mop up” oxygen, preventing this from happening.

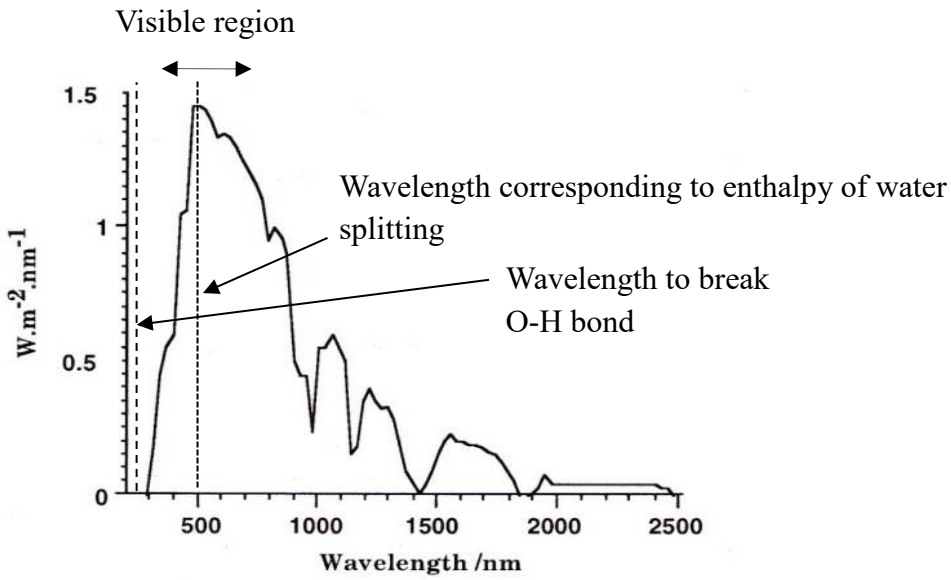

Figure 1.6. Solar spectrum showing visible region and wavelengths corresponding to thermodynamic and kinetics barriers

1.2.6 Photocatalysts

Currently there are two main approaches to water splitting using a heterogeneous catalyst;

- Two step system in which the reaction is split into two parts; H_2 production and O_2 production (z-scheme) as shown in Figure 1.7.
- One step system where light is used to split H_2O into H_2 and O_2 in one step. These require a narrow band gap, stability under irradiation and suitable valence and conduction bands for H_2 and O_2 production

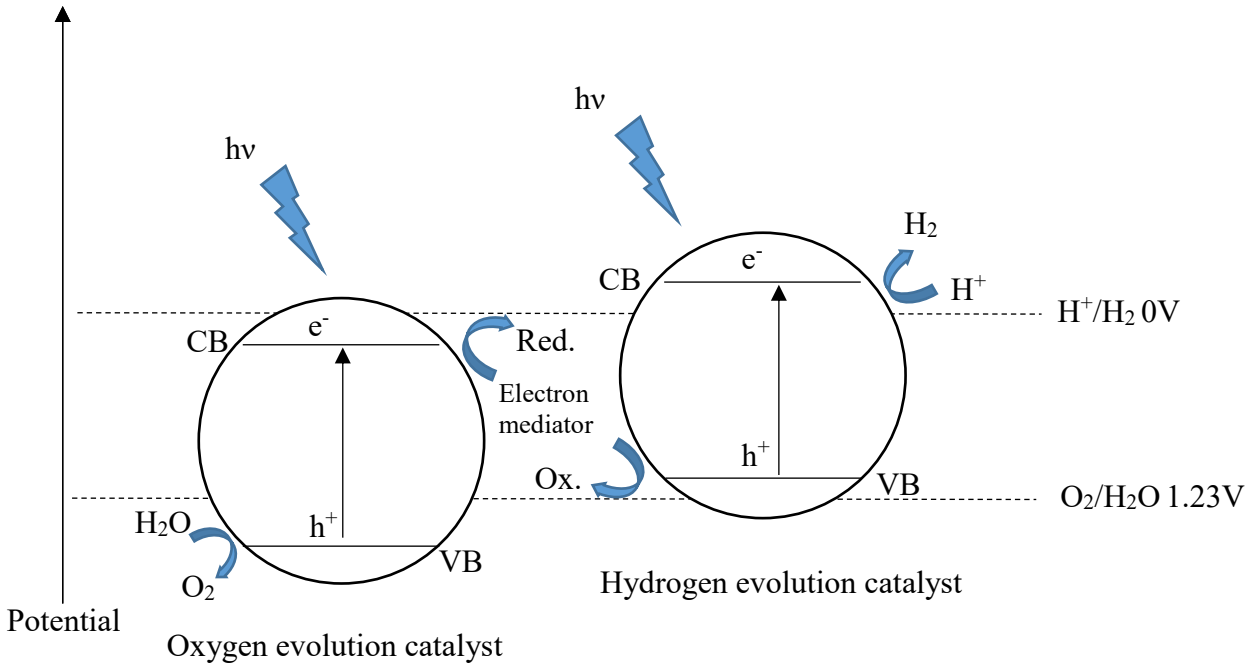

Figure 1.7. Schematic of Z-scheme photocatalyst

In a Z-scheme photocatalyst there is an oxygen evolution catalyst and a hydrogen evolution catalyst. The process involves the reduction and oxidation of the redox mediators; an electron acceptor (A) and an electron donor (D). The forward reactions that occur on the oxygen evolution catalyst are shown in reactions 1.5 and 1.6. The electron acceptor is reduced by conduction band electrons producing an electron donor and the water is oxidised by the holes to produce H^+.

$$A + e^- \rightarrow D \qquad (1.5)$$

$$H_2O + 2h^+ \rightarrow O_2 + 2H^+ \qquad (1.6)$$

The forward reactions that occur on the hydrogen evolution catalyst are shown in reactions 1.7 and 1.8. The electron donor produced by the oxygen evolution catalyst is oxidised by the holes in the valance band of the hydrogen evolution catalyst and the H^+ is reduced by the conduction band electrons to hydrogen.

$$D + h^+ \rightarrow A \qquad (1.7)$$

$$2H^+ + 2e^- \rightarrow H_2 \qquad (1.8)$$

A Fe^{3+}/Fe^{2+} redox mediator catalyst is an example of a Z-scheme catalyst.[9, 10, 11] This is where Rh, Cr^{3+}/Ta^{5+} or Cr^{3+}/Sb^{5+} is loaded onto $SrTiO_3$ in the presence of $FeCl_3$. The Fe^{3+}/Fe^{2+} redox mediator acts a redox shuttle which controls the reactivity of the electrons and holes. Another example of a redox shuttle is IO^{3-}/I^- where possible catalysts are $SrTiO_3$:Cr/Ta, $BaTaO_2N$ WO_3.[12, 13, 14] Some systems do not require a redox shuttle for example (Ru/$SrTiO_3$:Rh)-($BiVO_4$). When irradiated with visible light it is claimed that it produced one of the highest yields to date for a powdered photocatalyst.[15] An example of a one-step system is the photocatalyst, GaN:ZnO $(Ga_1\text{-}xZn_x)(N_{1-x}O_x)$, designed by Domen *et al.* which absorbs in the visible region and claims it can perform pure water splitting.[16] TiO_2 loaded with noble metals (Pd, Pt, Au etc) [17] is another example of a one-step system. Unfortunately, the catalyst is not very active for pure splitting however if a sacrificial agent is employed, high yields of hydrogen can be reached. Sacrificial agents boost hydrogen yields by acting as reducing agents and extracting the oxygen from water preventing the backwards reaction.[18-20] The most commonly used sacrificial agent for photocatalytic water splitting is methanol.[19, 21-23]

1.2.6.1 Methanol reforming

Using methanol as a sacrificial agent was first reported by Kawai and Sakata in 1980 using Pd/TiO_2, Pt/TiO_2 and RuO/TiO_2.[24] Ethanol has also been used as a sacrificial agent and it is seen a more sustainable resource.[25] The work on using methanol as the sacrificial agent was developed by Bowker and co-workers.[21] In this study the mechanism of methanol reforming was discussed. Figure 1.8 illustrates the steps involved for photocatalytic methanol reforming for hydrogen production.

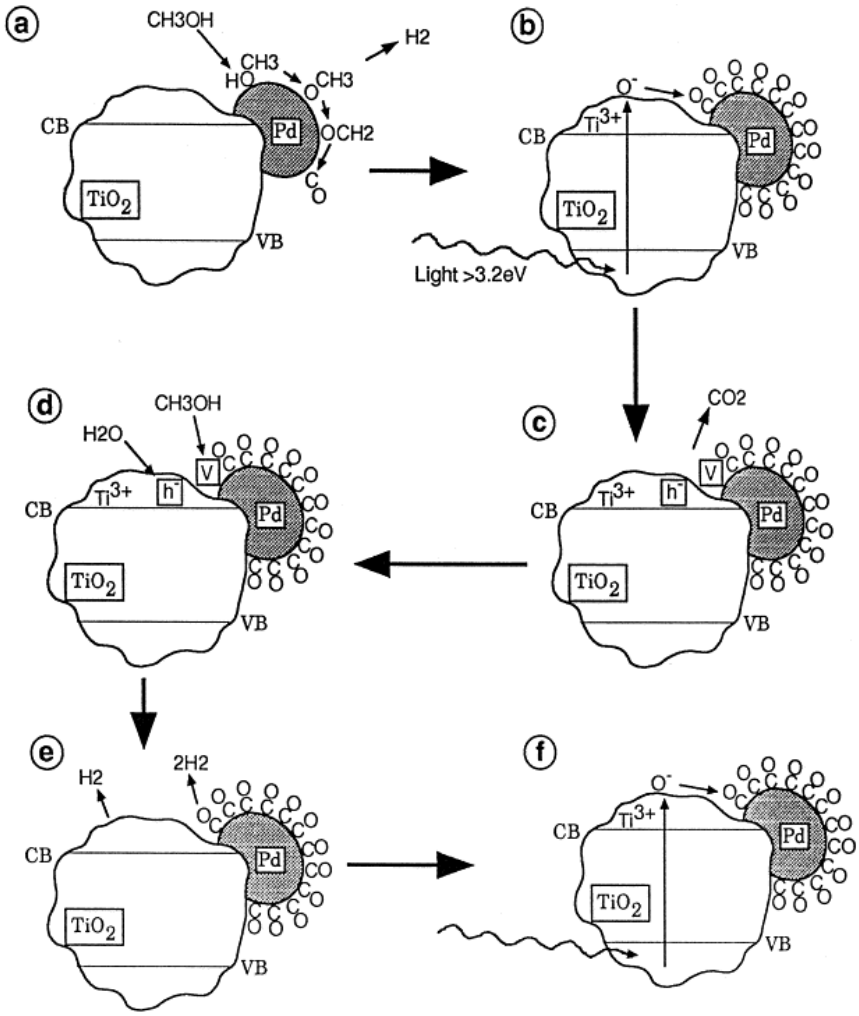

Figure 1.8. Schematic of photocatalytic methanol reforming for hydrogen production on Pd/TiO_2.[21]

The first step (a) is the catalytic decomposition of methanol on Pd. This step does not require UV light to proceed. The surface of the Pd gradually becomes poisoned by CO. In step (b) light excites electrons in the valence band of the TiO_2 into the conduction band. The excited electron in the conduction band oxidises the CO on the surface of the Pd and produces CO_2 in step (c). This leaves a vacancy on the metal and an anion vacancy (hole) in the titania lattice as shown in step (d). The methanol fills the vacancy and decomposes on the metal, in step (e), liberating hydrogen and water fills the hole, also releasing hydrogen. The cycle continues (step (f)) with the excitation of electrons in the valence band of the TiO_2. Step (a) is catalytic whereas steps (b-f) are photocatalytic and

require light to proceed. In the paper by Dickinson *et al.*[21] it is suggested that the rate determining step is catalytic rather than photocatalytic. It being, either the chemisorption of methanol onto the Pd or the decomposition of the methoxy into CO. This conclusion was made because increasing the concentration of methanol in the system had little effect on the rate of hydrogen production. If this is the case it could be assumed that the reaction rate would increase if the temperature of the reaction was increased.

A number of different metals loaded on TiO_2 have been used for this reaction. A comparison of the significant findings are summarised in Table 1.2. This includes the catalyst used, hydrogen production and reaction conditions.

Catalyst	Hydrogen production/ μmol H_2 h^{-1}	Hydrogen production/ μmol H_2 h^{-1} g^{-1}	Conditions
5%Pt/TiO_2[24]	460	1533	10 mL CH_3OH, 10 mL H_2O
1%Pt/TiO_2[26]	400	570	10 mL CH_3OH
1%Pt/TiO_2[27]	186	186	2% CH_3OH/3% H_2O/95% N_2 continuous flow (40mL min^{-1})
5%Pd/TiO_2[24]	220	733	10 mL CH_3OH, 10 mL H_2O
0.5%Pd/TiO_2[21]	400	2000	100μl CH_3OH, 100 mL H_2O
2%Au/TiO_2[22]	600	3000	110μl CH_3OH, 100 mL H_2O

1%Au/TiO_2[27]	133	133	2% CH_3OH/3% H_2O/95% N_2 continuous flow (40mL min^{-1})
1%Au-1%Ag/TiO_2[27]	128	128	2% CH_3OH/3% H_2O/95% N_2 continuous flow (40mL min^{-1})
1%Au/TiO_2[27]	11.7	11.7	2% CH_3OH/3% H_2O/95% N_2 continuous flow (40mL min^{-1})
10%Cu/TiO_2[28]	250	250	500 mL CH_3OH, 500 mL H_2O
1%NiO/TiO_2[29]	30	30	10 mL CH_3OH, 290 mL H_2O
10%RuO/TiO_2[24]	37	123	10 mL CH_3OH, 10 mL H_2O
TiO_2[24]	27	90	10 mL CH_3OH, 10 mL H_2O

Table 1.2. Hydrogen production from alcohols using UV light and a photocatalyst under an inert atmosphere

Table 1.2 shows that it is clear that the metal has a significant effect on the activity of the catalyst. Many things can influence the hydrogen yield including the power of the light source, distance between reaction vessel and the light source and the material of the reaction vessel, all of which makes the comparison of literature very difficult.

1.2.6.2 Sacrificial agents

Methanol is not the only sacrificial agent that has been used for photocatalytic hydrogen production. Many different alcohols, polyols and sugars have also been used. Bahruji *et*

al.[30] did an extensive study on primary, secondary and tertiary alcohols using Pd/TiO_2. The alcohols used and the hydrogen produced is shown in Figure 1.9.

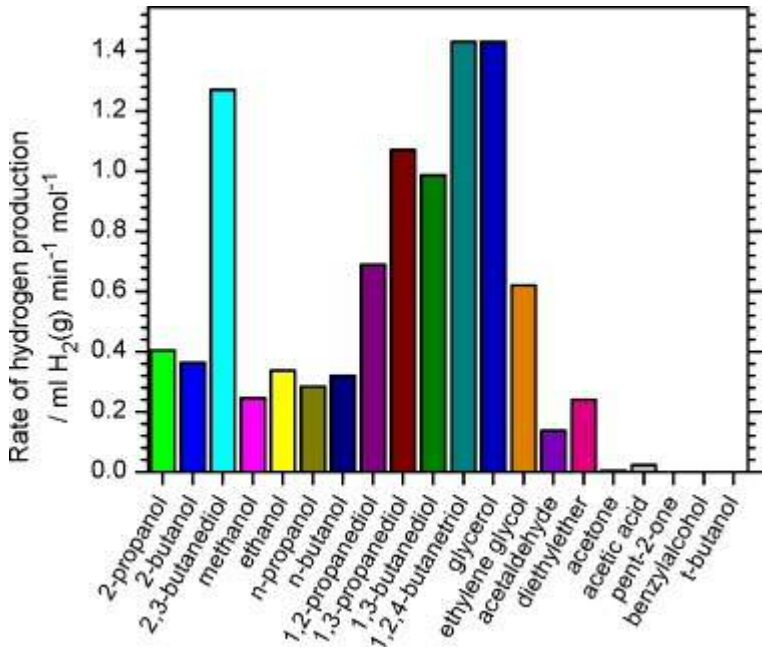

Figure 1.9. Hydrogen production from a range of sacrificial agents using $0.5\%Pd/TiO_2$.[30]

From this study it was observed that the sacrificial agent must have a hydrogen atom alpha to the hydroxyl group in order to react. The study also suggested that with more hydroxyl groups, the higher the hydrogen yield. A study by Leung *et al.* in 2011 tested C-3 polyols for hydrogen production in an attempt to establish whether there was a relationship between number of hydroxyl groups and hydrogen production. The experimental hydrogen yields are shown in Table 1.3.

Polyol	Hydrogen production/ μmol H_2 h^{-1}
Glycerol	300
Propylene glycol	196
Isopropanol	86

Table 1.3. Hydrogen production from different C-3 polyols.[31]

Table 1.3 shows that hydrogen production increases with more hydroxyl groups. In fact the ratio of hydrogen produced is 1:2:3 for isopropanol, propylene glycol and glycerol. This suggests that there is a relationship between the number of hydroxyl groups and hydrogen production.

1.2.7 Semi-conductors

The band gap of a semiconductor is what makes it a possible photocatalyst. The valence band in a semi-conductor is the highest in energy, fully filled band. The conduction band is where electrons are more weakly bound. The positions of the valence and conduction bands give semi-conductors different properties and the energy difference between them is called the band gap. When energy greater than the band gap is applied *e.g.* light energy, an electron is excited from the valence band to the conduction band. This process produces an excited electron (e^-) and also leaves a positive hole (h^+) in the valence band. It is these photogenerated charge carriers that aid the catalysis of reaction. The photogenerated holes and electrons have three possible pathways after being produced.

1. Migration to the surface and reducing the adsorbed species
2. Migration to the surface and oxidising the adsorbed species
3. Recombination with each other

The third pathway is obviously unfavourable to the desired reaction and will decrease the efficiency of the photocatalyst. Doping with metals has been reported to trap the electrons, due to the Schottky Barrier at the interface between the metal and the semi-conductor, preventing recombination.[32]

The deposition of metal nanoparticles has been shown to increase the efficiency of interfacial charge transfer from the semi-conductor into the metal.[33, 34] The Fermi level in a semi-conductor is related to the number of accumulated electrons. If more electrons

accumulate in a system, the Fermi level shifts negatively towards the conduction band which in turn improves the energetics of the system. In a semi-conductor the Fermi level generally lies in the middle of the valence and conduction band. When metal nanoparticles are deposited onto the surface of a semi-conductor, the Fermi level shifts towards the conduction band (Figure 1.10). The transfer of electrons from the semi-conductor into the metal continues until the system achieves equilibration, otherwise known as the Fermi equilibrium.

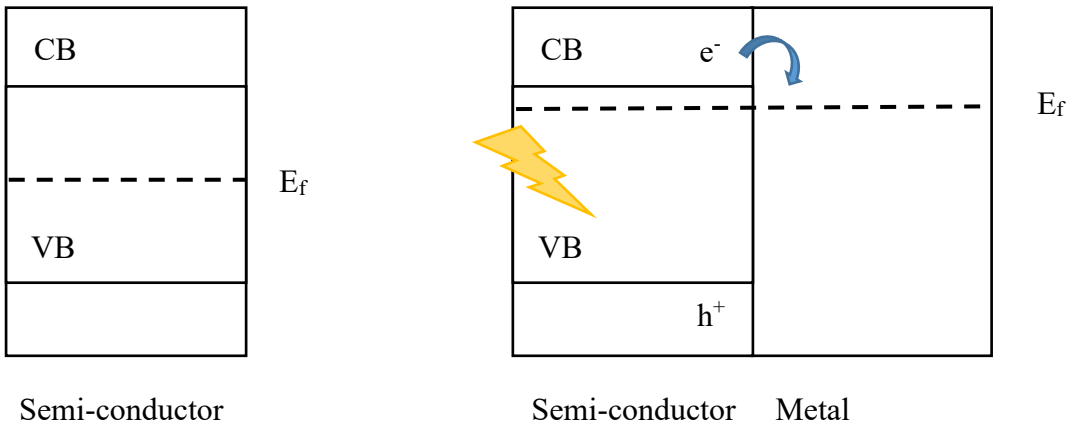

Figure 1.10. Position of Fermi level in semi-conductor (left) and semi-conductor with metal nanoparticle deposited (right).

The shift in Fermi level means that there is an increase in electrons with more energy and so electrons can more easily pass into the metal. This process increases charge separation which been reported to be a factor that significantly increases the activity of a photocatalyst.[35]

The size of the nanoparticle has also been shown to affect the position of the Fermi level in a metal semi-conductor system. Subramanian *et al*.[36] studied the effect of depositing different sized Au nanoparticles on TiO_2 and how this affected Fermi equilibration.

Catalyst	Size of nanoparticle/ nm	Position of Fermi level/ mv
TiO_2	-	-230
Au/TiO_2	8	-250
Au/TiO_2	5	-270
Au/TiO_2	3	-290

Table 1.4. Size of Au nanoparticle deposited on TiO2 and the apparent Fermi level.[36]

Table 1.4 shows that the smaller the nanoparticles, the more negative the Fermi level and therefore the higher electron accumulation. This suggests that the smaller the nanoparticles, the better the charge separation which ultimately increases the performance of the photocatalyst.

The size of Au nanoparticles can also have an effect on the position of the plasmon resonance peak position in UV-vis spectroscopy.[37, 38] Larger nanoparticles of gold will absorb light of greater wavelength, making them appear bluer in colour. Smaller nanoparticles of gold will appear redder in colour as they absorb shorter wavelengths of light. The size dependence of the plasmon absorption was studied for 9, 15, 22, 48, and 99 nm gold nanoparticles in aqueous solution.[39] The peak of the plasmon peak for different sized nanoparticles is shown in Table 1.5.

Au nanoparticle size/ nm	Position of plasmon peak/ nm
8.9	517
14.8	520
21.7	521
48.3	533
99	573

Table 1.5. Plasmon peak position and Au nanoparticle size.

For photocatalytic water splitting it is essential that the valence band and conduction band of the semiconductor overlap with the redox potentials of the water splitting half reactions. This is shown for some examples in Figure 1.11.

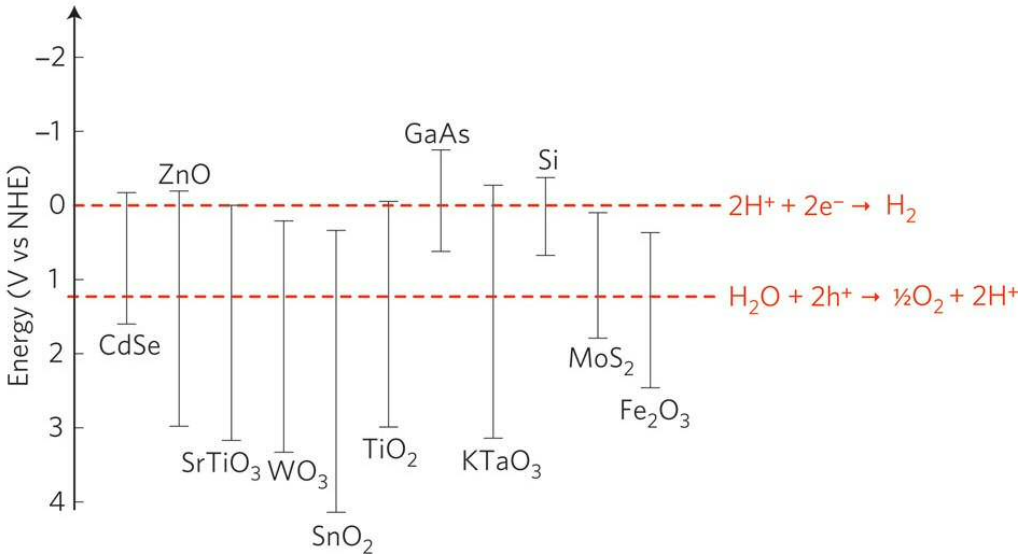

Figure 1.11. Energy level diagram for the conduction and valence bands of common semi-conductors and how they overlap with water splitting half reactions on a potential scale (V) versus the normal hydrogen electrode (NHE).[40]

Figure 1.11 shows that CdSe, ZnO, TiO_2 and $KTaO_3$ overlap with the potential required for water splitting. For this study TiO_2 was chosen as the semiconducting support as the band gap of TiO_2 is at the right potential for water splitting but also because it is considerably more stable and more efficient than the other semi-conductors at the right potential. The stability of CdSe is low and is prone to oxidation, [41] ZnO suffers from photocorrosion in aqueous solution [42] and $KTaO_3$ has been reported to have a low effiency of < 1%.[43]

1.2.7.1 TiO_2

The band gap of TiO_2 is 3.2 eV which means that it can absorb radiation in the UV region and therefore is an appropriate semi-conducting support for photocatalytic hydrogen production. There are three different polymorphs of titanium oxide; anatase, rutile and brookite. The three distinct forms of TiO_2 differ in their assembly of TiO_6^{2-} octahedral. (Figure 1.12).

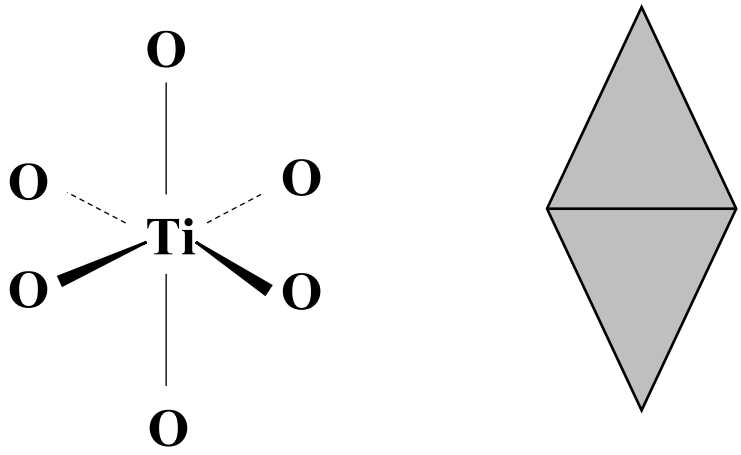

Figure 1.12. TiO_6^{2-} octahedral

Anatase octahedra are connected via the vertices of the octahedral, in rutile via the edges and in brookite they are connected by both edges and vertices as shown in Figure 1.13.[44]

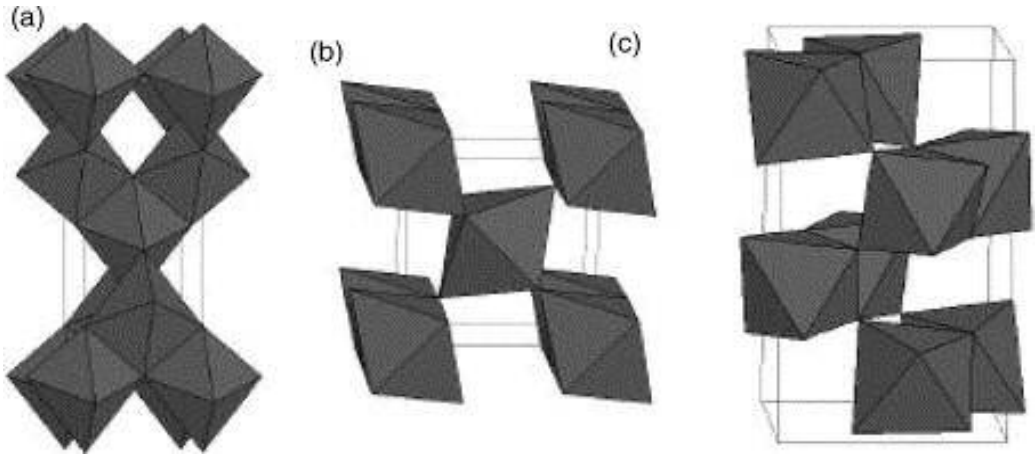

Figure 1.13. Assembly of TiO_6^{2-} octahedra in a) anatase b) rutile and c) brookite.[31]

The stability of the three structures depends on the size of the TiO_2 particles. At less than 11 nm, anatase is the most stable form. From 11-35 nm brookite is most stable and at more than 35 nm, rutile. [45] The enthalpy change from anatase to rutile is relatively small (-1.3 to -6 kJ mol^{-1}).[46, 47] However, anatase can be stable up to 1000 °C if the particles are kept small using certain preparation methods or doping.[48] Once the critical size of nucleus of TiO_2 is formed, anatase conversion to rutile can happen at temperatures as low as 400 °C.[49]

The band gap for anatase and rutile are well known to be 3.26 and 3.05 eV respectively.[50, 51] However the band gap of brookite is unclear. Studies have suggested that the direct band gap of brookite must be larger than 3.5 eV and that it has an indirect band gap of 1.9 eV.[52]

1.2.7.2 TiO_2 activity

The different polymorphs of titania have significantly different activities towards photocatalytic water splitting. Abe *et al*. conducted a comparative study on Pt/TiO_2-anatase and Pt/TiO_2-rutile, using co-catalyst IO^{3-}/I^-.[53] The activities of the catalysts are shown below in Table 1.6.

Photocatalyst	Rate of hydrogen production/ μmol h^{-1}
Pt/TiO_2-anatase	20
TiO_2-anatase	0
Pt/TiO_2-rutile	Tr.
TiO_2-rutile	0
Pt/TiO_2-anatase + TiO_2-rutile	125
Pt/TiO_2-rutile + TiO_2-anatase	<1

Table 1.6. Anatase and rutile activity

Rutile is considered to be a much less effective catalyst compared to anatase.[54] Studies have shown that electron hole recombination in rutile is much quicker than in anatase, making it a poor photocatalyst.[55-57] Some suggest that because rutile has a lower flat band potential, which is close to the NHE potential (H^+/H_2), there is not enough driving force for water reduction.[58] Mixing anatase and rutile mechanically (as above) or chemically (TiO_2-P25 Degussa) has shown to have synergistic effects which has been attributed to longer electron hole lifetimes.[59]

Brookite nanocrystals have been reported to have high photocatalytic activity.[60, 61] The hydrothermal synthesis of titanium bis(ammonium lactate) dihydroxide in the presence of urea can produce brookite/anatase mixtures.[62] At higher concentrations of urea, a higher ratio of brookite to anatase is produced. The brookite phase can be characterised using XRD, especially Rietveld analysis of XRD patterns. In some studies anatase/brookite mixtures have been reported to be more active than TiO_2-P25 for photocatalytic hydrogen production.[63, 64] The flat band of brookite is more cathodic than anatase which promotes interfacial electron transfer, giving better charge separation and therefore better photoactivity.[35]

For the majority of the work in this thesis TiO_2-P25 was used as the literature has suggested that the highest hydrogen yields are achieved using TiO_2-P25 as the mixture of anatase and rutile present has synergistic effects.

1.3 Aims and objectives

The purpose of this study is to develop photocatalysts which are active for the production of hydrogen from water and to further understanding of the factors involved in promoting the reaction. The thesis is divided into three bodies of work. The relevant literature for each section will be at the beginning of each chapter.

As a preliminary measure it is important to define a couple of crucial terms. In this thesis when the term catalysis is used, it refers to non-photocatalytic reactions that do not require light to proceed. An example of this is the decomposition of methanol on Pd. On the other hand, photocatalysis will be used for photocatalytic reactions, and also as a broader definition to discuss reactions which combine photocatalytic and catalytic steps. The term catalyst will be in reference to a non-photoactive material, and finally the word photocatalyst will denote a material that is photoactive encompassing those with or without a catalytic component.

The first results chapter explores the use of different metals loaded onto titania for use as photocatalysts for photocatalytic methanol reforming for hydrogen production. The photocatalysts are characterised using XPS and TPR to develop the relationship between high photocatalytic performance and metal reducibility. Other properties such as work function and how the metal affects the band gap is also investigated. The best M/TiO_2 photocatalysts (M = metal) reported in the literature are Pt/TiO_2, Pd/TiO_2 and Au/TiO_2. These are expensive metals and so it would be beneficial to find a metal that is effective but also economical. The fundamental aim of the chapter is to provide a fair comparison of different M/TiO_2 photocatalysts as comparative studies in the literature are limited. The novelty in this work is attempting to correlate the performance of the photocatalysts with the properties that drive high performance.

The second part of study will focus on using different sacrificial agents with varying numbers of hydroxyl species for photocatalytic hydrogen production. From the literature it is clear that a wide range of sacrificial agents for photo-reforming has already been considered. Chapter 4 will develop this work by using longer chain polyols such as erythritol and xylitol. The mechanism for the photoreforming of longer chain polyols will

be investigated. Finally, by investigating these molecules an attempt will be made to establish a relationship between the number of hydroxyl groups and hydrogen yield.

The final results chapter will probe the effect of using different polymorphs of TiO_2 and using different preparation methods of TiO_2 in an attempt to produce active photocatalysts for photocatalytic methanol reforming for hydrogen production. The different polymorphs of TiO_2 have been extensively researched for photocatalytic processes. Sol-gel TiO_2 is a promising photocatalyst. There is little literature concerning sol-gel TiO_2 and photocatalytic methanol reforming. Chapter 5 will concentrate on tuning sol-gel TiO_2 for use as a photocatalyst for photocatalytic methanol reforming. The photocatalysts will be characterised using XRD and BET to derive the properties of TiO_2 that will produce the most active photocatalysts.

It is important to consider the impact of this research and therefore the final chapter will highlight the key findings of this work and suggest possible further research to build upon the conclusions made.

1.4 References

1. J. Gribbin and M. Gribbin, *New Scientist*, 1996, 151, A1.

2. M. Granovskii, I. Dincer and M. A. Rosen, *International Journal of Hydrogen Energy*, 2006, 31, 337.

3. L. Schlapbach and A. Zuttel, *Nature*, 2001, 414, 353.

4. S. T. Weir, A. C. Mitchell and W. J. Nellis, *Physical Review Letters*, 1996, 76, 1860.

5. R. H. Baughman, A. A. Zakhidov and W. A. de Heer, *Science*, 2002, 297, 787.

6. M. V. Twigg, *Catalyst Handbook*, Wolfe, London, UK, 2nd Edition edn., 1989.

7. J. T. Richardson, M. Lei, K. Forster and M. V. Twigg, *Applied Catalysis a-General*, 1994, 110, 217.

8. A. Fujishima and K. Honda, *Nature*, 1972, 238, 37.

9. H. Kato, M. Hori, R. Konta, Y. Shimodaira and A. Kudo, *Chemistry Letters*, 2004, 33, 1348.

10. H. Kato, Y. Sasaki, A. Iwase and A. Kudo, *Bulletin of the Chemical Society of Japan*, 2007, 80, 2457.

11. Y. Sasaki, A. Iwase, H. Kato and A. Kudo, *Journal of Catalysis*, 2008, 259, 133.

12. K. Sayama, K. Mukasa, R. Abe, Y. Abe and H. Arakawa, *Chemical Communications*, 2001, 2416.

13. R. Abe, K. Sayama and H. Sugihara, *Journal of Physical Chemistry B*, 2005, 109, 16052.

14. R. Abe, T. Takata, H. Sugihara and K. Domen, *Chemical Communications*, 2005, 3829.

15. Y. Sasaki, H. Nemoto, K. Saito and A. Kudo, *Journal of Physical Chemistry C*, 2009, 113, 17536.

16. K. Maeda, T. Takata, M. Hara, N. Saito, Y. Inoue, H. Kobayashi and K. Domen, *Journal of the American Chemical Society*, 2005, 127, 8286.

17. J. Greaves, L. Al-Mazroai, A. Nuhu, P. Davies and M. Bowker, *Gold Bulletin*, 2006, 39.

18. E. Pulido Melian, O. Gonzalez Diaz, A. Ortega Mendez, C. R. Lopez, M. Nereida Suarez, J. M. Dona Rodriguez, J. A. Navio, D. Fernandez Hevia and J. Perez Pena, *International Journal of Hydrogen Energy*, 2013, 38, 2144.

19. N. L. Wu and M. S. Lee, *International Journal of Hydrogen Energy*, 2004, 29, 1601.

20. R. M. Navarro, M. C. Sanchez-Sanchez, M. C. Alvarez-Galvan, F. del Valle and J. L. G. Fierro, *Energy & Environmental Science*, 2009, 2, 35.

21. A. Dickinson, D. James, N. Perkins, T. Cassidy and M. Bowker, *Journal of Molecular Catalysis a-Chemical*, 1999, 146.

22. M. Bowker, L. Millard, J. Greaves, D. James and J. Soares, *Gold Bulletin*, 2004, 37.

23. L. Saeed Al-Mazroai, M. Bowker, P. Davies, A. Dickinson, J. Greaves, D. James and L. Millard, *Catalysis Today*, 2007, 122.

24. T. Kawai and T. Sakata, *Journal of the Chemical Society-Chemical Communications*, 1980.

25. A. Gasparotto, D. Barreca, D. Bekermann, A. Devi, R. A. Fischer, P. Fornasiero, V. Gombac, O. I. Lebedev, C. Maccato, T. Montini, G. Van Tendeloo and E. Tondello, *Journal of the American Chemical Society*, 2011, 133, 19362.

26. F. Chojnowski, P. Clechet, J. R. Martin, J. M. Herrmann and P. Pichat, *Chemical Physics Letters*, 1981, 84, 555.

27. G. L. Chiarello, M. H. Aguirre and E. Selli, *Journal of Catalysis*, 2010, 273.

28. H.-J. Choi and M. Kang, *International Journal of Hydrogen Energy*, 2007, 32, 3841.

29. A. Kudo, K. Domen, K. Maruya and T. Onishi, *Chemical Physics Letters*, 1987, 133, 517.

30. H. Bahruji, M. Bowker, P. R. Davies and F. Pedrono, *Applied Catalysis B-Environmental*, 2011, 107.

31. X. Fu, X. Wang, D. Y. C. Leung, Q. Gu, S. Chen and H. Huang, *Applied Catalysis B-Environmental*, 2011, 106, 681.

32. M. Jakob, H. Levanon and P. V. Kamat, *Nano Letters*, 2003, 3, 353.

33. Y. Nakato, M. Shioji and H. Tsubomura, *Chemical Physics Letters*, 1982, 90, 453.

34. V. Subramanian, E. Wolf and P. V. Kamat, *Journal of Physical Chemistry B*, 2001, 105, 11439.

35. A. Zachariah, K. V. Baiju, S. Shukla, K. S. Deepa, J. James and K. G. K. Warrier, *Journal of Physical Chemistry C*, 2008, 112, 11345.

36. V. Subramanian, E. E. Wolf and P. V. Kamat, *Journal of the American Chemical Society*, 2004, 126, 4943.

37. W. Haiss, N. T. K. Thanh, J. Aveyard and D. G. Fernig, *Analytical chemistry*, 2007, 79, 4215.

38. V. Amendola and M. Meneghetti, *Journal Of Physical Chemistry C*, 2009, 113, 4277.

39. S. Link and M. A. El-Sayed, *J. Phys. Chem. B*, 1999, 103, 4212.

40. S. Linic, P. Christopher and D. B. Ingram, *Nature Materials*, 2011, 10, 911.

41. J. Aldana, Y. A. Wang and X. G. Peng, *Journal of the American Chemical Society*, 2001, 123, 8844.

42. C. Ye, Y. Bando, G. Shen and D. Golberg, *Journal of Physical Chemistry B*, 2006, 110, 15146.

43. D. Xu, S. Yang, Y. Jin, M. Chen, W. Fan, B. Luo and W. Shi, *Langmuir*, 2015, 31, 9694.

44. O. Carp, C. L. Huisman and A. Reller, *Progress in Solid State Chemistry*, 2004, 32.

45. H. Z. Zhang and J. F. Banfield, *Journal of Physical Chemistry B*, 2000, 104, 3481.

46. Bobyrenk.Yy, A. B. Zholin and Konovalo.Vb, *Zhurnal Fizicheskoi Khimii*, 1972, 46, 1305.

47. A. Dassler, A. Feltz, J. Jung, W. Ludwig and E. Kaisersberger, *Journal of Thermal Analysis*, 1988, 33, 803.

48. G. Colon, M. C. Hidalgo and J. A. Navio, *Applied Catalysis a-General*, 2002, 231, 185.

49. R. D. Shannon, *Journal of Applied Physics*, 1964, 35, 3414.

50. H. Tang, F. Levy, H. Berger and P. E. Schmid, *Physical Review B*, 1995, 52, 7771.

51. J. Pascual, J. Camassel and H. Mathieu, *Physical Review B*, 1978, 18, 5606.

52. R. Zallen and M. P. Moret, *Solid State Communications*, 2006, 137, 154.

53. R. Abe, K. Sayama, K. Domen and H. Arakawa, *Chemical Physics Letters*, 2001, 344, 339.

54. M. R. Hoffmann, S. T. Martin, W. Y. Choi and D. W. Bahnemann, *Chemical Reviews*, 1995, 95.

55. R. Katoh, M. Murai and A. Furube, *Chemical Physics Letters*, 2008, 461, 238.

56. K. M. Schindler and M. Kunst, *Journal of Physical Chemistry*, 1990, 94, 8222.

57. A. Yamakata, T.-a. Ishibashi and H. Onishi, *Chemical Physics*, 2007, 339, 133.

58. T. Sreethawong, Y. Suzuki and S. Yoshikawa, *Journal of Solid State Chemistry*, 2005, 178, 329.

59. C. Y. Wu, Y. H. Yue, X. Y. Deng, W. M. Hua and Z. Gao, *Catalysis Today*, 2004, 93-5, 863.

60. B. Ohtani, J. Handa, S. Nishimoto and T. Kagiya, *Chemical Physics Letters*, 1985, 120, 292.

61. G. L. Chiarello, A. Di Paola, L. Palmisano and E. Selli, *Photochemical & Photobiological Sciences*, 2011, 10, 355.

62. A. A. Ismail, T. A. Kandiel and D. W. Bahnemann, *Journal of Photochemistry and Photobiology a-Chemistry*, 2010, 216, 183.

63. T. A. Kandiel, A. Feldhoff, L. Robben, R. Dillert and D. W. Bahnemann, *Chemistry of Materials*, 2010, 22, 2050.

64. Q. Tay, X. Liu, Y. Tang, Z. Jiang, T. C. Sum and Z. Chen, *Journal of Physical Chemistry C*, 2013, 117, 14973.

Chapter 2

Chapter 2

2.1 Introduction

The aim of this chapter is to outline and describe the procedures and techniques used during the study including photocatalyst preparation methods, experimental setup and instrument calibration. The photocatalysts were characterised using a number of techniques including X-ray diffraction (XRD), Brunaur-Emmett-Teller (BET), X-ray photoelectron spectroscopy (XPS), Temperature programmed reduction (TPR) and Raman spectroscopy.

2.2 Photocatalyst Preparation

Two methods of photocatalyst preparation were used in this study; incipient wetness and a colloidal method. For the bulk of the photocatalysts prepared, P25 (Degussa) was used as the photocatalyst support but other types of TiO_2 from different manufacturers and preparation methods were also used. These include anatase (Sigma Aldrich), rutile (Sigma Aldrich) and TiO_2 (sol-gel) (titania synthesised in laboratory from tetraisopropyl titanate).

2.2.1 Incipient wetness

Incipient wetness, used for the synthesis of the majority of photocatalysts used in this study, involves dissolving the metal salt in the amount of water required to fill the pores of the support. This was determined by adding water dropwise from a graduated pipette to the support until it did not absorb anymore. $PdCl_2$ (Sigma Aldrich) was dissolved in the appropriate amount of deionised water and 2 drops of HCl added using a sonicator bath for 15 minutes. Table 2.1 shows the amount of water required to fully saturate different TiO_2 supports. HCl is required for the complete dissolution of $PdCl_2$. The Pd solution was added slowly to TiO_2 using a pipette. The mixture of the Pd solution and TiO_2 was ground and mixed together thoroughly using a pestle and mortar. The

photocatalyst was then dried at 120 ºC for 2 hours and then calcined at 400 ºC for 3 hours. A scheme of the preparation of Pd/TiO_2 (IW) is shown in Figure 2.1. The photocatalyst was then passed through a 53 μm sieve to ensure a homogeneous particle size. The photocatalyst samples were then characterised using XRD, BET and XPS.

TiO_2	Incipient wetness point for 2 g of TiO_2/ ±0.1 mL
P25	1.5
Anatase	1.5
Rutile	2.0
$sTiO_2$	1.0

Table 2.1. Summary of incipient wetness points for titania used

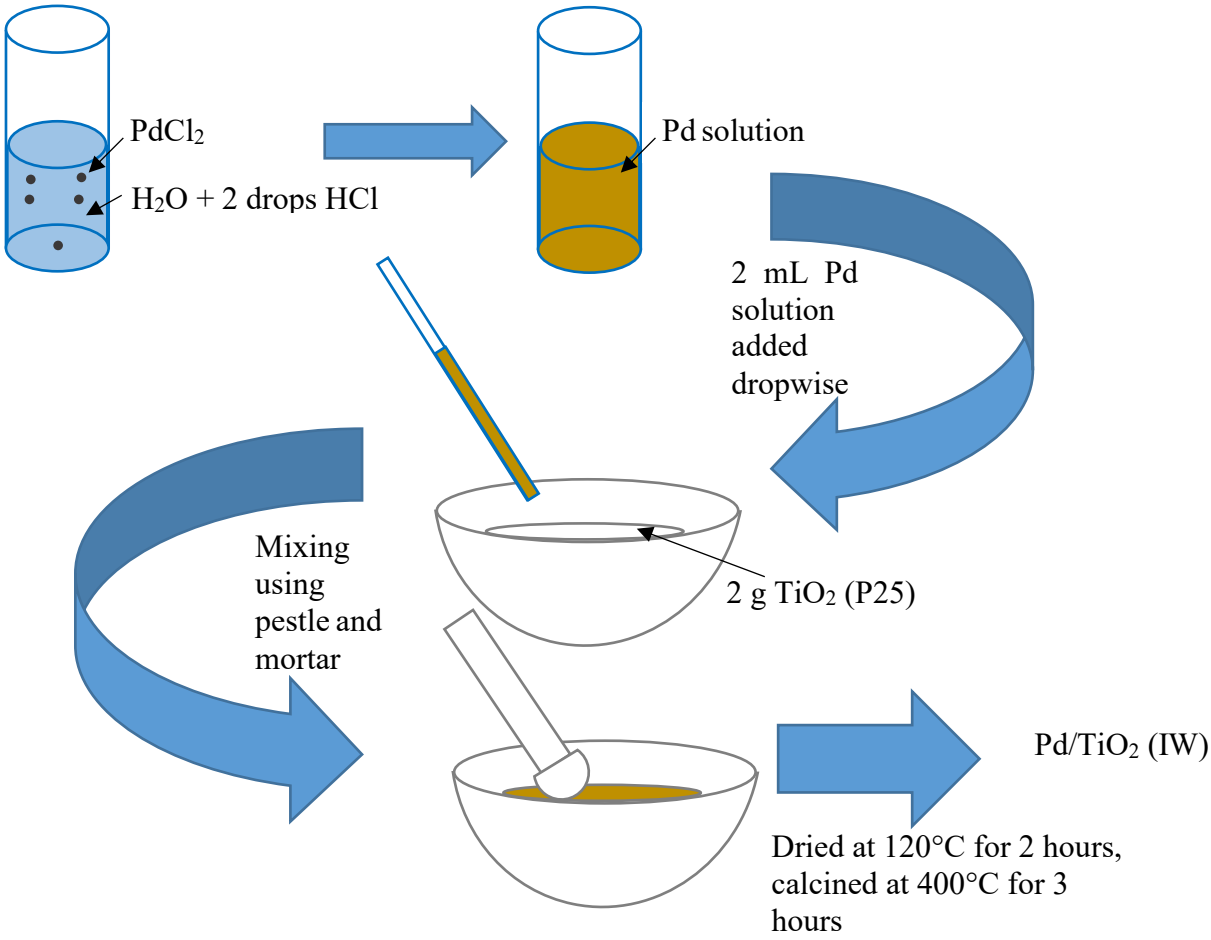

Figure 2.1. Scheme showing incipient wetness preparation of Pd/TiO_2 (IW)

A range of different metal catalysts were prepared following the same method but using the corresponding metal salt. These are summarised in Table 2.2. The loading of the metal catalysts was 0.5 wt%.

Metal Salt	Mass of precursor used/ g
$PdCl_2$	0.0167
H_2PtCl_6	0.0265
$HAuCl_4$	0.0181
$RhCl_3.3H_2O$	0.0255
$RuCl_3.H_20$	0.0223
$IrCl_3.H_2O$	0.0165
$CuNO_3$	0.0295
$NiNO_3$	0.0500
$AgNO_3$	0.0157

Table 2.2. Summary of metal precursors used for incipient wetness preparation of photocatalysts and the mass used for 2g of photocatalyst.

For the preparation of 2 g 0.5 wt% of Pd on TiO_2, the mass of $PdCl_2$ required was determined is shown in Equation 2.1.

Equation 2.1. Calculation of mass of precursor used

2.2.2 Colloidal gold and impregnation

To obtain a more controlled metal nanoparticle size a colloidal method was also used for gold catalysts. The Turkevich method[1] uses citrate (sodium citrate, 98% Sigma Aldrich)

as a reducing agent and capping agent for the synthesis of gold nanoparticles. After the nanoparticles were produced, they were impregnated onto TiO_2.

Figure 2.2 shows the colloidal method of Au nanoparticle synthesis. 1% Au solution was produced by dissolving $HAuCl_4.3H_2O$ (99% Sigma Aldrich) in water. The solution was heated to 90 ºC and 1% citrate solution added. The solution continued to be heated until the Au nanoparticles had formed indicated by the colour change from very pale yellow to black to red.[1] TiO_2 was added to the mixture and stirred for 5 hours. The mixture was filtered and washed with water. The photocatalyst was dried at 120 ºC for 2 hours and sieved to an aggregate size of 53 µm. The photocatalysts were characterised using XPS, XRD and UV-vis spectroscopy.

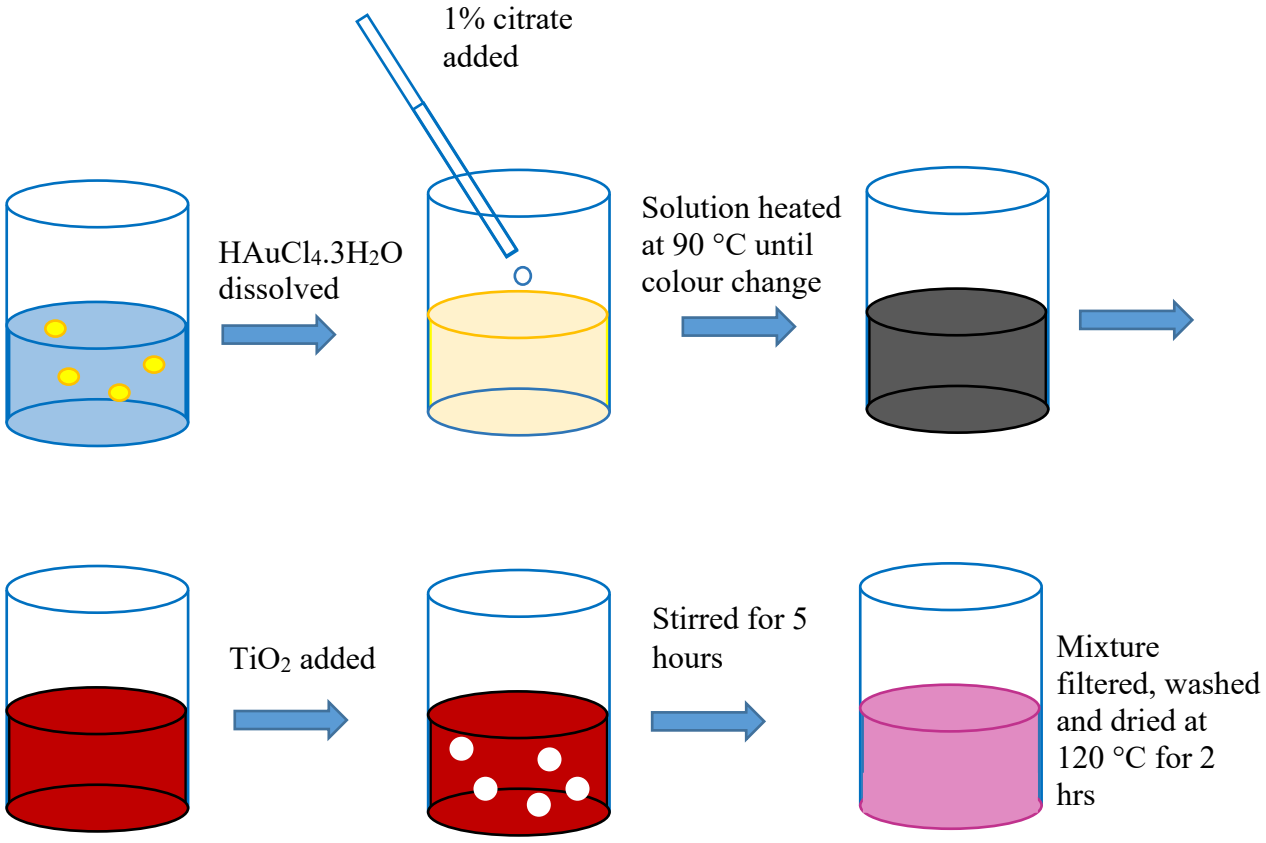

Figure 2.2. Colloidal gold synthesis following Turkevich method.

2.3 Synthesis of TiO_2 (TiO_2-sol-gel)

TiO_2-sol-gel was synthesised in the laboratory by a method used by Addamo *et al.*[2] The materials used are listed here; titanium (IV) tetraisopropoxide (Sigma Aldrich), Isopropyl alcohol (Sigma Aldrich), nitric acid and deionized water.

Tetraisopropropyl titanate (2.5mL) was added to isopropyl alcohol (42.5 mL). Water (400 mL) was acidified using nitric acid (5 drops) to pH 2.5. The tetraisopropyl titanate solution was added to the acidified water and immediately a milky white precipitate was formed. The mixture was stirred for 24 hours at room temperature followed by heating at 75-80 ºC for 5 hours. The solution was then dried at 100 ºC overnight to remove alcohol.

Pd was impregnated onto TiO_2-sol-gel using the same incipient wetness technique described above. The TiO_2-sol-gel was calcined at different temperatures (300, 500 and 700ºC) and characterised using XRD, BET and Raman.

2.4 Experimental Set Up

2.4.1 Photoreactor

Dickinson's original experimental set up for photocatalysis was used for the reactions in this study.[3] This comprised a photoreactor, light source and analysis by gas chromatography (GC), Figure 2.3. The photoreactor involved using a Pyrex two necked flask, one for purging with nitrogen and the other for sampling. The size of vessel was 200 mL in total and the thickness of the glass was 2 mm (minimising light absorption). The vessel was clamped above a hot plate so that the reaction could be stirred and heated if necessary. The light source was placed 30 cm away from the front of the vessel. The reactor and lamp were placed inside a black Perspex box to minimise interference from

other light sources. Injection samples were taken at regular intervals from the reactor before, during and after the experiment and analysed using a GC.

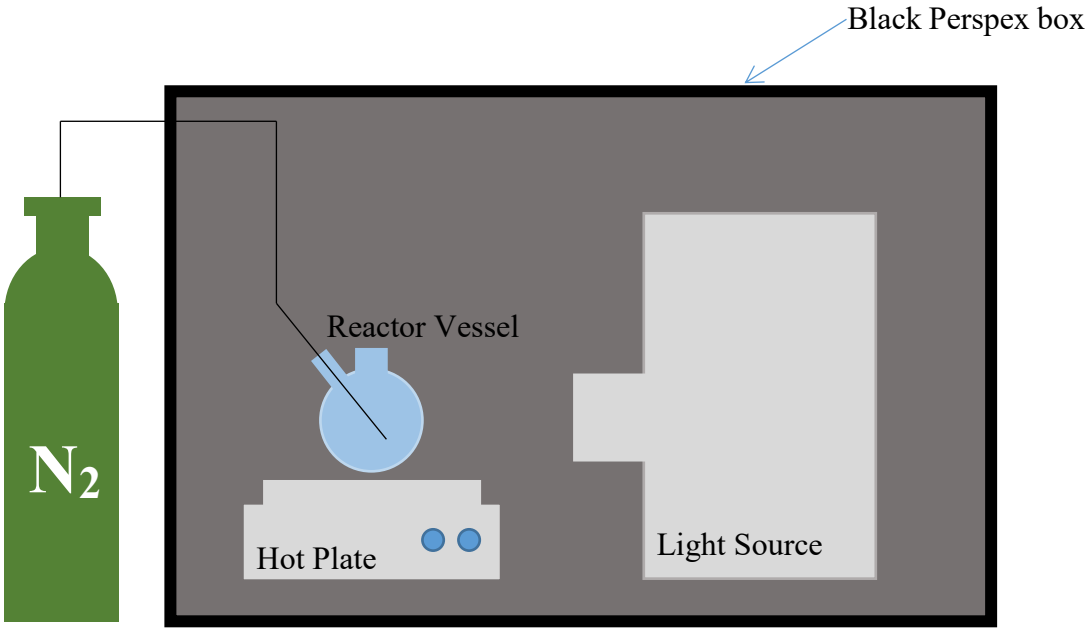

Figure 2.3. Schematic diagram showing reaction set up with reactor and light source

2.4.2 Reaction procedure (Photocatalytic alcohol reforming)

In the reaction vessel, the catalyst (0.2g) and deionised water (100 mL) were purged with nitrogen for 30 mins to remove oxygen and other gases. The alcohol (0.00247 mol) was added to the reaction mixture via syringing through a rubber bung. Table 2.3 details the alcohols tested for hydrogen production. The mixture was stirred using a magnetic stir bar. The lamp was then turned on illuminating the front of the flask. 0.2 mL samples were taken every 30 minutes and analysed using a GC to detect hydrogen. Some reactions required another GC to detect CO_2, CO and CH_4. For gas phase reactions the catalyst (0.2 g) was fixed on to a glass slide and secured above the water (10 mL) alcohol (0.0024 mol) mixture. The catalyst was fixed onto the slide using a couple of drops of deionised

water to make a paste and then the slide was dried in the oven at 50°C for 30 minutes (Figure 2.4).

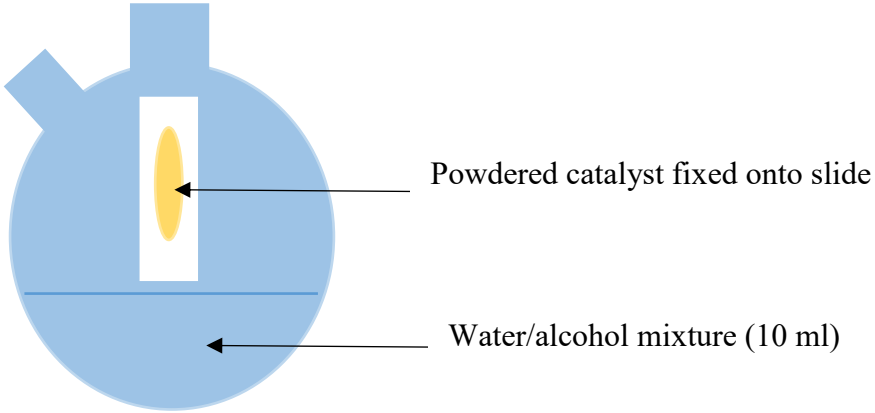

Figure 2.4. Gas phase reactor setup with catalyst mounted on slide above the water/alcohol mixture.

Alcohol	Amount used		Source
	Volume/ mL	Mass/ g	
Methanol	0.1		Fischer
Ethanol	0.143		Sigma Aldrich
Propan-2-ol	0.188		Fischer
Ethylene Glycol	0.139		Fischer
Glycerol	0.18		Sigma Aldrich
Erythritol		0.301	Sigma Aldrich
Xylitol		0.376	Sigma Aldrich
Glucose		0.445	Sigma Aldrich
Fructose		0.445	Sigma Aldrich
Sucrose		0.845	Sigma Aldrich

Table 2.3. Table showing details of the alcohols used for photocatalytic hydrogen production

2.4.3 Light Source

A Xenon arc lamp (Oriel Model No: 6271) was used to replicate sunlight in the photocatalytic experiments. It provided light ranging from UV, visible and infra-red regions (200-1100 nm, Figure 2.5). The lamp along with the ignitor, condensing optics, rear reflector and lamp cooling fan were placed in an arc lamp housing (Oriel Model No: 66921). This was then connected to a power supply (Newport Model No: 69920).

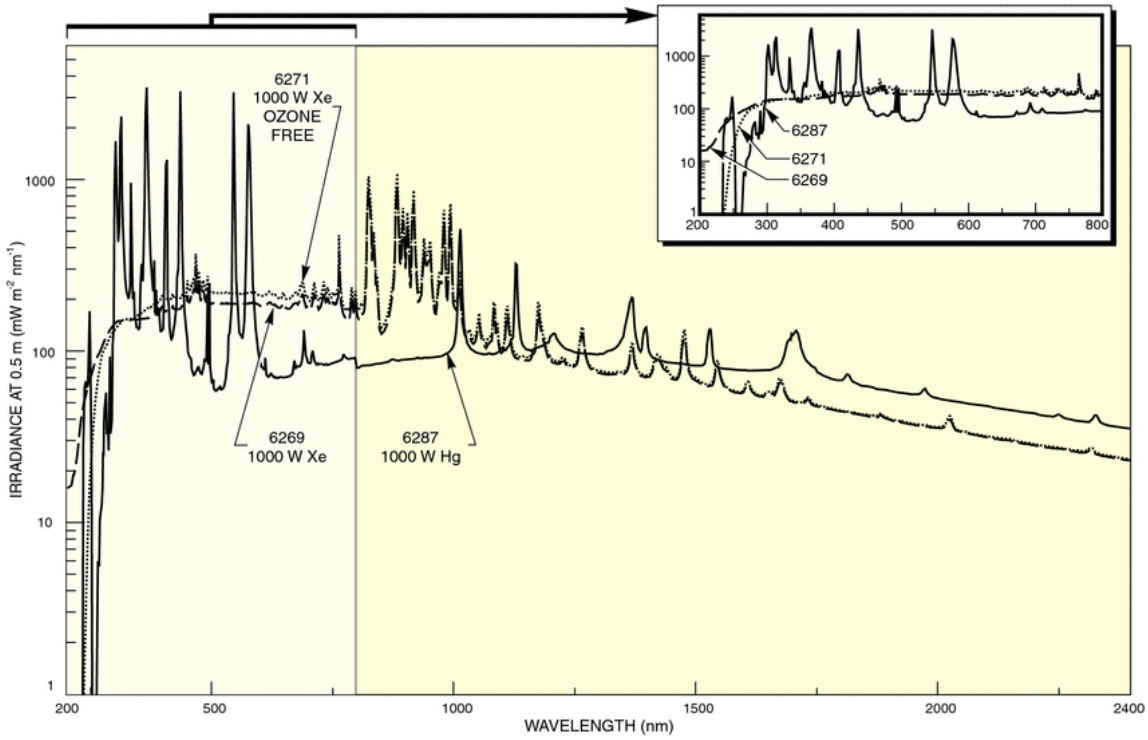

Figure 2.5. Spectral Irradiance of Arc Lamp Xenon Model 6272.[4]

2.4.4 Gas Chromatography

Gas chromatography was used to identify and quantify the products from photocatalytic reactions. Samples were taken before during and after reaction using a syringe. The gas samples can flow directly into the column whereas liquid samples are vaporised in the

chamber before continuing to the column. The column is where the products are separated, each compound will have a different affinity for the stationary phase of the column. The higher the affinity, the more time it takes for the molecule to elute from the column. In this study two types of detector was used; thermal conductivity detector (TCD) for gas samples and flame ionisation detector (FID) for liquid samples. A TCD responds to changes in thermal conductivity. When the compound elutes the column, it passes a filament and the detector compares the thermal conductivity of the carrier/compound mix to the reference flow of carrier gas. In contrast in an FID, the compound is combusted with hydrogen, producing ions which are then be detected.

2.4.4.1 Hydrogen analysis

Two GCs were used during this study to analyse hydrogen production. The first was a Varian 3300 using a 2 m long, molecular sieve, 13X column and a TCD. When this GC became inoperable, analysis was continued using a Perkin Elmer Clarus 480 equipped with a 2 m x 1/8 in, silicostel molecular sieve and TCD. 0.2 mL was extracted from the reaction system using a gas tight syringe (from SGE) and injected into the GC. The column used was capable of separating hydrogen, oxygen, nitrogen and CO. A basic schematic of a GC is shown in Figure 2.6. Due to the difference in thermal conductivity between argon and hydrogen, argon was used as the carrier gas. When the difference in thermal conductivity between the carrier gas and the product is higher, the sensitivity of the measurement is greater.

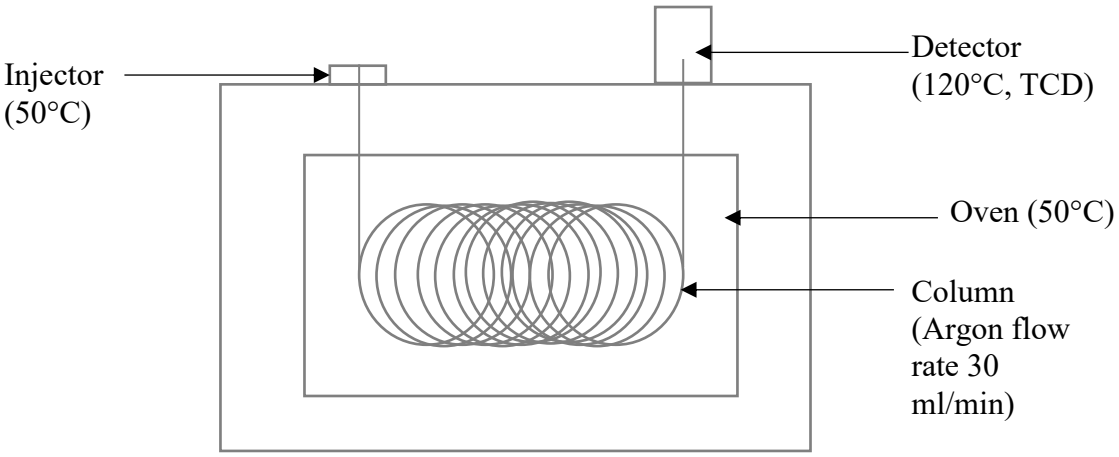

Figure 2.6. Schematic of basic GC with configuration, heating programme and flow rates.

The GC was calibrated using 10% hydrogen in argon (BOC). Known volumes were extracted from the cylinder using a gas tight syringe and injected into the GC. The area under the peak for hydrogen was recorded and repeated three times for each volume. A linear plot of volume of hydrogen against area is shown in Figure 2.7. The gradient of the slope could be used to calculate the hydrogen present in the reactor. The formula used to calculate the amount to hydrogen produced is shown below in Equation 2.2.

Equation 2.2 Hydrogen calibration

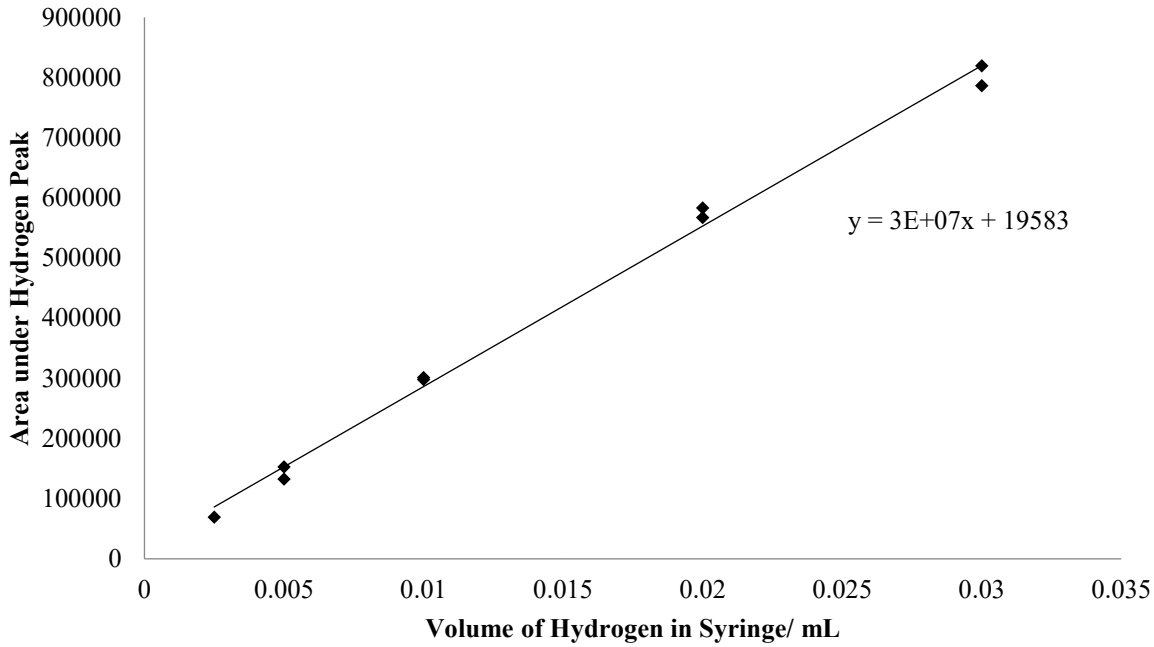

Figure 2.7. Hydrogen calibration plot

2.4.4.2 Other gaseous product and liquid analysis

To measure other gaseous products and liquid products a Perkin Elmer Clarus 480 was used. This system was equipped with two detecters; a TCD and FID. The method for analysing other gas samples was the same as for hydrogen but using a different column and carrier gas. The column used was a 5 ft x 1/8 in x 2.1 mm SS (Suplico Analytical) and the carrier gas was helium. The other gas products calibrated for were CO_2 and CH_4. These calibration plots are shown in Figures 2.7 and 2.8. The calculation to obtain the volume of product in the reactor vessel uses the same equation as above (Equation 2.2)

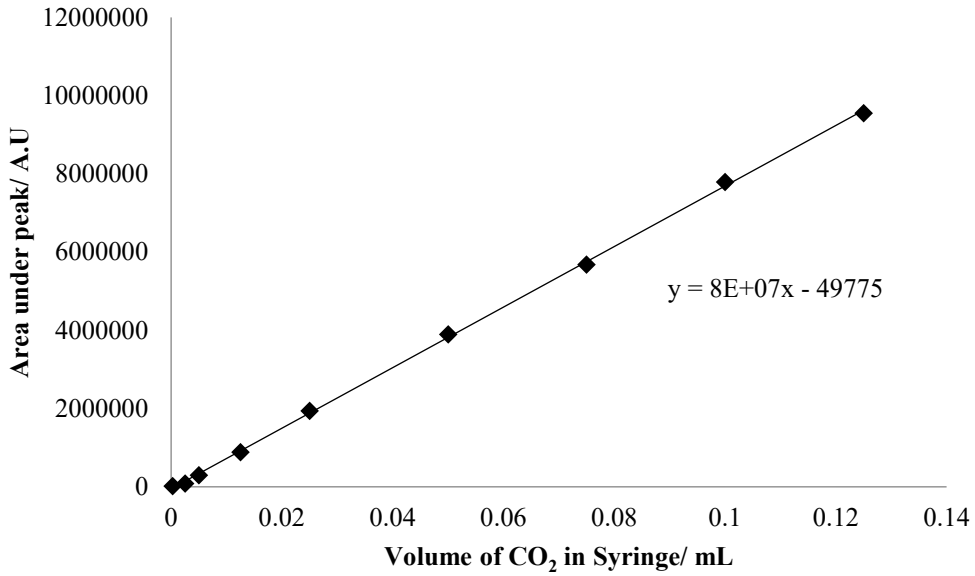

Figure 2.7. CO_2 calibration plot

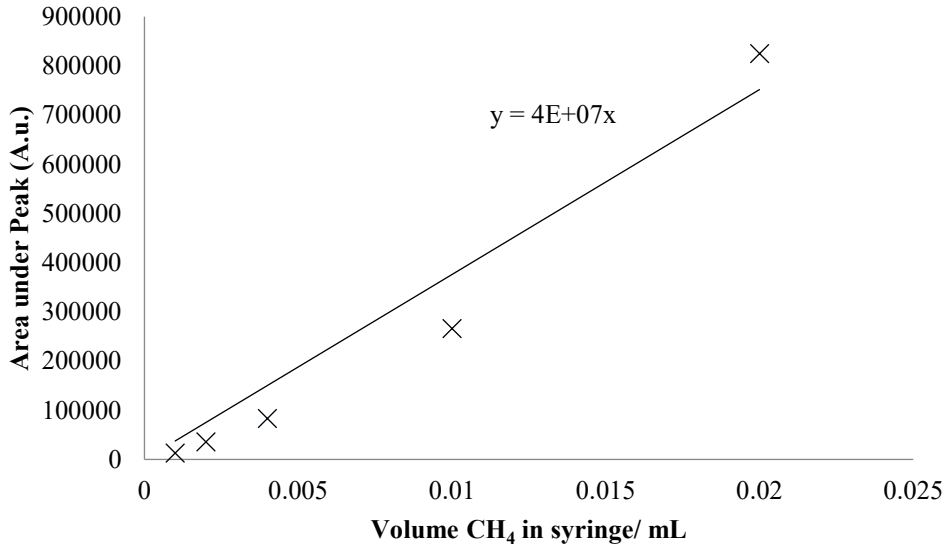

Figure 2.8. CH_4 calibration plot

2.5 Catalyst Characterisation

2.5.1 X-ray Diffraction

X-ray diffraction is technique that can be used to characterise crystalline materials and define their lattice structure. Specifically, this technique can measure the average

spacings between layers in a crystal lattice, determine the crystal structure of an unknown material, signify whether the structure is amorphous and can determine the orientation of crystal. The technique was developed by William and Lawrence Bragg in the early 20th century. When X-rays are reflected off a crystal, they form an interference pattern that can be analysed. This diffraction pattern is produced when a set of parallel X-rays intercept a set of parallel lattice planes separated by a distance, d. The atoms in these planes will scatter the incident rays at an angle of θ. These properties are related in the Bragg Law shown below in Equation 2.3 and shown in Figure 2.9.

Equation 2.3. Bragg Law

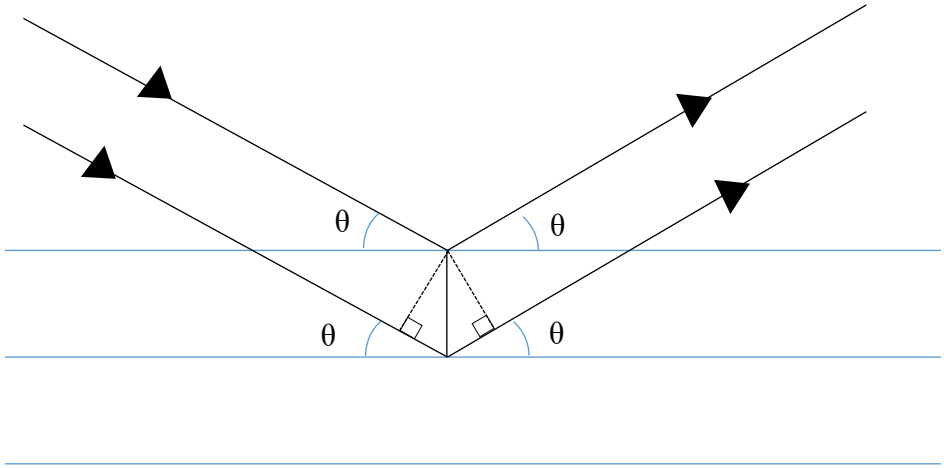

Figure 2.9**.** Schematic of diffracted beams in a crystal lattice

In this study, XRD patterns were obtained by an Enraf Nonus FR590 diffractometer equipped with a hemispherical analyser using Cu Kα radiation (α = 1.54 Å). The current was 30 mA and a voltage of 40 kV. XRD patterns were used to acquire information about the phases of TiO2 present in the catalysts and also to obtain characterisation of crystal size using the Scherrer equation (Equation 2.4).

τ = mean size of crystallite

k = shape factor (usually 0.9) dependent on shape

λ = X-ray wavelength

β = line broadening at half maximum intensity (FWHM)

θ = Bragg angle

Equation 2.4 Scherrer Equation

2.5.2 BET Analysis

The surface areas of the catalysts were characterised using BET analysis. This technique was developed by Brunauer, Emmett and Teller and published in 1938. The technique involves adsorption and desorption of a molecule onto the surface of the catalyst. There are two types of adsorption; physisorption and chemisorption. Physisorption involves weak interactions between the surface and the adsorbate whereas chemisorption involves chemical bonds (sharing of electrons) between the surface and the adsorbate. As a result, chemisorption requires much more energy for desorption to occur compared to physisorption. The adsorption isotherm used in BET analysis is based on similar assumptions as the Langmuir isotherm. The assumptions of the BET isotherm are listed below.

1. Adsorptions occur only on well-defined sites of the sample surface (one per molecule)
2. A molecule can act as a single adsorption site for a molecule of the upper layer.

3. The uppermost molecule layer is in equilibrium with the gas phase
4. The desorption is a kinetically-limited process, i.e. a heat of adsorption must be provided:
5. At the saturation pressure, the molecule layer number tends to infinity (i.e. equivalent to the sample being surrounded by a liquid phase)

The catalyst was weighed, degassed and then exposed to nitrogen at different pressures (usually 5 different pressures). From the amount of adsorbed gas and the surface area of the adsorbate (N_2), the surface area can be calculated using the following equation (Equation 2.5).

$$\frac{P}{V(P_0 - P)} = \frac{1}{V_m C} + \frac{(C-1)}{V_m C}\left(\frac{P}{P_0}\right)$$

V = the total volume of adsorbate (N_2)

V_m = the volume of gas molecules corresponding to the monolayer

P = pressure

P_0 = saturation vapour pressure

C = BET constant

Equation 2.5. BET isotherm

Equation 2.5 can be plotted as a straight line graph with $\frac{P}{V(P_0 - P)}$ on the y axis and $\frac{P}{P_0}$ on the x axis to produce a BET plot. The slope (S) and the intercept (I) are then used to determine the monolayer volume and the BET constant using Equations 2.6 and 2.7.

Equations 2.6 and 2.7

To obtain the surface area of the catalyst the Equation 2.8 is used.

N = avogadros number

S = diameter of adsorbate

V_m = molar volume of adsorbate gas

Equation 2.8 BET surface area

2.5.3 XPS (X-ray photoelectron spectroscopy)

XPS is a useful technique to analyse the surface of the catalyst. It can identify the elements present, approximate surface coverage and their oxidation state. In the present work, XPS was used to determine the oxidation state of the metal nanoparticles on the surface of the catalyst before and after reaction. X-rays of a known wavelength are fired at the catalyst sample resulting in the emission of electrons via the photoelectric effect. The kinetic energy of the emitted electrons can be related back to their "binding energy" using Equation 2.9.

$E_{binding}$ = binding energy of electron

E_{photon} = energy of X-ray photons

$E_{kinetic}$ = kinetic energy of electron

Ø = work function (dependent on instrument and sample)

Equation 2.9 XPS binding energy

All XPS studies were carried out by Dr David Morgan using a Kratos Axis Ultra-DLD photoelectron spectrometer with a monochromatic Al Kα x-ray source and the "hybrid spectroscopy" mode resulting in an analysis area of 700×300 μm at a pass-energy of 40 eV for high resolution scans and 160 eV for survey scans. The XPS data was analysed using CasaXPS [9] with all binding energies referenced to the C(1s) peak at 284.7 eV with an uncertainty of ~0.2 eV. Curve fits were made using Gaussian-Lorentzian (GL(30)) lineshapes.

2.5.4 TPR (Temperature programmed reduction)

TPR monitors how easily the oxidised metal nanoparticles can be reduced. All of the metal nanoparticles used in this study are in their oxidised states prior to use as catalysts with the exception of gold. During the reaction, it is suggested that the metal nanoparticles need to be reduced before they can start acting as catalysts. Therefore the ease of reducibility can play a part in the activity of the different catalysts.

The procedure begins with adding the catalyst to a glass U-tube. The u-tube is fixed into the machine and an inert gas (N_2) is passed through the catalyst to remove any other gasses that were present. A mixture of N_2 and H_2 is then passed over the catalyst and the tube and its contents are heated using a low ramp rate (typically 5 K/min). As the catalyst

is heated, reduction can take place. The level of H_2 flowing out of the U-tube is measured and a decrease in H_2 indicates that reduction at that temperature has taken place.

2.5.5 Raman spectroscopy

Raman spectroscopy probes the vibrational and rotational modes present in a molecule. The set of peaks produced by Raman spectroscopy can be used to classify the molecule including identifying what phases are present. Light from a laser of a specific wavelength is fired at the sample and interacts with the vibration within the molecule. Two types of scattering occurs; inelastic (Stokes and anti-Stokes) and elastic scattering (Rayleigh) as shown in Figure 2.10. Radiation elastically scattered with the same wavelength as the incident laser is filtered out. The inelastic scattered radiation is detected, producing a Raman spectrum. Raman spectroscopy was used to determine the presence of different phases of TiO_2 (anatase, rutile and brookite). The Raman spectroscopy in this study was carried out using a Renishaw inVia Raman microscope.

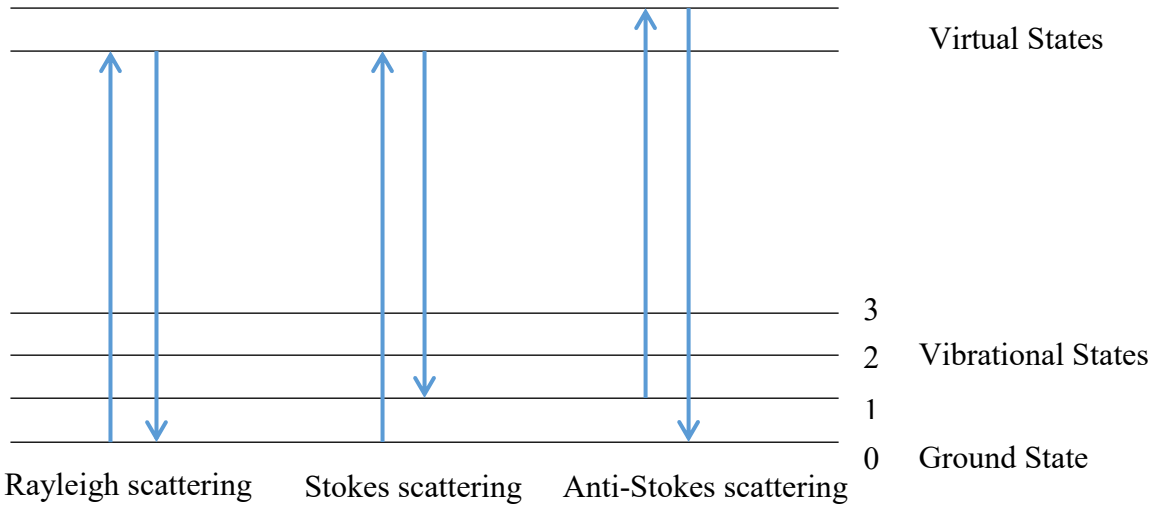

Figure 2.10. Energy level transitions for Rayleigh, Stokes and Anti-Stokes Raman scattering

2.5.6 Mass spectrometry

Mass spectrometry is an analytical technique in which different masses within a sample are detected. The sample is firstly ionised and fragmented, then based on the mass/charge ratio separated and finally detected using an ion detector. A mass spectrometer consists of three main parts; an ion source, mass analyser, and a detector. Electron ionisation has been used in this study as the samples being analysed were gaseous. Electrons are emitted from a filament and bombard the sample, producing ionised fragments.

The ionised fragments are then separated according to their mass/charge ratio by the mass analyser. The mass analyser used was a quadrupole mass filter where oscillating electric fields are used to control the pathways of the ions passing between four steel cylinders. The potential applied to the cylinders allows specific ionised fragments to pass through. The potential then changes so that fragments with other mass/charge ratios can move through. This effectively filters the fragments according to their mass/charge ratios. The ions are then detected by the ion detector producing a plot showing the relative amounts of fragments present in the sample. In order to detect the presence of gases other than H_2, CO_2, CO and CH_4, gas samples were injected into a sampling system attached to a Hiden Analytical quadrupole Hal 201 mass spectrometer using He as the carrier gas. The cracking fractions for the gases detected are shown in Table 2.4.

Gas	Cracking fraction
H_2	2 (1000), 1 (21)
CO_2	44 (1000), 16 (94)
C_3H_8	29 (1000), 28 (615), 44 (402)
C_4H_{10}	43 (1000), 29 (442), 27 (371)

Table 2.4 Cracking fractions for gases detected using mass spectrometry.[5]

2.6 References

1. J. Turkevich, P. C. Stevenson and J. Hillier, Discuss. Faraday. Soc, Editon edn., 1951, vol. 85, p. 3317.
2. M. Addamo, V. Augugliaro, A. Di Paola, E. Garcia-Lopez, V. Loddo, G. Marci and L. Palmisano, *Thin Solid Films*, 2008, **516**, 3802-3807.
3. Dickenson, A. J., *Photocatalytic Hydrogen Production,* in Chemistry Department, 1997, University of Reading : Reading.
4. http://assets.newport.com/webDocuments-EN/images/Light_Sources.pdf
5. Cornu, A. Massot, R., Compilation of Mass Spectroscopic Data, 1966, London: Heyden in co-operation with Presses Universitaires le France.

Chapter 3

3.1.Introduction

The photocatalytic, ambient temperature, reforming of methanol, used to generate hydrogen gas, can be an alternative source to sustain global energy demand. Photocatalysis offers green hydrogen production with the reaction solely driven by solar energy. TiO_2 is an ideal semiconductor for this purpose as it has a 3.2 eV band gap which allows photon absorption in the UV region. P25 TiO_2 has been shown to exhibit better photocatalytic activity than other TiO_2 types due to the presence of anatase-rutile heterojunctions, which are said to be the active sites of the catalyst.[1, 2] Photocatalysts with high photon absorption and long charge separation have higher activity. One way of achieving this is to dope TiO_2 with a metal. The metal acts as an electron sink, prolonging charge carrier separation, improving the lifetime of the active species.[3, 4, 5] Also the interaction between the TiO_2 and the metal allows electrons to move easily from the conduction band in the TiO_2 to the Fermi of the metal, increasing the activity. Pure water splitting is very difficult. Using a sacrificial agent can increase hydrogen yields. Methanol can be used as a sacrificial agent as seen in early work by Kawai *et al.*[6] and Naito *et al.*[7] Methanol acts as a sacrificial reductant, extracting oxygen from water which in turn produces hydrogen. An important experiment to point out is photocatalytic methanol reforming in D_2O.[8] Here the hydrogen yield is far lower than with unlabelled water indicating that water is needed for the reaction to proceed to its full extent. Also that water is in fact split to produce hydrogen *i.e.* the hydrogen is not coming from only the methanol. As well as the photocatalyst and sacrificial agent, the method used to produce the photocatalyst is an important factor and can affect the hydrogen yield of the reaction.

3.1.1 Photocatalytic hydrogen production from methanol

In 1972, Fujishima and Honda[9] proposed a method of splitting water using electrochemical photolysis. Here, light equal to less than 413 nm illuminated the reactor and a voltage was applied between a TiO_2 electrode and a platinum electrode. It was partly this work that sparked an interest in photocatalytic water splitting. As mentioned before pure water splitting is very difficult and the use of a sacrificial agent greatly increases hydrogen yields. The next section will focus on the literature on photocatalytic methanol reforming for hydrogen production using metal loaded TiO_2.

The early work of Kawai and Sakata demonstrated that high hydrogen yields could be achieved using Pd/TiO_2, Pt/TiO_2 and RuO_2/TiO_2 with methanol in aqueous solution.[6, 10] The main finding was that Pt/TiO_2 had the highest activity, followed by Pd/TiO_2 and then RuO_2/TiO_2. The maximum quantum yield was 40% which was for Pt/TiO_2. They reported that using TiO_2 alone produced much lower yields of hydrogen which they attributed to the charge separation being inefficient and/or the fact there was not a methanol oxidation catalyst present. Electrode catalysts were compared to powdered photocatalysts and it was reported that the powdered photocatalysts produced higher yields as they have larger surface areas.

Similar work was done by Domen *et al*. and Naito *et al.* on photocatalytic alcohol reforming. Different semiconductors were explored using water and propan-2-ol.[11] Pd/TiO_2 , Pt/TiO_2 and Rh/TiO_2 were used for the photodecomposition of methanol and the presence of alkali metal cations for selectivity.[12] Again Pt/TiO_2 produced the highest yields of hydrogen, with Rh/TiO_2 coming a close second. The hydrogen yields reported for Pd/TiO_2 were much lower in relation to the other two photocatalysts. Addition of alkali metal cations such as Li, Na and Rb improved the selectivity towards hydrogen with Na being the most effective.

3.1.1.1 Platinum

Pt/TiO_2 achieves high hydrogen yields, more recently this photocatalyst has been researched further. In 2005 Galinska *et al.*[13] published research on Pt/TiO_2 for photocatalytic methanol reforming and using other sacrificial agents. Better hydrogen yields were achieved at 60˚C compared to 40˚C. Other gaseous products were also recorded including CO_2 and CH_4. EDTA and Na_2S were also used as sacrificial agents however methanol produced the highest hydrogen yields. It was postulated that this was because some hydrogen is produced directly from methanol decomposition. Lin *et al.*[14] used a micro-emulsion method of synthesising 0.1%-0.7% wt $Pt/TiO_{2-x}N_x$ and $TiO_{2-x}N_x$. No activity was observed without Pt present. Ethanol and propan-1-ol were also used as sacrificial agents, however methanol produced the highest yield of hydrogen. This was suggested to be because using ethanol and propan-1-ol would require the cleavage of C-C bond, slowing the reaction. Rosseler *et al.*[15] compiled a study on Pt/TiO_2 and Au/TiO_2 using different supports with varying anatase and rutile components. The best catalyst for hydrogen production was Au/TiO_2-P25 and it was suggested that this was because Au can store electrons at the Au-TiO_2 interface (the active site) and that Pt is a better catalyst for the backwards reaction. A study which contradicts this was done by Naldoni *et al.*[16] in 2013 which also compared Au/TiO_2 and Pt/TiO_2 found that Pt/TiO_2 was the better photocatalyst due to Pt having greater electron sink abilities. The levels of other products; H_2CO, CO_2 and CO were recorded as well as H_2. It was found that the ratio of H_2:CO_2 was greater than expected (higher than 3) indicating that the oxidation of methanol was not complete. The ratio of CO_2:CO for Pt/TiO_2 was higher than for Au/TiO_2 which was attributed to the fact that Pt is a better oxidation catalyst.

PtO clusters have been deposited on TiO_2 nanosheets at different weight and size loadings for solar water splitting.[17] It was found that the smaller the cluster, the better the activity

of the catalyst. The best being 0.15 wt% PtO/TiO_2 (nanosheet) producing 86.1 μmol g^{-1} h^{-1} where the nanocluster was 0.2 nm. It was suggested that the smaller the nanocluster, the lower the adsorption energy and the easier the removal of H_2 from the surface of the photocatalyst.

3.1.1.2 Gold

Gold has been used a catalyst for many years, sparking from the observation by Haruta *et al*. in the 1980s that nano-gold is an active catalyst.[18, 19] Using Au/TiO_2 for alcohol reforming for hydrogen production was first explored by Bamwenda *et al*. using ethylene glycol and ethanol as sacrificial agents.[20, 21] It was found that the preparation method of the Au/TiO_2 and Pt/TiO_2 was very important and gave very different activities. Photo-deposition (FP), deposition precipitation (DP), impregnation (IMP) and physical mixing (MIX) methods were employed; the most promising being photo-deposition for Au and Pt photocatalysts (Table 3.1).

Catalyst	Hydrogen production rate/μmol g^{-1} min^{-1} m^{-2}
1.8%Au/TiO_2 (DP)	2.56
1.0%Au/TiO_2 (FD)	7.81
3.0%Au/TiO_2 (MIX)	0.84
1.0%Pt/TiO_2 (DP)	3.70
1.0%Pt/TiO_2 (IMP)	3.53
0.9%Pt/TiO_2 (FD)	8.85

Table 3.1. Au/TiO_2 and Pt/TiO_2 catalysts prepared using different methods and hydrogen production from ethanol reforming.[20]

In 2011 a very interesting paper was published by Murdoch *et al.*[22] Here the effect of using different loadings and different types of TiO_2 was explored for photocatalytic

ethanol reforming. In general Au nanoparticles on anatase are usually smaller as anatase has a higher Fermi level which generates more metal-support electronic interactions, hindering growth. Anatase hydrogen yields were almost 2 orders of magnitude larger than those of the rutile photocatalysts. This was attributed to rutile having much higher charge recombination rates which has been documented in previous literature.[23-25] Another point addressed in this paper was the effect of particle size on the yield of hydrogen. With lower loadings of Au, smaller nanoparticles were seen. TEM was used get an average Au nanoparticle size (Table 3.2).

Catalyst	Average Au nanoparticle size/ nm	Rate of hydrogen production/ mol min^{-1}
1%Au/TiO_2 (anatase)	3	0.4 x 10^{-6}
2%Au/TiO_2 (anatase)	9	0.5 x 10^{-6}
4%Au/TiO_2 (anatase)	13	1.2 x 10^{-6}
8%Au/TiO_2 (anatase)	18	0.6 x 10^{-6}
1%Au/TiO_2 (rutile)	25	0.3 x 10^{-8}
2%Au/TiO_2 (rutile)	25	0.3 x 10^{-8}
4%Au/TiO_2 (rutile)	30	0.4 x 10^{-8}
8%Au/TiO_2 (rutile)	32	1.1 x 10^{-8}

Table 3.2. Au/TiO_2 photocatalysts, Au nanoparticle size and hydrogen production rate

Table 3.2 shows that with higher loadings, the particle size increases and also that the Au nanoparticles on anatase are smaller than on rutile. It has been reported that smaller nanoparticles can shift the Fermi level negatively towards the conduction band which, in theory can increase electron hole lifetimes and therefore the activity of the photocatalyst.[22] 4%Au/TiO_2 (anatase) exhibited the highest rate of hydrogen production. This was attributed to 4%Au/TiO_2 (anatase) having a higher number of active sites (sites

at the perimeter of the Au nanoparticles). At 8% Au loading there was a decrease in the rate of hydrogen production. It was suggested that at this weight loading, there was less TiO_2 exposed which led to a reduction in activity. The paper commented that it was not possible to access whether size had an effect as the catalysts had different loadings. The authors addressed this by normalising the data using XPS to attain the Au/TiO_2 ratio. The normalised data is shown in Table 3.3.

Au loading/ %	XPS Au 4f/Ti 2p	Rate /mol m^{-1} min^{-1}	Normalised rate
1	0.003	4.7×10^{-7}	1.4×10^{-4}
2	0.004	5.1×10^{-7}	1.0×10^{-4}
4	0.008	11.0×10^{-7}	1.4×10^{-4}

Table 3.3. Normalised hydrogen production rates using Au/TiO_2

When the hydrogen production rate values were normalised, the rates were very similar. This indicates that from ~3-13 nm the size of the nanoparticles doesn't have a big effect on the rate of hydrogen production.

It is important to note however, that sub nanoclusters have been shown to enhance photocatalytic activity. In a study by Zhao *et al.*[26] a range of Au clusters and nanoparticles were photo-deposited on CdS using Na_2S as the sacrificial agent. The photocatalyst with 0.95 nm Au clusters deposited on the surface achieved hydrogen production rates of 400 μmol h^{-1} whereas the photocatalyst with 9 nm Au nanoparticles deposited on the surface produced a rate of around 30 μmol h^{-1}.

The first study using Au/TiO_2 for hydrogen production from methanol reforming was done in 2004 by Bowker *et al.*[27] A range of Au loadings were tested producing various amounts of hydrogen and interestingly a dual peak in rates was found at 0.2 and 2 wt%. It was postulated that because Au can take on two different morphologies when deposited on TiO_2,[28] the two peaks seen were a reflection of this. Since then many more studies on

Au/TiO_2 for methanol reforming have been conducted. One example being a study compiled by Oros-Ruiz *et al.*[29] on Au loading on TiO_2 and it was found that the optimum was 0.5 wt% when compared to 0.25 wt% and 1 wt%. The preparation method used was deposition precipitation which could be why it was different to the findings in the paper by Bowker *et al.*[25] where incipient wetness was used. It was concluded that there had to be a compromise between the presence of Au (electron sink) and the amount of TiO_2 exposed to light.

3.1.1.3 Palladium

Palladium on TiO_2 is an effective catalyst for photocatalytic methanol reforming. In 1999 Bowker *et al.* [30] tested a range of loadings of Pd on TiO_2 and different methanol concentrations. Changing the initial methanol concentration had little effect on the hydrogen yield, suggesting that the reaction was close to zero order. Conversely changing the loading of Pd on TiO_2 had an interesting effect. Increasing the loading from 0.001 to 0.5 wt% increased the activity of the catalyst by a factor of 3. However when the loading was increased from 0.5 to 5 wt% almost no activity was observed. The increase in activity was ascribed to an increase in the interface between the metal and the support due to increased presence of palladium. The decrease in activity was attributed to, at higher loadings, the particles overlapping, decreasing the perimeter active area.[31] A mechanism for the reaction was also proposed, detailing methanol decomposition as the first step with PdO being reduced via CO_2 and H_2O production.[32]

Pd has been compared to other metals for photocatalytic alcohol reforming by Yang *et al.*[33] Pd/TiO_2, Pt/TiO_2, Rh/TiO_2 and Pt-Rh/TiO_2 prepared via impregnation were compared for ethanol reforming. Pd/TiO_2 and Pt/TiO_2 were equally effective photocatalysts for the reaction. Rh/TiO_2 was a less active catalyst and interestingly the bimetallic Pt-Rh/TiO_2 catalyst had the lowest activity. Although the photocatalysts were

calcined in air, the XPS suggests that only Rh is in oxide form and Pt and Pd are metallic. It was proposed this observation explains the trend in activity.

3.1.1.4 Other metals

Other metals loaded on TiO_2 have been studied for photocatalytic methanol reforming for hydrogen production. Copper loaded on TiO_2 has given shown to improve photocatalytic activity when compared to TiO_2 alone.[34-36] XPS studies on Cu/TiO_2 suggest before the reaction Cu is present as CuO in Cu^{2+} oxidation state. After reaction the XPS suggests that the CuO is reduced to either Cu_2O or Cu metal (the peaks are difficult to distinguish).[37] Different preparation techniques have been investigated.[38] Chemical reduction using $NaBH_4$ yielded the highest hydrogen yields with Cu being present in the active catalyst as Cu_2O. Wet impregnation and sol gel methods producing CuO were found to show reasonable activity. However photo-deposition method showed low activity and produced Cu metal loaded on TiO_2. The trend in activity of the catalysts was attributed to the oxidation state of the Cu in the active catalyst.

There is a little literature on the activity of Ni/TiO_2 as a photocatalyst for this reaction. Ni/TiO_2 was found to show some activity by Jing *et al*.[39] however this was only when platinum was present as a co-catalyst. Ni/TiO_2- TNT (TiO_2 nano-tubes) was found to show some level of hydrogen production when compared to TiO_2-TNT alone.[40]

Another noble metal that has been studied is silver. A study by Chiarello *et al*.[41] compared Ag/TiO_2 to Au/TiO_2, Pt/TiO_2, Pd/TiO_2 and TiO_2. It was found that Ag/TiO_2 was less effective than the other noble metals tested but had some positive effect when compared to TiO_2.

Table 3.4 summarises the literature discussed in this chapter including the nature of preparation method, oxidation state of the metal on the photocatalyst and the rate of hydrogen production from photocatalytic methanol reforming.

Catalyst	Preparation method	Oxidation state	Rate of hydrogen production/ μmol h^{-1} g^{-1}
0.3%Pt/TiO_2[42]	Dry impregnation	-	440
0.3%Pt/TiO_2[15]	Wet impregnation	Pt(0)	900
0.64%Pt/TiO_2[16]	Deposition precipitation	Pt(0)/Pt(2+)	2200
5%Pt/TiO_2[6]	Physical mixing	Pt(0)	1553
5%Pd/TiO_2[6]	Physical mixing	Pd(0)	733
0.5%Pd/TiO_2[30]	Incipient wetness	Pd(2+)	2000
2%Au/TiO_2[15]	Direct anionic exchange	Au(0)	1320
0.7%Au/TiO_2[16]	Deposition precipitation	Au(0)	1600
2%Au/TiO_2[27]	Incipient wetness	Au(0)	3000
10%RuO_2/TiO_2[6]	Physical mixing	Ru(4+)	123
8%Cu/TiO_2[38]	Sol-gel	Cu(2+)	1500
8%Cu/TiO_2[38]	Chemical reduction with $NaBH_4$	Cu(2+)	2000
8%Cu/TiO_2[38]	Wet impregnation	Cu(2+)	1600
8%Cu/TiO_2[38]	In situ photodeposition	Cu(0)	900
1%Ag/TiO_2[41]	Flame spray pyrolysis	-	117

1%NiO/TiO_2[43]	Wet impregnation	Ni(2+)	30

Table 3.4. Different M/TiO_2 photocatalysts, preparation method, oxidation state and rate of hydrogen production from photocatalytic methanol reforming.

It is clear that there has been a substantial amount of work investigating photocatalytic methanol reforming for hydrogen production using a range of different metals deposited on TiO_2. Pt, Pd and Au look to be promising metals as does Cu when deposited on TiO_2 for use as photocatalysts for photocatalytic methanol reforming. Despite this there are limited publications in the literature which provide direct comparisons of the different TiO_2 supported metals that are prepared and tested in the same manner. As discussed in Chapter 1 there are many experimental variables which can significantly influence the hydrogen production rate. This body of work makes a fair comparison regarding the activity of a series of metals for photocatalytic methanol reforming. In addition to the testing of these catalysts, characterisation techniques such as XPS, TPR and UV-vis of the catalysts was also conducted, in an attempt to establish the properties that govern high performance for photocatalytic hydrogen production.

3.2 Results and Discussion

3.2.1 Different metal/TiO_2 catalysts

A range of metal/TiO_2 photocatalysts were prepared via incipient wetness impregnation at a loading of 0.5 wt%. The TiO_2 used for these photocatalysts was P25 Degussa. Hydrogen production was monitored over time during the photocatalytic methanol reforming reaction. 0.1% v/v methanol solution and 0.2 g catalyst was used for all experimental runs. The activity of the photocatalysts tested is shown below in Figure 3.1.

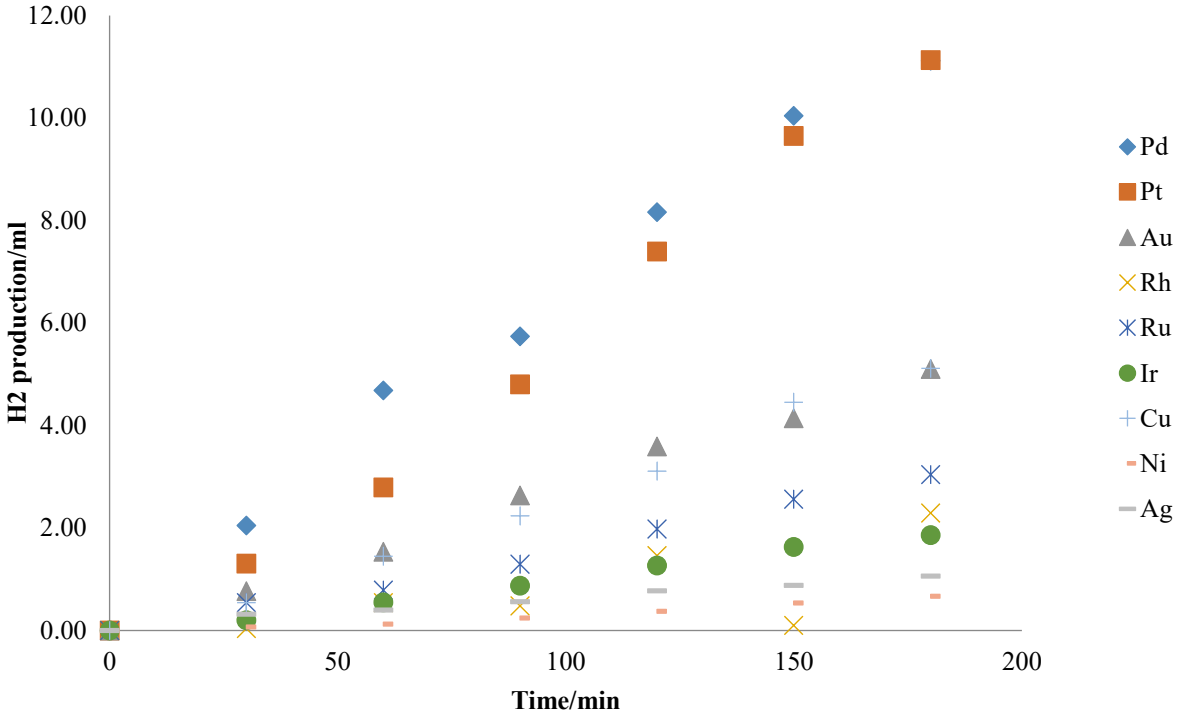

Figure 3.1. Hydrogen produced using different 0.5 wt% metal/TiO_2 catalysts and a 0.1% methanol solution

Figure 3.1 shows that loading TiO_2 with metal nanoparticles produces active catalysts for photocatalytic hydrogen production from methanol reforming as TiO_2 alone produces negligible hydrogen with or without the presence of UV light. Hydrogen is produced at a linear rate signifying a zero order reaction. This indicates that methanol has saturated the catalyst surface. There also appears to be no induction time for 0.5 wt% catalysts.

Different metals exhibited different activities as summarised in Figure 3.2. Pt and Pd were the most active photocatalysts with a rate of hydrogen production of ~ 820 µmol h^{-1} g^{-1}. Although this is lower than the rates reported in other studies for the same metals,[6, 16, 27] it is not a fair comparison because, as mentioned previously, many experimental factors can greatly affect the rate of hydrogen production. Au and Cu followed with rate of ~ 370 µmol h^{-1} g^{-1}. Rh, Ru, Ir and Ag showed low activity and Ni was found to be the least active metal.

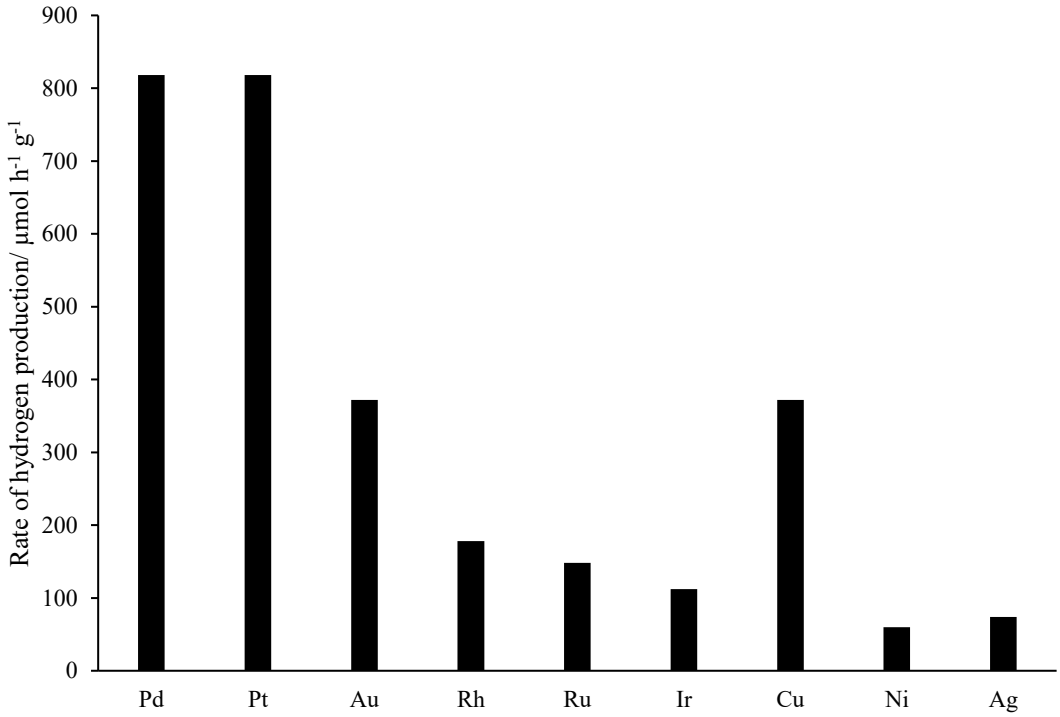

Figure 3.2. Rate of hydrogen production by each metal, per gram photocatalyst

Figure 3.2 compares M/TiO_2 photocatalysts using the same wt% of metal, a better comparison might be per mole metal as shown in Figure 3.3.

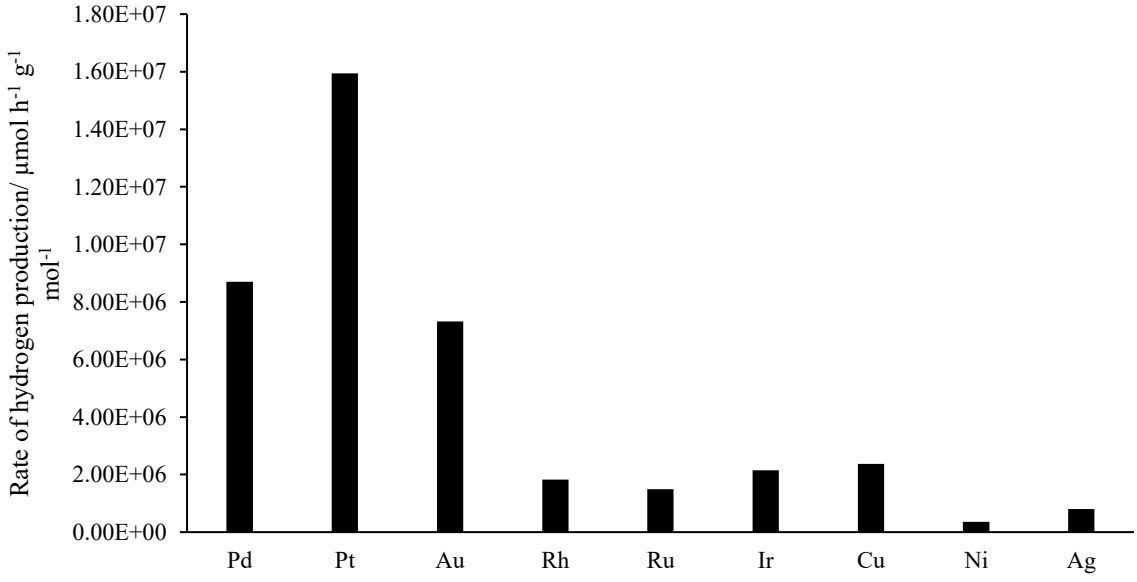

Figure 3.3. Rate of hydrogen production per mole metal

When comparing the metals by mole of metal present, it is clear that Pt is the most active metal, followed by Pd and Au. The relative activity of Cu has fallen however it is a much

cheaper resource compared to Pt, Pd and Au. The current prices of metals and the activity per dollar is shown in Table 3.5.

Metal	Price / USD tOz	Rate of hydrogen production / mL min^{-1}	Rate of hydrogen production per gram metal / mL min^{-1} g^{-1}	Rate of hydrogen production per gram per Dollar / mL min^{-1} g^{-1} USD
Pd	608	0.061	6.11	0.010
Pt	1079	0.061	6.11	0.006
Au	1289	0.028	2.83	0.002
Rh	725	0.011	1.11	0.001
Ru	42	0.017	1.67	0.040
Cu	13.4	0.028	2.83	0.211
Ir	500	0.011	1.10	0.002
Ni	0.263	0.004	0.39	1.475
Ag	17	0.006	0.61	0.036

Table 3.5. Current price of metals (May 2016) and activity

Table 3.5 shows that although Pt is a more active catalyst per mol, Pd is more economical. Interestingly Ni is the most economical metal for this process, followed by Cu. Therefore although they may have lower have activities compared to Pd and Pt, they still are promising metals for the future.

These experiments have further demonstrated the need for metal nanoparticles to be present on the TiO_2 as highlighted from previous literature.[4] The metal nanoparticles act as an electron sink, increasing electron-hole lifetime and therefore the activity of the photocatalyst. The metal also plays an important role in the adsorption and decomposition of methanol. The trend in activity by metal appears to agree with the majority of literature, [20, 33, 41] with Pt being the most active metal followed by Pd and Au. The inactivity of Ag and Ni is not surprising as the literature reported for these metals is in agreement. Higher yields of hydrogen using these metals has only been reported when using of a co-catalyst [39] or with high temperatures.[44]

3.2.2 Loading of metal/TiO_2 catalysts

The weight loading of the photocatalyst has been reported to greatly affect activity. Here the effect of different weight loadings for Pd, Au and Cu has been investigated.

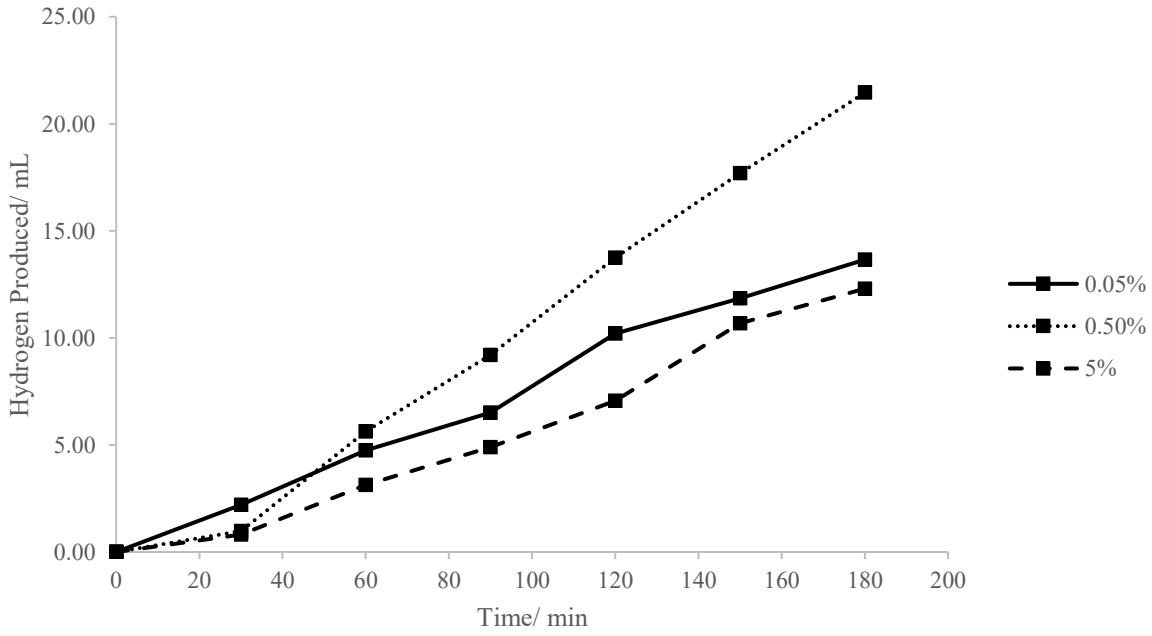

Figure 3.4. Hydrogen production from photocatalytic methanol reforming using different Pd wt% loadings

The weight loading for Pd/TiO_2 was varied from 0.05% to 5% and the catalysts were tested for photocatalytic methanol reforming using a 1% methanol solution as shown in Figure 3.4. 0.5 wt% Pd/TiO_2 gives the highest yield of hydrogen after 3 hours which is in keeping with previous literature.[30] The trend in the activity using different loadings can be explained as follows. The active site for this reaction is the interface between the metal and the TiO_2. As the loading of Pd increases from 0.05% to 0.5%, the perimeter around the nanoparticles (active sites) increases. After 0.5% the activity drops because the nanoparticles are now overlapping, reducing the perimeter and therefore the amount of active sites.[31] An induction time for the higher loadings of Pd (0.5% and 5%) of around 30 min can be seen in this data. The Pd/TiO_2 is calcined in air during its preparation, suggesting that the catalyst before the reaction is PdO/TiO_2. The induction time at higher loadings of Pd suggests that reduction of the PdO to Pd by methanol is necessary for the reaction to proceed.

The same experiment was also carried out for Au/TiO_2 using 0.2, 0.5, 1 and 2 wt% Au/TiO_2. The results are shown below in Figure 3.5.

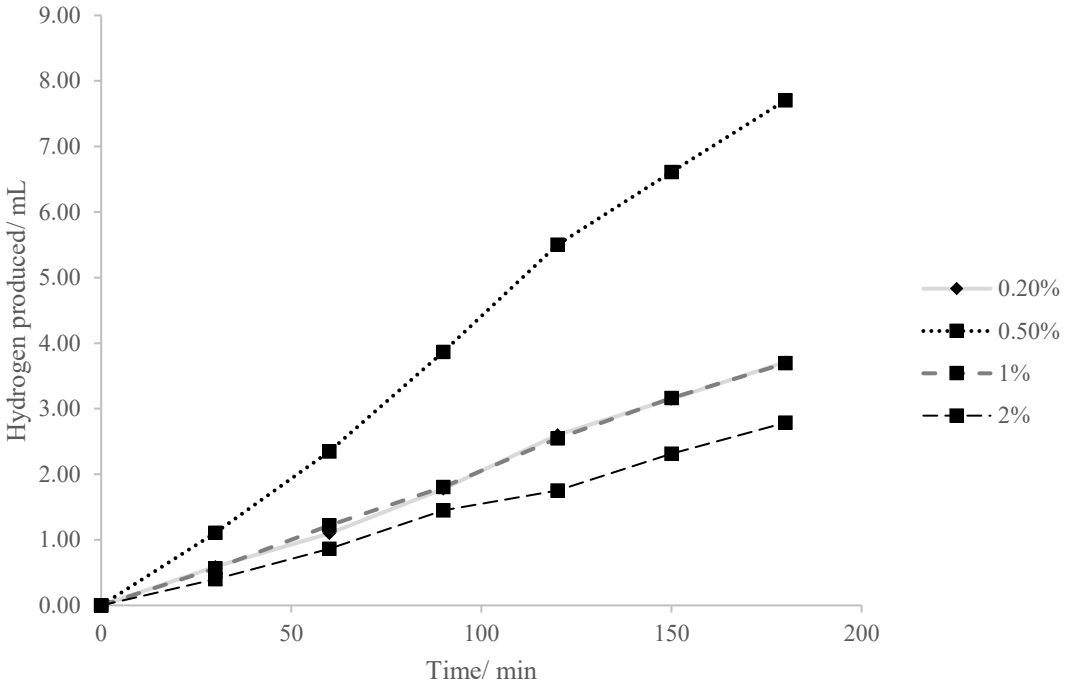

Figure 3.5. Hydrogen production from photocatalytic methanol reforming using different wt% Au/TiO_2

The highest yield for Au was obtained at a wt% loading of 0.5% as seen in Figure 3.5. Contrary to previous work, a "double maximum" at 0.5% and 2% was not observed.[27] However if higher loadings were investigated; a "double maximum" may be seen. No induction time is apparent with Au/TiO_2. It is well known that Au forms metallic gold nanoparticles, even when calcined in air. Therefore reduction is not required when using this catalyst as the active catalyst is already present.

The weight loading of Cu/TiO_2 was investigated using 0.1, 0.5 and 1 wt% using 1% methanol solution. The experiment was carried out for 90 minutes only but at more frequent intervals. The results are shown in Figure 3.6.

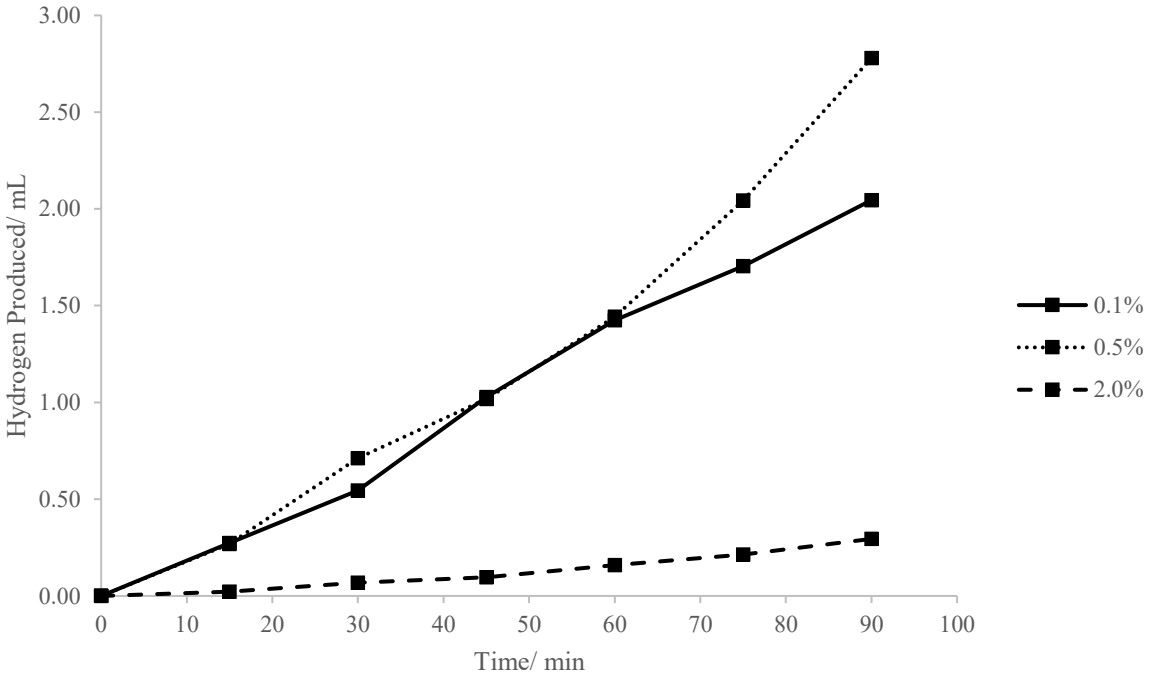

Figure 3.6. Hydrogen production from photocatalytic methanol reforming using different wt% Cu/TiO_2

0.5% Cu/TiO_2 was found to be the most active photocatalyst. However interestingly, 0.1% Cu/TiO_2 also showed high activity. 2% Cu/TiO_2 showed very low activity, however it is likely that Cu has a longer induction time.

3.2.3 XPS

XPS was used to investigate the oxidation state of the active catalyst. The induction time at higher loadings of Pd/TiO_2 suggests that reduction takes place during the reaction to produce the active species (PdO to Pd metal). XPS was carried out before and after the reaction for Pt/TiO_2, Pd/TiO_2, Cu/TiO_2 and Ni/TiO_2.

Analysis of the Ti 2p peaks on the XPS spectra indicates that there is no change in the TiO_2 during the reaction or with the addition of metals (Figure 3.7). Peaks are present at 458 and 464 eV corresponding to Ti $2p_{3/2}$ [45] and Ti $2p_{1/2}$.[46]

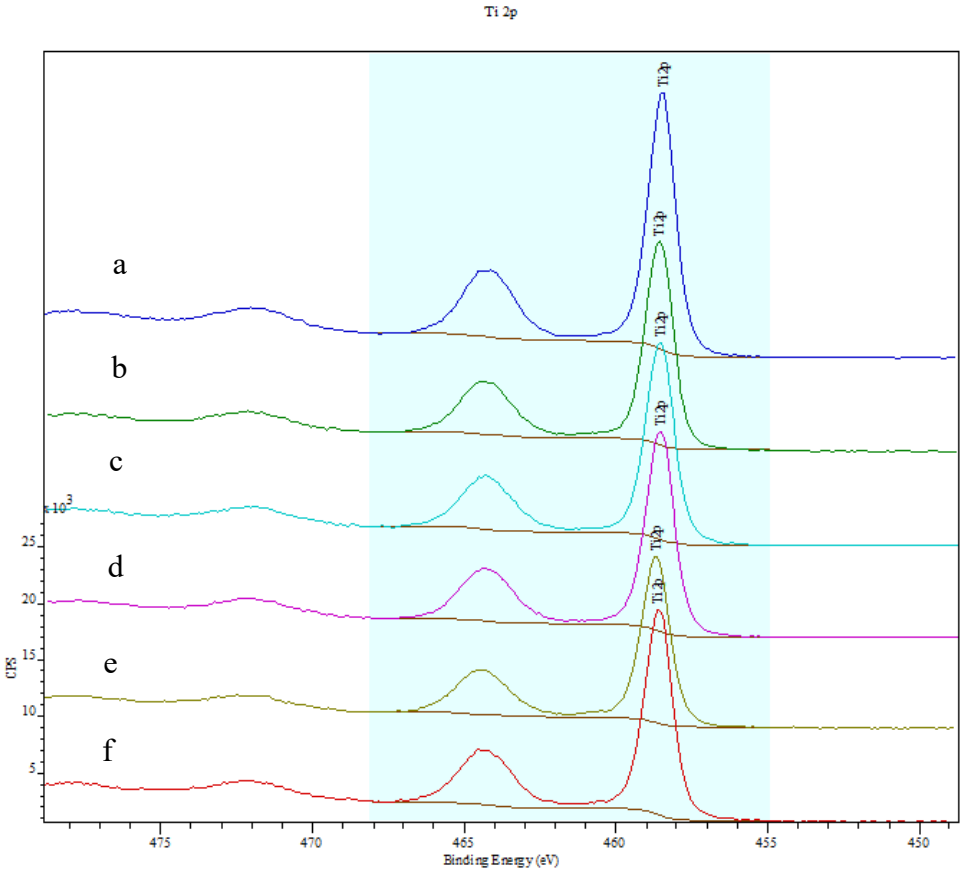

Figure 3.7. XPS of Ti 2p for Pt/TiO_2 before (a) and after (b) reaction, Cu/TiO_2 before (c) and after (d) reaction and Ni/TiO_2 before (e) and after (f) reaction

Looking at the O 1s peaks for the catalysts tell a similar story in that all the oxygen species present are the same in each catalyst, and before and after reaction. Peaks are present at 529 eV corresponding to O^{2-} and at 531 eV corresponding to OH^- (Figure 3.8).

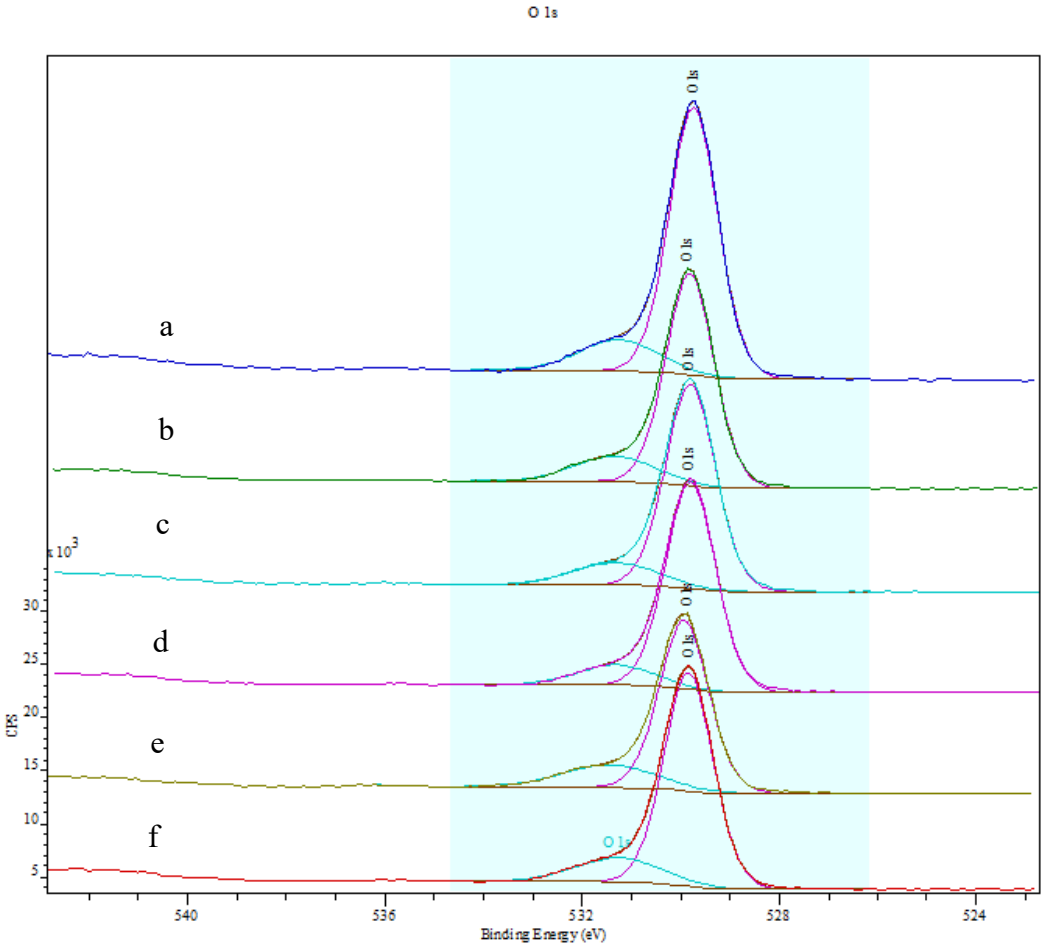

Figure 3.8. XPS for O 1s peaks for Pt/TiO_2 before (a) and after (b) reaction, Cu/TiO_2 before (c) and after (d) reaction and Ni/TiO_2 before (e) and after (f) reaction

The XPS for Pt $4f_{7/2}$ shows two different oxidation states of Pt present in the sample before reaction. The peak 72.08 eV corresponds to Pt^{2+} (PtO) [47] and the peak at 73.92 eV corresponds to Pt^{4+} (PtO_2).[48] The peak areas have a ratio of 7:3 ($PtO:PtO_2$). The peaks are also split with a difference in eV of 3.3. After reaction it appears that the platinum oxide has been reduced somewhat to Pt metal with the presence of a new peak as seen in Figure 3.9 at 70.6 eV.[49] The ratio of area of the peaks present is 30:50:17 ($PtO:PtO_2$:Pt). This data is summarised in Table 3.6

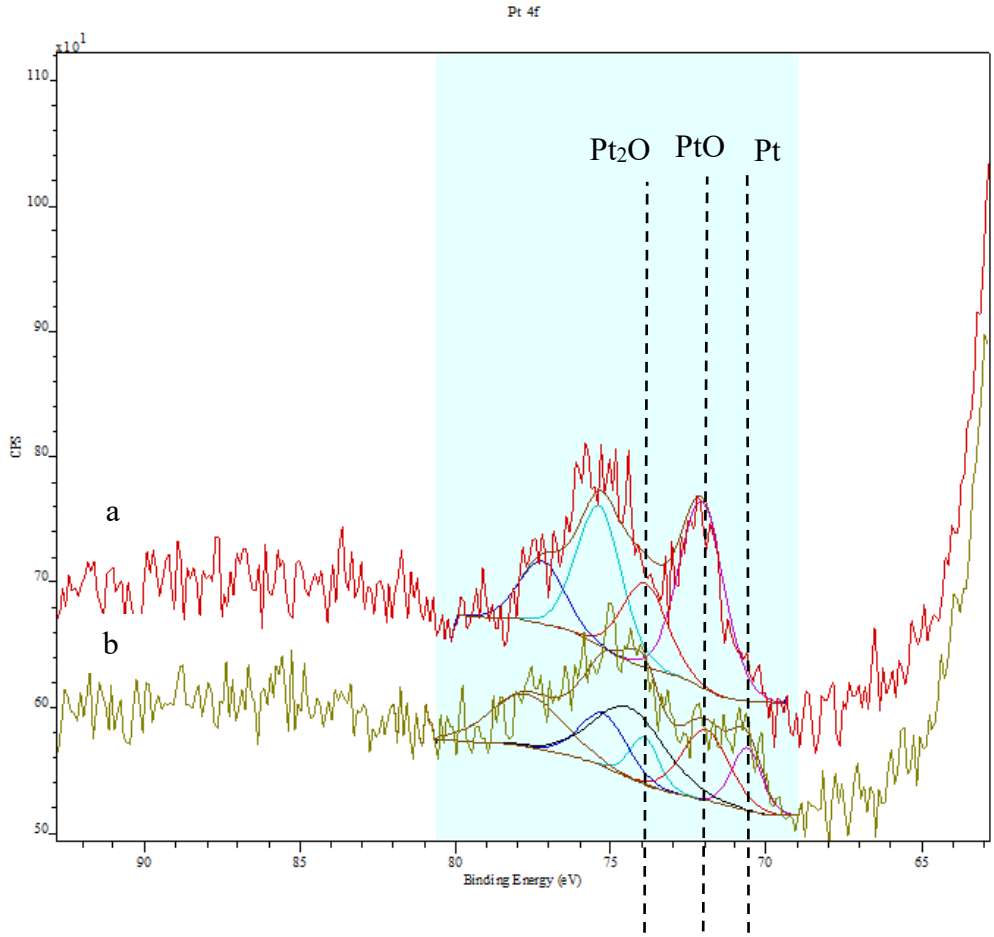

Figure 3.9. XPS of Pt 4f for Pt/TiO_2 before (a) and after (b) reaction

Species	Peak position/ eV	Percentage of species present before reaction	Percentage of species present after reaction
Pt	70.6	0%	17.5%
PtO	72.1	70%	51.5%
Pt_2O	73.9	30%	31%

Table 3.6. Pt species present in $0.5\%Pt/TiO_2$ before and after reaction

The Pd $3d_{5/2}$ XPS shows that before the reaction there is only PdO present on the surface of the catalyst (Figure 3.10). The peak at 336.8 eV corresponds to Pd^{2+} in PdO.[50] The peak is split by 5.4 eV (characteristic of this species). After reaction, there is a new peak at 334.8 eV signifying the presence of Pd metal, [51] indicating that Pd is reduced during the reaction.

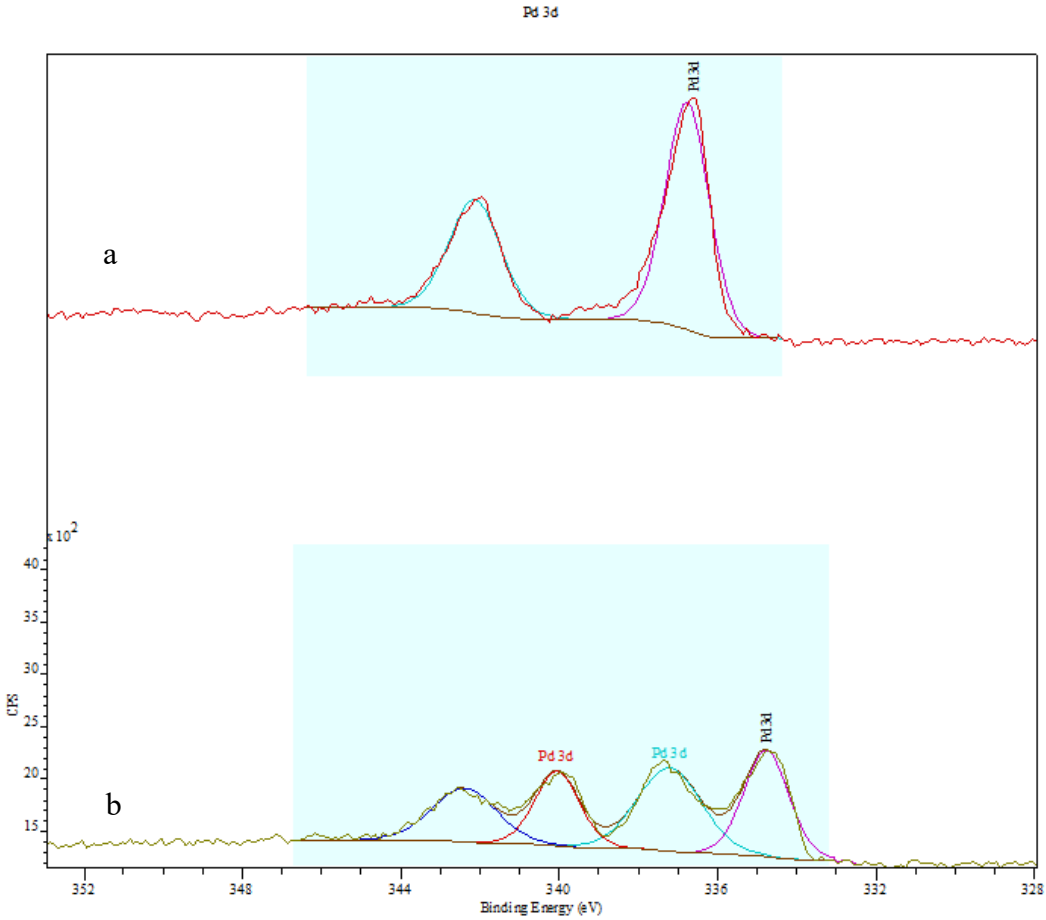

Figure 3.10. XPS of Pd 3d for Pd/TiO_2 before (a) and after (b) reaction

The Cu $2p_{3/2}$ XPS in Figure 3.11 shows peaks at 932.17 and 934.13 eV. The peak at 932.17 eV could correspond to either to Cu metal [52] or Cu^{2+} but it is difficult to distinguish between them. The peak at 934.13 is likely to correspond to Cu^{2+} in Cu(OH). [53] The high binding energy of 934.13 eV indicates that Cu^{2+} is present as $Cu(OH)_2$ but also the presence of the shake up structure at around 342 eV which is characteristic of $Cu(OH)_2$. [54] Although the peak for Cu^{1+} also corresponds to the binding energy ~933 eV, Cu_2O is red in colour and the catalyst was green which makes the presence of Cu_2O improbable. After reaction, the same peaks were present but the peak at ~933 eV increased which could suggest that some of the Cu^{2+} has been reduced to Cu metal.

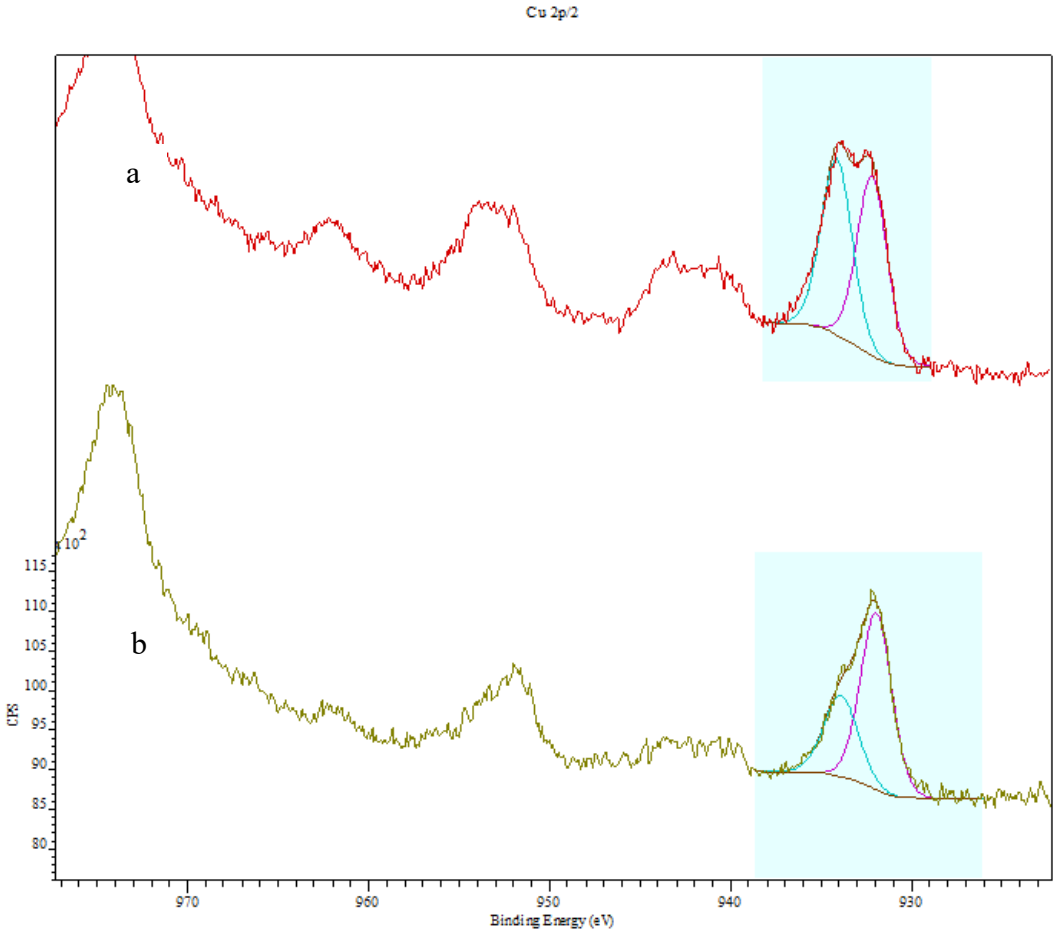

Figure 3.11. XPS of Cu 2p for Cu/TiO_2 before (a) and after (b) reaction

The XPS for Ni $2p_{3/2}$ was the same for both before and after reaction (Figure 3.12). The XPS has a peak at 855 eV which is split, producing another peak at 873 eV. Each of the peaks has satellites at 861 and 879 eV which is characteristic of Ni^{2+}.[55] There is no peak at ~852 eV in either spectrum indicating that there no Ni metal present before or after the reaction. Therefore, this suggests that the Ni^{2+} is not reduced during the reaction.

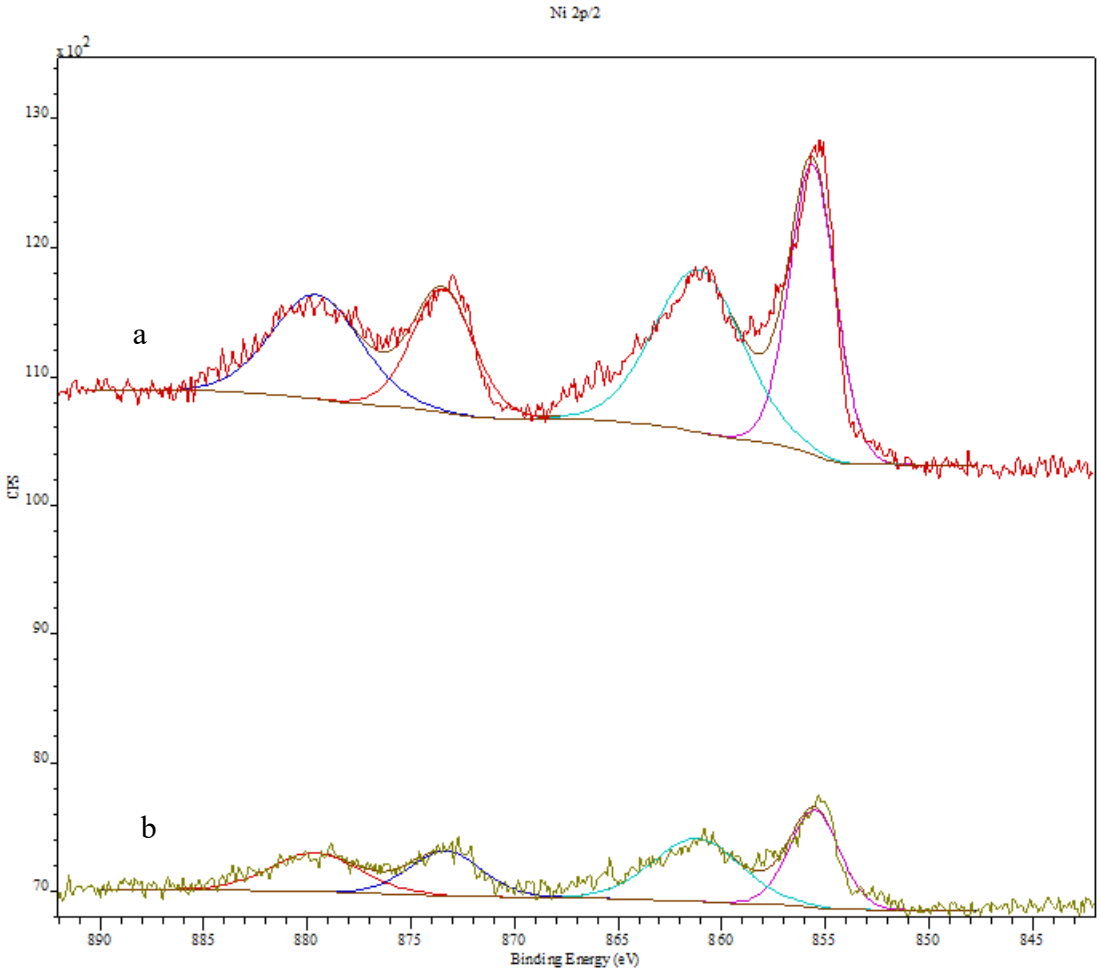

Figure 3.12. XPS of Ni 2p for Ni/TiO_2 before (a) and after (b) reaction

Overall the XPS shows that the catalysts that are active are reduced during reaction. Ni/TiO_2 is nearly inactive for photocatalytic methanol reforming and from the XPS it is clear that there is no change in the Ni species after reaction.

3.2.4 TPR

Temperature programmed reduction (TPR) is a useful technique to probe the temperature at which a species will reduce. The reductant used was hydrogen and the catalysts studied were Pd/TiO_2, Pt/TiO_2, Cu/TiO_2 and Ni/TiO_2. Different ramp rates were also investigated. The TPR of Pd/TiO_2 is shown below in Figure 3.13.

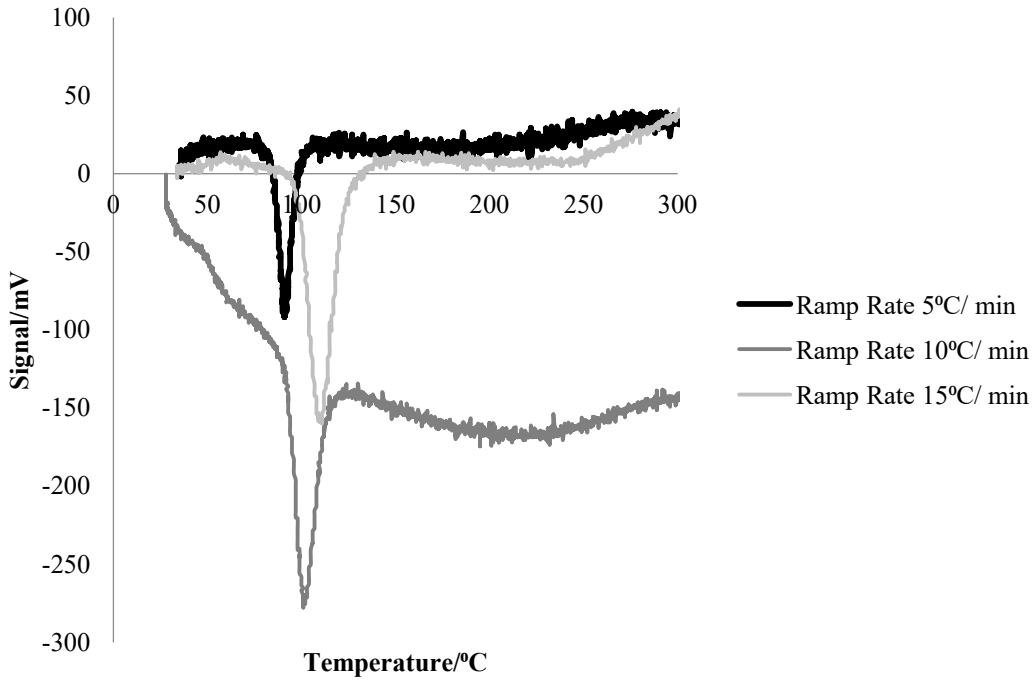

Figure 3.13. TPR plot for Pd/TiO_2 at different ramp rates

Figure 3.13 shows the TPR data for $0.5\%Pd/TiO_2$ giving a negative peak. It is possible that PdO is reduced at a low temperature (<100°C). The Pd metal present then absorbs hydrogen atoms into the lattice.[56] Then at a certain temperature (here ~100°C), all of the hydrogen in the structure is expelled producing a negative peak.

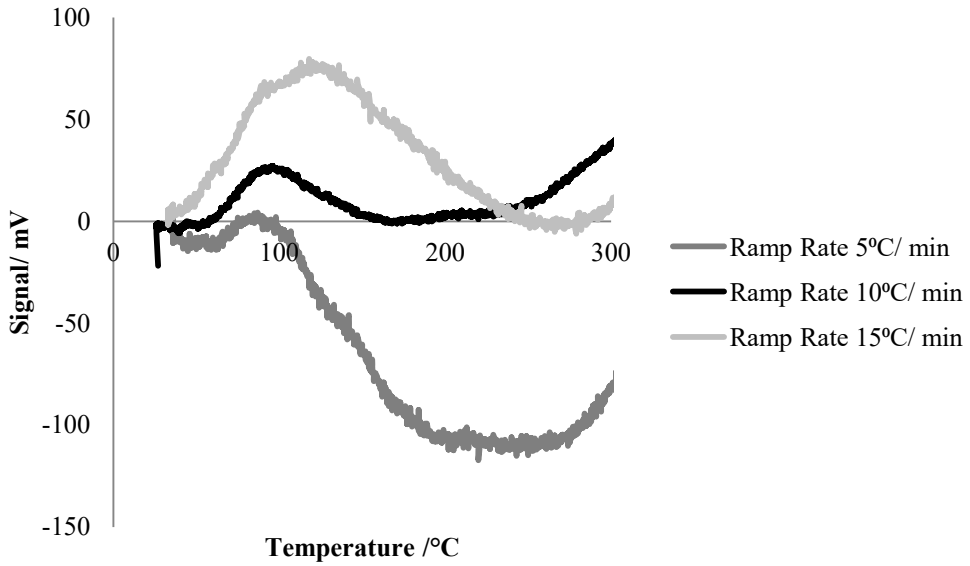

Figure 3.14. TPR plot for 0.5% Pt/TiO_2 at different ramp rates

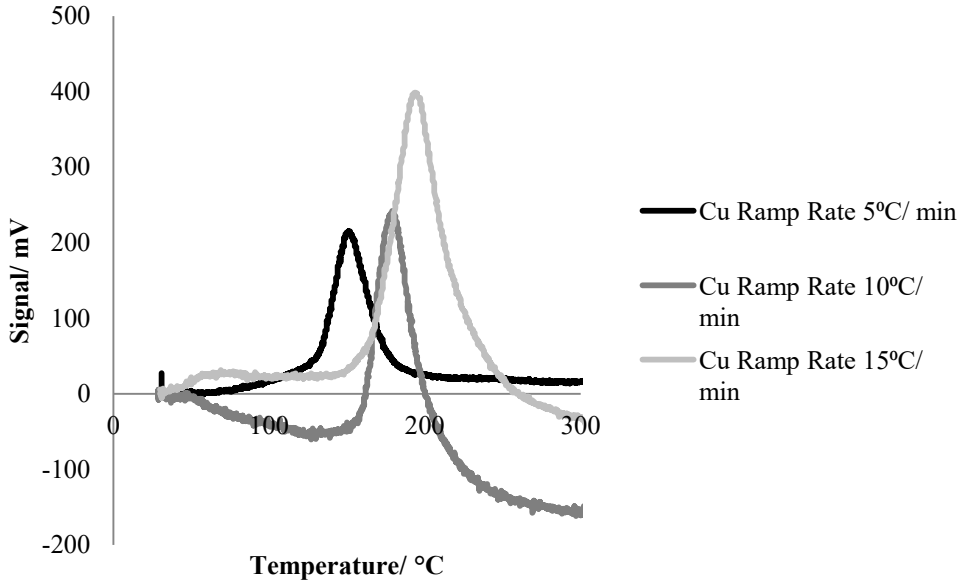

Figure 3.15. TPR plot for 0.5% Cu/TiO_2 at different ramp rates

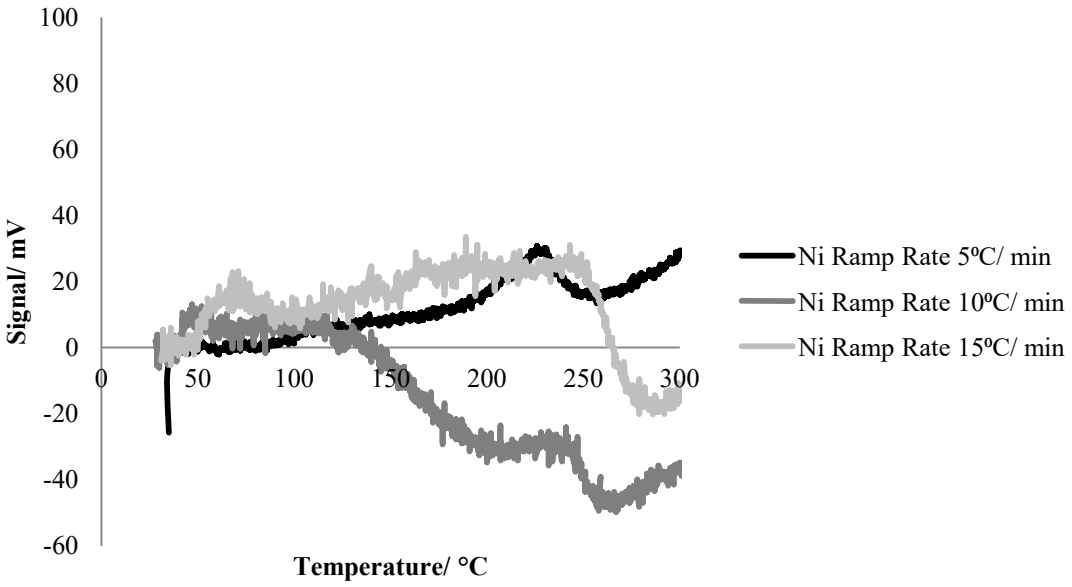

Figure 3.16. TPR plot for 0.5% Ni/TiO_2 at different ramp rates

The TPR plot for 0.5% Pt/TiO_2 shows weak reduction peaks from around 80-120 °C as seen in Figure 3.14. When the ramp rate is increased from 5 °C min^{-1} to 15 °C min^{-1}, the temperature at which reduction takes place shifts higher. Figure 3.15 shows the TPR profile for 0.5% Cu/TiO_2. The reduction of Cu/TiO_2 takes place between 150-200 °C. This is higher than Pt/TiO_2 indicating that the reduction of the Cu species requires more energy than the Pt species. The 0.5% Ni/TiO_2 TPR profile (Figure 3.16) exhibits very weak peaks at around 220-250 °C, making it the least reducible out of the three. The peak maximum temperatures from these data can be used to calculate the activation energy of reduction using a Kissinger plot.[57]

The relationship between the shift in temperature peak maximum (T_{max}) and the ramp rate (β) is given by the Kissinger equation (Equation 3.1). The pre exponential factor and the activation energy can be then be calculated from a plot of $\ln(\beta/T_{max}^2)$ against $1/T_{max}$. The gradient of this plot is equal to $-E_a/R$ and the intercept is gives $\ln(AR/E_a)$.

$$\ln\left(\frac{\beta}{T^2}\right) = \frac{-E_a}{RT} + \ln\left(\frac{AR}{E_a}\right)$$

Equation 3.1. Kissinger Equation

Using the temperature peak maximum and the ramp rate from the TPR, Table 3.7 has been composed.

Catalyst	(β) Ramp rate/ºC min^{-1}	Temperature of Peak Maximum/°C	Temperature of Peak Maximum/K	ln (β/T^2)	1/T
Ni	5	226	499	-10.8	0.0020
Ni	10	235	508	-10.1	0.0019
Ni	15	245	518	-9.79	0.0019
Cu	5	149	422	-10.4	0.0023
Cu	10	180	453	-9.9	0.0022
Cu	15	196	469	-9.5	0.0021
Pt	5	87	360	-10.1	0.0027
Pt	10	111	384	-9.5	0.0026
Pt	15	128	401	-9.2	0.0024

Table 3.7. Data and calculations for Kissinger plot for 0.5%Ni/TiO_2, 0.5%Cu/TiO_2 and 0.5%Pt/TiO_2

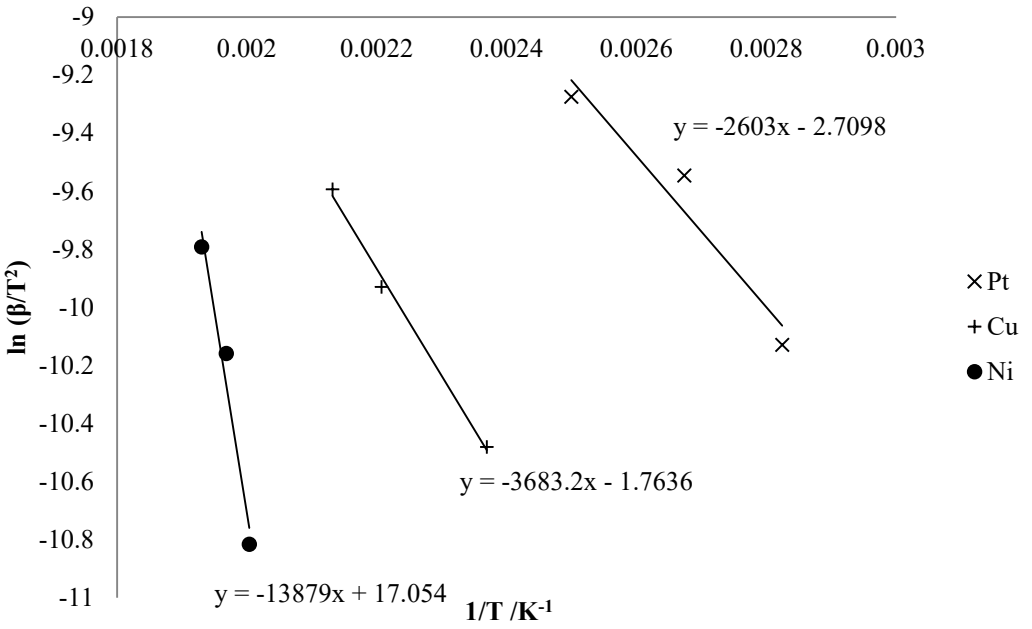

Figure 3.17. Kissinger plot

The Kissinger plot for 0.5%Ni/TiO_2, 0.5%Cu/TiO_2 and 0.5%Pt/TiO_2 is shown above in Figure 3.17. According Equation 3.1, from the slope of the plots, the activation energy of reduction can be calculated (Table 3.8).

Catalyst	Slope	Activation energy kJ mol^{-1}
Ni/TiO_2	-13879	115.39
Cu/TiO_2	-3683	30.62
Pt/TiO_2	-2603	21.64

Table 3.8. Activation energy of reduction calculation

From these calculations the platinum catalyst is the easiest to reduce with a calculated activation energy of 21.64 kJ mol^{-1}. The most difficult is the Ni catalyst with an activation energy of 115.39 kJ mol^{-1}. The XPS has shown that Ni shows no change in oxidation state before and after reaction, with Ni remaining as NiO which agrees with the TPR data.

From the XPS both Pt/TiO_2 and Cu/TiO_2 are reduced somewhat during reaction, which is consistent with this TPR data as both exhibit low activation energies.

3.2.5 Metal Properties

3.2.5.1 Metal Reducibility

The enthalpy of reduction for each metal oxide during the reaction was estimated using Equation 3.2 according to Equation 3.3. The reactants being the metal oxide present on the catalyst at the beginning of the reaction and methanol. The products being the metal, carbon dioxide and hydrogen. An example of this reaction is shown in Equation 3.3.

Equation 3.2. Calculation for enthalpy of reduction

$$MO_x + xCH_3OH \rightarrow M + xCO_2 + 2xH_2$$

E.g. $PdO + CH_3OH \rightarrow Pd + CO_2 + 2H_2$

Equation 3.3. Generalised mechanism for photocatalytic methanol reforming

Most of the metals are present in oxidised form before the reaction with the exception of Au which is present in metallic state. The metals, their estimated enthalpy of reduction and activity are summarised below in Figure 3.18.

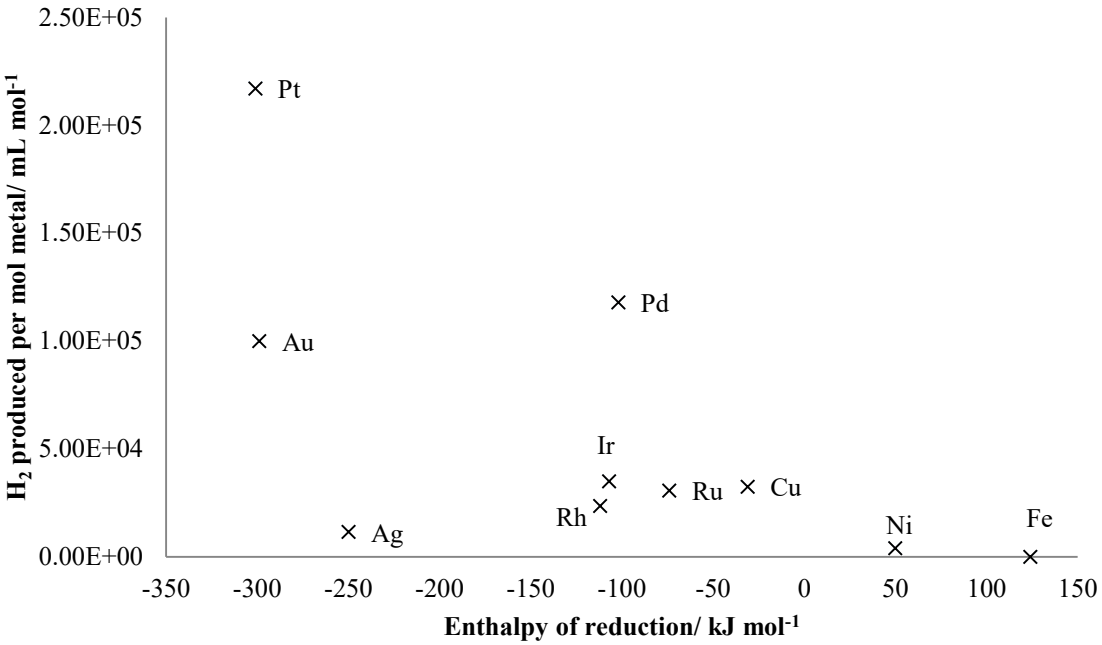

Figure 3.18. Enthalpy of reduction for each metal oxide compared to activity towards photocatalytic methanol reforming

Figure 3.18 shows that metals with positive enthalpies of reduction *i.e.* Ni, have poor activity for photocatalytic methanol reforming. Generally speaking, the metals with more negative enthalpies of reduction *e.g.* Pt and Pd, exhibit higher activity. This suggests that the reduction of the metal oxide prior to reaction is an activation barrier to the reaction continuing on to water splitting. From these calculations, the enthalpy of reduction of Ag is -250 kJ mol^{-1}. This should mean that silver is an active catalyst for photocatalytic methanol reforming however it's activity is much lower than other metals with similar enthalpies of reduction.

3.2.5.2 Work Function

A paper published by Chiarello *et al.* speculated that the work function, Φ, of the metal could be related to the activity of the catalyst.[41] The greater the difference in work function between the TiO_2 and the metal, the more electron transfer, producing a more

active photocatalyst. Ag has a low work function of 4.74 eV, only just higher than TiO_2 (4.6-4.7 eV), [58] which could explain why it is inactive even though it is readily reducible.

The work functions of the metals are tabulated below in Table 3.9.[59]

Metal	Work Function Φ/ eV
Pd	5.6
Pt	5.93
Au	5.47
Cu	5.10
Ru	4.71
Rh	4.98
Ir	5.00
Ni	5.04
Ag	4.26

Table 3.9. Metal and work function in eV

The work function of the metal and the activity of the catalysts by metal have been plotted below in Figure 3.19.

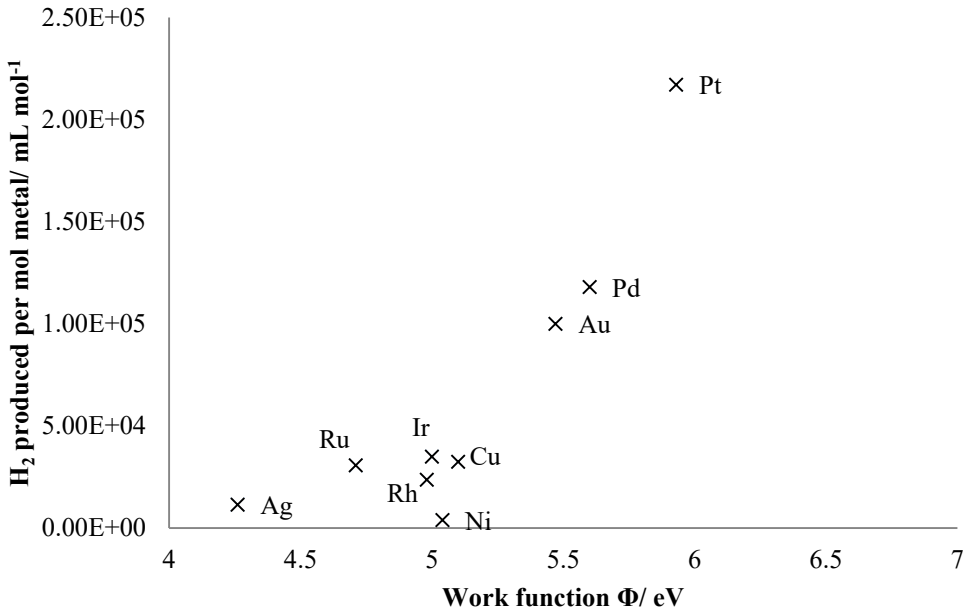

Figure 3.19. Work Function of metal against hydrogen production per mole metal

Figure 3.19 shows a good relationship between the work function of the metal and hydrogen production. Platinum has a high work function of 5.93 eV and has the best activity and Ru has a low work function of 4.71 eV and is a fairly inactive catalyst. On the other hand, Ni has a work function of 5.04 eV which is only 0.06 eV less than Cu, however Cu is an active catalyst for photocatalytic hydrogen production whereas Ni is not. This suggests that to obtain a highly active catalyst for photocatalytic methanol reforming, the metal needs have a high work function compared to TiO_2 and the ability to be reduced easily. The adsorption of metals on TiO_2 create a Schottky junction which increases charge separation.[60] The higher the difference in work function between the metal and TiO_2, the longer the charge separation time and therefore the better the photocatalyst.

3.2.5.3 Band gap

It is reported that metal nanoparticles can alter the band gap of TiO_2 and increase absorption into the visible region.[61, 62] UV-vis diffuse reflectance spectroscopy has been

used to probe whether the change in band gap has a relationship with the catalyst activity towards photocatalytic methanol reforming. The spectra are shown below in Figure 3.20.

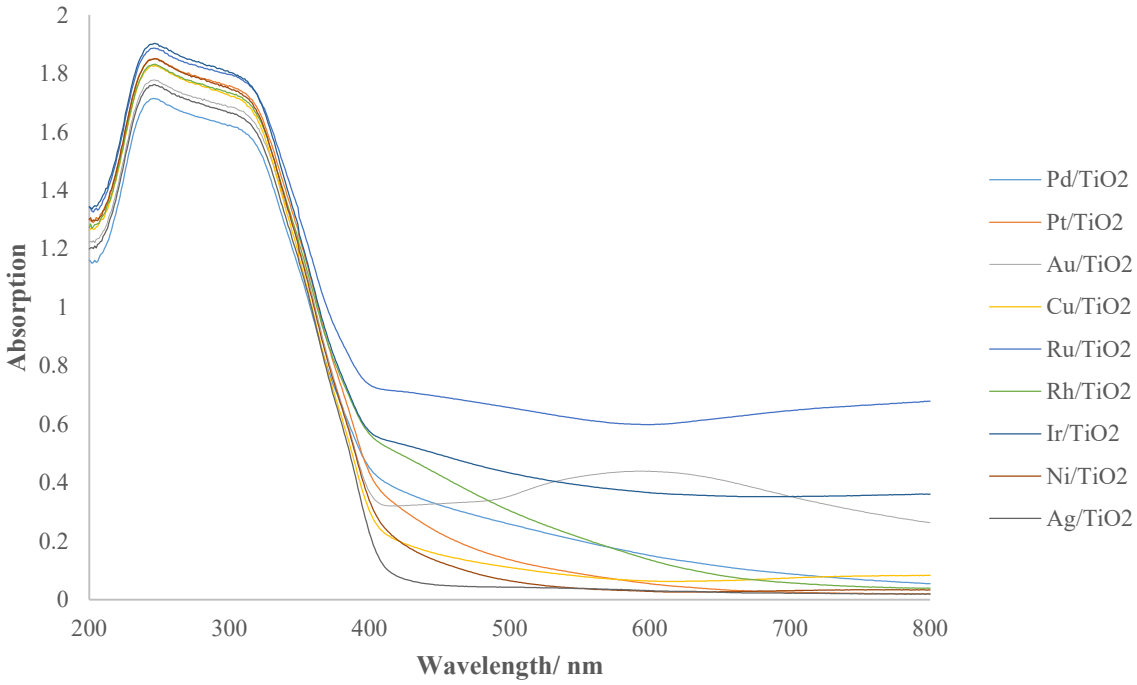

Figure 3.20. UV-vis spectroscopy of metal loaded TiO_2 catalysts

The absorption edge of TiO_2 alone is around 400 nm. As seen in Figure 3.20 the absorption edge with metal loaded TiO_2 increases to above 400 nm. An example of how this was calculated by extrapolation is shown in Figure 3.21 for 0.5%Au/TiO_2 and shows it be ~425 nm.

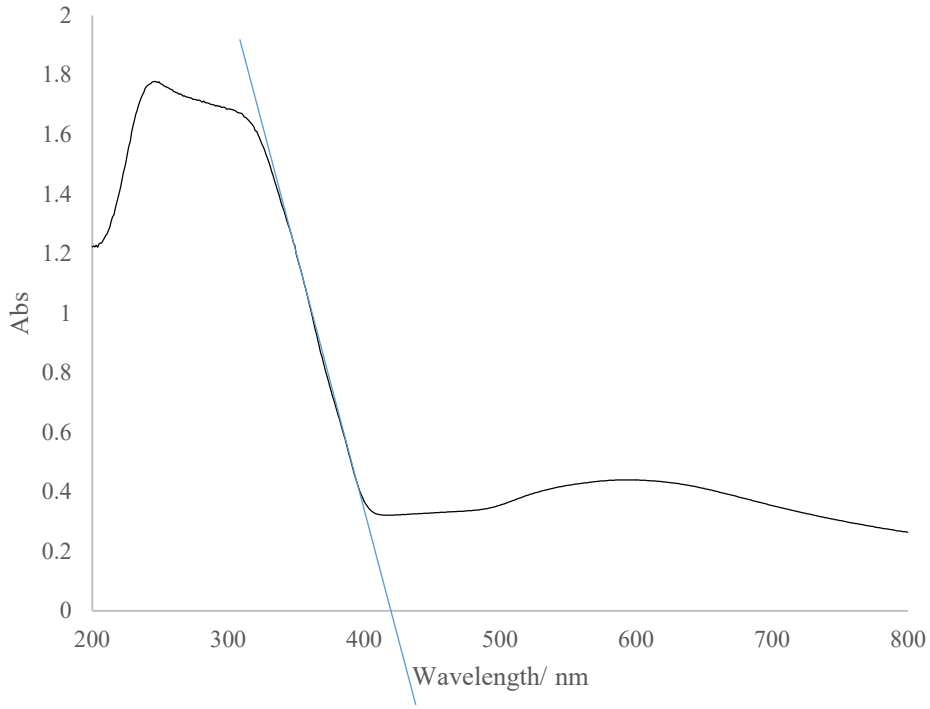

Figure 3.21. Example showing the absorption edge for 0.5%Au/TiO_2 found by extrapolation (blue line)

The direct band gap of the metal loaded photocatalysts can be calculated using a Tauc plot (Figure 3.22).[63] The equation used to construct the plot is shown below in Equation 3.4.[64]

α = absorption coefficient = absorbance

k= parameter related to the effective masses associated with the valence and conduction bands

n = ½ for direct band gap

E_g = band gap

Equation 3.4. Tauc plot equation

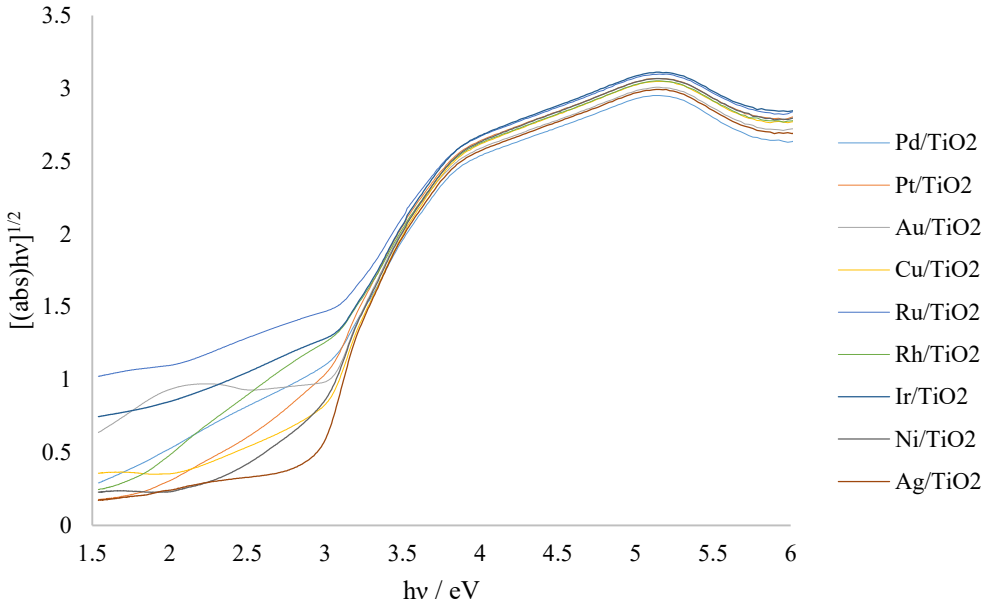

Figure 3.22. Tauc Plot for metal loaded TiO_2 catalysts

The Tauc plot shown in Figure 3.22 indicates that the band gap for Au/TiO_2 is 2.74 eV. This is considerably lower than TiO_2-P25 (3.2 eV) and suggests that Au/TiO_2 will absorb light of longer wavelengths *i.e.* in the visible region. Au shows a strong absorption around 600 nm due to the surface plasmon resonance phenomena. [65] The band gaps calculated using Tauc plots are summarised in Table 3.10.

Catalyst	Band gap/ eV
Pd/TiO_2	2.65
Pt/TiO_2	2.71
Au/TiO_2	2.74
Cu/TiO_2	2.71
Rh/TiO_2	2.68

Ru/TiO_2	2.62
Ir/TiO_2	2.68
Ni/TiO_2	2.68
Ag/TiO_2	2.74

Table 3.10. Metal loaded TiO_2 and their corresponding band gap according to Tauc plot

The Tauc band gaps for the photocatalysts were plotted against hydrogen production in Figure 3.23.

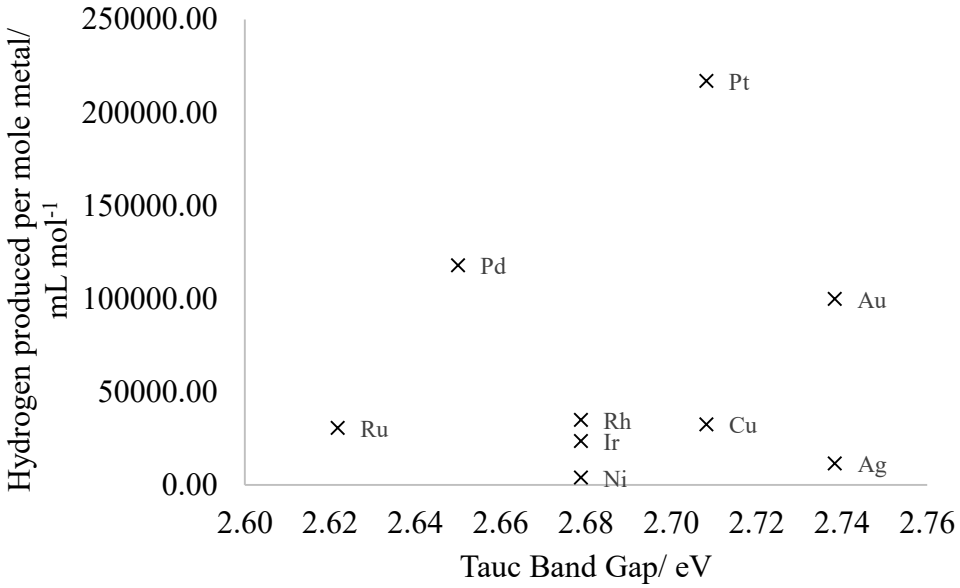

Figure 3.23. Tauc Band gap against hydrogen production per mole metal

Figure 3.23 shows that there no correlation between the band gap of the metal loaded TiO_2 and the activity of the catalyst. However the UV-visble diffuse reflectance spectroscopy has shown that loading TiO_2 with metal can increase absorption into the visible region.

3.3 Conclusion

The work in this chapter has focused on metal loaded TiO_2 for photocatalytic methanol reforming for hydrogen production. Different metals were loaded on TiO_2 and tested for their activity towards photocatalytic methanol reforming. The best catalyst was found to be Pt/TiO_2 followed by Pd/TiO_2 and Au/TiO_2. Ag/TiO_2 and Ni/TiO_2 were found to be nearly inactive catalysts for this process. An induction time was observed for high loadings of Pd/TiO_2 suggesting that before the reaction could proceed, the metal oxide has to be reduced. XPS analysis confirmed this for Pt/TiO_2, Pd/TiO_2 and Cu/TiO_2. Ni/TiO_2 was present as NiO before and after reaction. The enthalpy of reduction was calculated for each metal and plotted against activity. In general easily reduced metal oxide produced better catalysts whereas metal oxides with higher enthalpies of reduction were found to be less active. Another factor influencing activity was work function. Largely the greater the difference in work function between the metal and TiO_2, the better the catalyst. This was attributed to better electron transfer and longer charge separation time. UV-vis spectroscopy confirmed that loading metal nanoparticles onto TiO_2 can extend the band gap of TiO_2 into the visible region. However the band gap change for different metals had no relation to the catalyst activity. In conclusion, there are two factors that influence the activity of the M/TiO_2 catalyst. The first is the difference in work function between the metal and TiO_2. The second is the ease of reducibility of the metal oxide. The best catalyst for this reaction was Pt/TiO_2 because it has a high work function and platinum oxide is easily reduced to Pt.

3.4 References

1. J. Zhang, Q. Xu, Z. Feng, M. Li and C. Li, *Angewandte Chemie-International Edition*, 2008, 47, 1766.

2. Y. K. Kho, A. Iwase, W. Y. Teoh, L. Maedler, A. Kudo and R. Amal, *Journal of Physical Chemistry C*, 2010, 114, 2821.

3. L. Bonneviot and G. L. Haller, *Journal of Catalysis*, 1988, 113, 96.

4. F. Chojnowski, P. Clechet, J. R. Martin, J. M. Herrmann and P. Pichat, *Chemical Physics Letters*, 1981, 84, 555.

5. J. Tang, J. R. Durrant and D. R. Klug, *Journal of the American Chemical Society*, 2008, 130.

6. T. Kawai and T. Sakata, *Journal of the Chemical Society-Chemical Communications*, 1980.

7. M. Kawai, S. Naito, K. Tamaru and T. Kawai, *Chemical Physics Letters*, 1983, 98, 377.

8. F. Guzman, S. S. C. Chuang and C. Yang, *Industrial & Engineering Chemistry Research*, 2013, 52, 61.

9. A. Fujishima and K. Honda, *Nature*, 1972, 238, 37.

10. T. Kawai and T. Sakata, *Journal of the Chemical Society-Chemical Communications*, 1979, 1047.

11. K. Domen, S. Naito, T. Onishi and K. Tamaru, *Chemistry Letters*, 1982, 555.

12. S. Naito, *Journal of the Chemical Society-Chemical Communications*, 1985.

13. A. Galinska and J. Walendziewski, *Energy & Fuels*, 2005, 19, 1143.

14. W.-C. Lin, W.-D. Yang, I. L. Huang, T.-S. Wu and Z.-J. Chung, *Energy & Fuels*, 2009, 23, 2192.

15. O. Rosseler, M. V. Shankar, M. K.-L. Du, L. Schmidlin, N. Keller and V. Keller, *Journal of Catalysis*, 2010, 269, 179.

16. A. Naldoni, M. D'Arienzo, M. Altomare, M. Marelli, R. Scotti, F. Morazzoni, E. Selli and V. Dal Santo, *Applied Catalysis B-Environmental*, 2013, 130, 239.

17. Y. H. Li, *Chemistry – A European Journal*, 2014, 20, 12377.

18. M. Haruta, N. Yamada, T. Kobayashi and S. Iijima, *Journal of Catalysis*, 1989, 115, 301.

19. M. Haruta, T. Kobayashi, H. Sano and N. Yamada, *Chemistry Letters*, 1987, 405.

20. G. R. Bamwenda, S. Tsubota, T. Nakamura and M. Haruta, *Journal of Photochemistry and Photobiology a-Chemistry*, 1995, 89.

21. G. R. Bamwenda, S. Tsubota, T. Kobayashi and M. Haruta, *Journal of Photochemistry and Photobiology a-Chemistry*, 1994, 77.

22. M. Murdoch, G. I. N. Waterhouse, M. A. Nadeem, J. B. Metson, M. A. Keane, R. F. Howe, J. Llorca and H. Idriss, *Nature Chemistry*, 2011, 3, 489.

23. R. Katoh, M. Murai and A. Furube, *Chemical Physics Letters*, 2008, 461, 238.

24. K. M. Schindler and M. Kunst, *Journal of Physical Chemistry*, 1990, 94, 8222.

25. A. Yamakata, T.-a. Ishibashi and H. Onishi, *Chemical Physics*, 2007, 339, 133.

26. P. Shen, S. Zhao, D. Su, Y. Li and A. Orlov, *Applied Catalysis B: Environmental*, 2012, 126, 153.

27. M. Bowker, L. Millard, J. Greaves, D. James and J. Soares, *Gold Bulletin*, 2004, 37.

28. L. Zhang, R. Persaud and T. E. Madey, *Physical Review B*, 1997, 56, 10549.

29. S. Oros-Ruiz, R. Zanella, R. Lopez, A. Hernandez-Gordillo and R. Gomez, *Journal of Hazardous Materials*, 2013, 263, 2.

30. A. Dickinson, D. James, N. Perkins, T. Cassidy and M. Bowker, *Journal of Molecular Catalysis a-Chemical*, 1999, 146.

31. M. Bowker, D. James, P. Stone, R. Bennett, N. Perkins, L. Millard, J. Greaves and A. Dickinson, *Journal of Catalysis*, 2003, 217.

32. N. Aas, T. J. Pringle and M. Bowker, *Journal of the Chemical Society-Faraday Transactions*, 1994, 90, 1015.

33. Y. Z. Yang, C. H. Chang and H. Idriss, *Applied Catalysis B-Environmental*, 2006, 67, 217.

34. A. Sobczynski, *Monatshefte Fur Chemie*, 1991, 122, 645.

35. N. L. Wu and M. S. Lee, *International Journal of Hydrogen Energy*, 2004, 29, 1601.

36. P. Gomathisankar, T. Noda, H. Katsumata, T. Suzuki and S. Kaneco, *Frontiers of Chemical Science and Engineering*, 2014, 8, 197.

37. H.-J. Choi and M. Kang, *International Journal of Hydrogen Energy*, 2007, 32, 3841.

38. S. Xu, J. Ng, X. Zhang, H. Bai and D. D. Sun, *International Journal of Hydrogen Energy*, 2010, 35, 5254.

39. D. W. Jing, Y. J. Zhang and L. J. Guo, *Chemical Physics Letters*, 2005, 415, 74.

40. J. S. Jang, S. H. Choi, D. H. Kim, J. W. Jang, K. S. Lee and J. S. Lee, *Journal of Physical Chemistry C*, 2009, 113, 8990.

41. G. L. Chiarello, M. H. Aguirre and E. Selli, *Journal of Catalysis*, 2010, 273.

42. A. Galinska and J. Walendziewski, *Energy & Fuels*, 2005, 19, 1143.

43. A. Kudo, K. Domen, K. Maruya and T. Onishi, *Chemical Physics Letters*, 1987, 133, 517.

44. M.-S. Park and M. Kang, *Materials Letters*, 2008, 62, 183.

45. F. Lange, H. Schmelz and H. Knozinger, *Journal of Electron Spectroscopy and Related Phenomena*, 1991, 57, 307.

46. S. O. Saied, J. L. Sullivan, T. Choudhury and C. G. Pearce, *Vacuum*, 1988, 38, 917.

47. G. M. Bancroft, I. Adams, L. L. Coatsworth, C. D. Bennewitz, J. D. Brown and W. D. Westwood, *Analytical Chemistry*, 1975, 47, 586.

48. J. E. Drawdy, G. B. Hoflund, S. D. Gardner, E. Yngvadottir and D. R. Schryer, *Surface and Interface Analysis*, 1990, 16, 369.

49. J. Thiele, N. T. Barrett, R. Belkhou, C. Guillot and H. Koundi, *Journal of Physics-Condensed Matter*, 1994, 6, 5025.

50. A. Tressaud, S. Khairoun, H. Touhara and N. Watanabe, *Zeitschrift Fur Anorganische Und Allgemeine Chemie*, 1986, 541, 291.

51. R. Nyholm and N. Martensson, *Journal of Physics C-Solid State Physics*, 1980, 13, L279.

52. S. W. Gaarenstroom and N. Winograd, *Journal of Chemical Physics*, 1977, 67, 3500.

53. G. Deroubaix and P. Marcus, *Surface and Interface Analysis*, 1992, 18, 39.

54. M. C. Biesinger, L. W. M. Lau, A. R. Gerson and R. S. C. Smart, *Applied Surface Science*, 2010, 257, 887.

55. G. Ertl, R. Hierl, H. Knozinger, N. Thiele and H. P. Urbach, *Applied Surface Science*, 1980, 5, 49.

56. T. Graham, *Philosophical Transactions Royal Society*, 1866, 156, 399.

57. H. E. Kissinger, *Analytical Chemistry*, 1957, 29, 1702.

58. C. Young, T. M. Lim, K. Chiang, J. Scott and R. Amal, *Applied Catalysis B-Environmental*, 2008, 78, 1.

59. *CRC Handbook of Chemistry and Physics*, 87th edn., 2008.

60. M. Jakob, H. Levanon and P. V. Kamat, *Nano Letters*, 2003, 3, 353.

61. Y. Hu, X. Song, S. Jiang and C. Wei, *Chemical Engineering Journal*, 2015, 274, 102.

62. J. Fang, S.-W. Cao, Z. Wang, M. M. Shahjamali, S. C. J. Loo, J. Barber and C. Xue, *International Journal of Hydrogen Energy*, 2012, 37, 17853.

63. B. Karvaly and I. Hevesi, *Zeitschrift Fur Naturforschung Part a-Astrophysik Physik Und Physikalische Chemie*, 1971, A 26, 245.

64. D. Zhang, G. Li, F. Wang and J. C. Yu, *Crystengcomm*, 2010, 12, 1759.

65. S. Zhu, S. Liang, Q. Gu, L. Xie, J. Wang, Z. Ding and P. Liu, *Applied Catalysis B-Environmental*, 2012, 119, 146.

Chapter 4

4.1 Introduction

The use of fossil fuels since the industrial revolution has increased the levels of CO_2 in the atmosphere from 280 to 400 ppm.[1] CO_2 is a greenhouse gas and so with increasing CO_2 levels, the temperature of the Earth will increase leading to global warming. Fossil fuels are a finite source of energy and will eventually run out. Alternative, greener energy resources are being developed. One of these is hydrogen from water spitting using sacrificial agents. Methanol is said to be "the next chemical vector" after petrol as it is compatible with the existing petroleum infrastructure.[2] Other oxygen containing compounds have been used for photocatalytic hydrogen production including ethanol,[3] n-butanol,[4] glycerol,[5, 6] and sugars such as glucose.[7]

4.1.1 Methanol

Using methanol as a sacrificial agent for photocatalytic methanol reforming was first achieved in 1980 by Kawai and Sakata where hydrogen was efficiently produced using metal loaded titania.[8] This work was continued using IR spectroscopy to study the mechanism of photocatalytic methanol reforming by Naito *et al.* in 1983.[9] The proposed mechanism is shown below in reaction (4.1) and (4.2). It was concluded that the presence of CO_2 indicated that water was split.

$$CH_3OH \rightarrow CH_3O_{(ads)} + H_{(ads)} \qquad (4.1)$$

$$CH_3O_{(ads)} + H_2O \rightarrow CO_{2\,(g)} + 5/2\ H_{2\,(g)} \qquad (4.2)$$

More recently, Bowker *et al.* proposed a full mechanism for photocatalytic methanol reforming on Pd/TiO_2.[10] Different concentrations of methanol were used to establish how this affected the reaction rates. It was found that after ~20 µl of methanol, the increase in the rate of reaction slowed. At around 20 µl it was suggested that a full monolayer of methanol was adsorbed on the surface and the order of reaction after this point was near

zero. This was attributed to saturation type kinetics (Langmiur Hinselwood model). [11, 12] The mechanism suggested is depicted below in Figure 4.1.

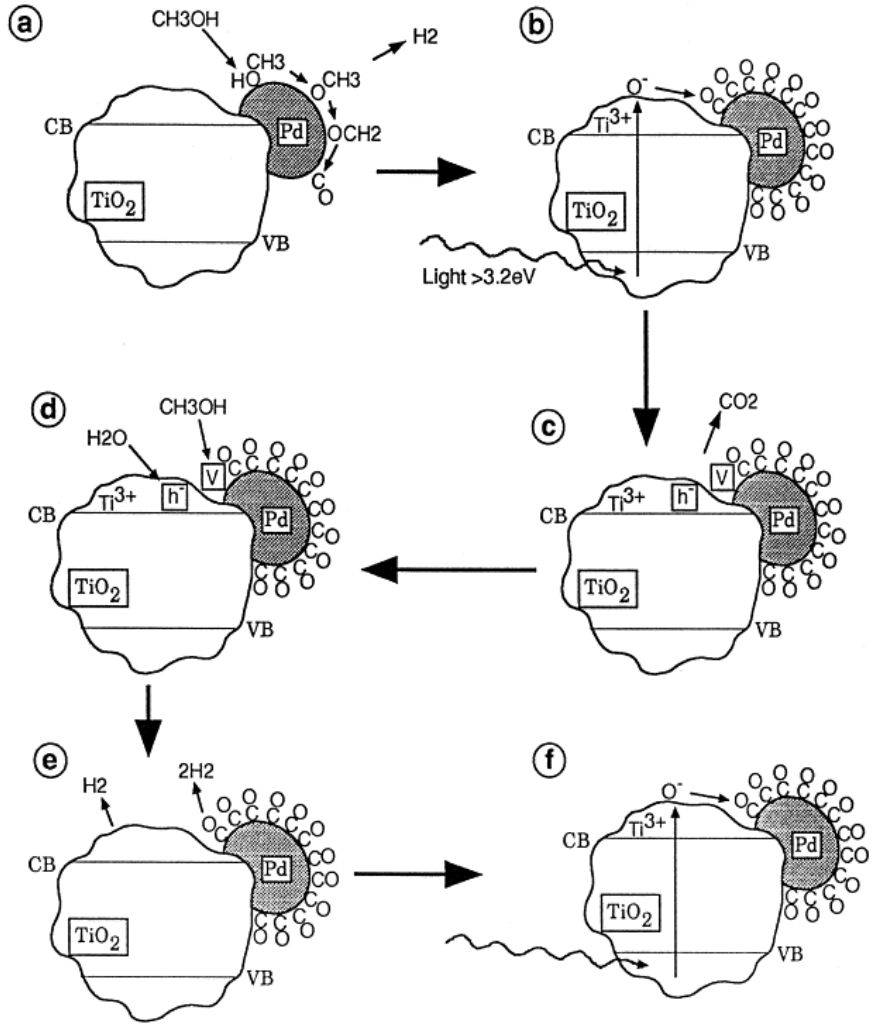

Figure 4.1. Mechanism for photocatalytic methanol reforming.[10]

The first step (a) involves methanol adsorption and decomposition on Pd. This occurs without light leading to saturation and poisoning of Pd with CO. In (b) light excites electrons to produce a highly active oxidising species (O^-). CO_2 is produced by this reaction leaving vacant metal site and anion vacancy (h^+) in the oxide in (c). Step (d/e) involves methanol adsorption to metal site and water filling the hole (h^+), releasing 3 mole hydrogen. Finally the catalyst is regenerated in step (f). The oxidising species was suggested to be OH^-, OH• or O•.[13] No intermediates were reported. In a recent study by

Nomikos *et al.* it was suggested that formic acid and formaldehyde stay adsorbed to the photocatalyst until full decomposition and oxidation to CO_2.[14]

Methanol is known to adsorb to metal oxides via the methoxy species.[15] Methanol readily produces formaldehyde under UV illumination.[16, 17] Decomposition to formaldehyde has been investigated by FTIR spectroscopy and the proposed mechanism is shown below in reactions (4.3), (4.4) and (4.5).[18]

$$CH_3OH \rightarrow CH_3O^-{}_{(ads)} + H^+ \quad (4.3)$$

$$CH_3O^-{}_{(ads)} + H^+ \rightarrow CH_3O\bullet{}_{(ads)} \quad (4.4)$$

$$CH_3O\bullet{}_{(ads)} + h^+ \rightarrow CH_2O_{(ads)} + H^+ \quad (4.5)$$

It was suggested that the formaldehyde species does not desorb but undergoes further oxidation using surface oxygen ion ($O_{(s)}$) to form dioxymethylene, reaction (4.6).

$$CH_2O_{(ads)} + O_{(s)} \rightarrow H_2CO_{2\,(ads)} + H^+ \quad (4.6)$$

Dioxymethylene can then further consume photogenerated holes to produce formic acid and release photons. Finally the surface formic acid can be decarbonylated via the photo-Kolbe reaction,[7, 19, 20] resulting in CO_2 and H_2 as shown in reaction (4.7).

$$H_2CO_{2\,(ads)} + h^+ \rightarrow HCOO_{(ads)} + H^+ \rightarrow CO_2 + H_2 \quad (4.7)$$

Intermediates have been reported for steam photo-reforming of methanol and the photo oxidation of methanol. Formaldehyde, formic acid and CO were detected for steam photo reforming.[21] Formaldehyde and formic were reported for photo-oxidation.[22]

4.1.2 Alcohols

Many alcohols have been used as sacrificial agents for photocatalytic hydrogen production with varying degrees of hydrogen yields.[4, 23] Primary and secondary alcohols

produce similar results whereas negligible hydrogen yields are found for tertiary alcohols. Some rules were established to predict whether an alcohol will produce hydrogen.[4]

1. Hydrogen atom alpha to hydroxyl group must be present
2. Alkyl groups attached to alcohols yield corresponding alkanes
3. Methylene groups between alcohols are fully oxidised to CO_2
4. "Competing" methyls will further oxidise producing more H_2

These rules mean that the stoichiometry of a reaction can be predicted. An example of propane diol is shown below in reaction (4.8) and (4.9).

1,2-propane diol

$$C_3H_8O_2 + 2H_2O \rightarrow CH_4 + 2CO_2 + 4H_2 \qquad (4.8)$$

1,3-propane diol

$$C_3H_8O_2 + 4H_2O \rightarrow 3CO_2 + 8H_2 \qquad (4.9)$$

Some examples of alcohols and the products detected by mass spectroscopy are shown below in Table 4.1.[24]

Alcohol	Products
methanol	H_2, CO_2
ethanol	H_2, CO_2, CH_4
1-propanol	H_2, CO_2, C_2H_6
2-propanol	H_2, CO_2, CH_4
1-butanol	H_2, CO_2, C_3H_8
2-butanol	H_2, CO_2, C_2H_6

Table 4.1. Alcohols used as sacrificial agents for photocatalytic alcohol reforming and the products observed

4.1.3 Polyols

The use of polyols as sacrificial agents has been reported in literature.[25, 26] It was reported that the more OH groups in a molecule the higher the reforming efficiency obtained.[6] Glycerol, propylene glycol and 2-propanol were tested for photo reforming. The ratio of hydrogen production after 12 hours was 3:1.96:0.86 ≈ 3:2:1 showing a high correlation between the number of OH groups and hydrogen production. Scavenging efficiency was found to be better in polyols with more OH groups.[27] An equation for ideal polyol reforming was proposed reaction (4.10).

$$C_3H_{8-x}(OH)_x + (6-x)H_2O \rightarrow (10-x)H_2 + 3CO_2 \qquad (4.10)$$

The proposed equation was found for glycerol but not for propylene glycol and propan-2-ol. This led to the conclusion that only hydrogen atoms bonded to hydroxyl carbon will be evolved as H_2.

4.1.4 Sugars

Sugars are considered to be renewable resources of energy.[28, 29] Sugars also contain a high number of OH groups. Kondarides *et al.* tested a range of alcohols and sugars including glucose and proposed that the stoichiometry of the reaction can be predicted using the following reaction (4.11).[30]

$$C_xH_yO_z + (2x-z)H_2O \rightarrow xCO_2 + (2x-z+-)H_2 \qquad (4.11)$$

It was reported that all alcohols and sugars tested followed the stoichiometry. An interesting point made in the paper was the heat content of hydrogen produced compared to the heat content of biomass used. The heat content of glycerol (ΔH_c = 1660 kJ mol^{-1}) was calculated to be about 20% lower than the heat content of the hydrogen produced (7 x ΔH_c = 258.8 kJ mol^{-1} = 2000 kJ mol^{-1}).

Some literature has reported that the hydrogen production rate decreased with higher molecular weights of sugars *i.e.* starch < sucrose < glucose.[7] The higher rate of glucose was attributed to quicker diffusion in solution.

This chapter focuses on using different oxygenates with varying numbers of OH groups, particularly polyols as sacrificial agents for photocatalytic hydrogen production. The stoichiometric relationship between hydrogen and carbon dioxide produced has been probed in liquid phase and gas phase reactions in order to obtain further evidence of the mechanism previously proposed. Hydrogen production has been investigated using polyols, cyclohexanols, sugars and carboxylic acids in an attempt to gain higher hydrogen yields. The relationship between the number of oxygen containing groups and hydrogen yield has been explored and a formula for predicting hydrogen production has been proposed.

4.2 Results and Discussion

4.2.1 Hydrogen and Carbon dioxide stoichiometry

The proposed overall reaction scheme for methanol reforming is shown in reaction (4.12).[31] The stoichiometric relationship between hydrogen and carbon dioxide is 3 moles H_2 to 1 mole of CO_2.

$$CH_3OH + H_2O \rightarrow 3H_2 + CO_2 \qquad (4.12)$$

The yield of hydrogen and carbon dioxide was monitored over time to establish whether the reaction followed the stoichiometry (Figure 4.2). Both H_2 and CO_2 are produced simultaneously at a steady rate. The presence of CO_2 suggests that water has been split and is further evidence of the mechanism proposed by Bowker *et al.* [10] After 3 hours of reaction, 10.7 mL of H_2 has been evolved but only 1.27 mL CO_2. The H_2:CO_2 ratio here is higher than the expected 3:1. High H_2:CO_2 ratios have been reported in the literature

and it was suggested that it was due to incomplete oxidation of CO_2 with CO being detected.[32] During this experiment, however, no CO was detected suggesting that either CO is still adsorbed to the palladium surface or complete oxidation occurred only producing CO_2. The high H_2:CO_2 ratio could be attributed to CO_2 being dissolved in the reaction solution. This is discussed later in the chapter.

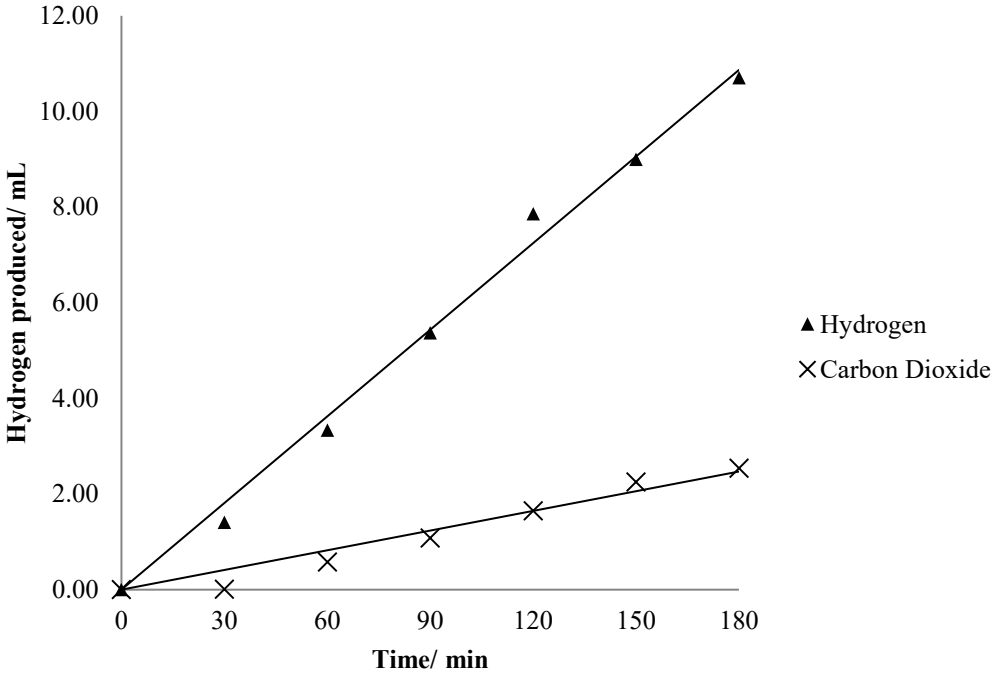

Figure 4.2. H_2 and CO_2 production over time for photocatalytic methanol reforming using 0.5%Pd/TiO_2 in the liquid phase (100 mL water)

The experiment was repeated in the gas phase to probe whether this would have an effect on the H_2:CO_2 ratio. Figure 4.3 shows hydrogen, carbon dioxide and carbon monoxide production over time using 10 mL water. Again H_2 (20.72 mL) and CO_2 (2.3 mL) are produced at a steady rate however CO (2.29 mL) was also observed.

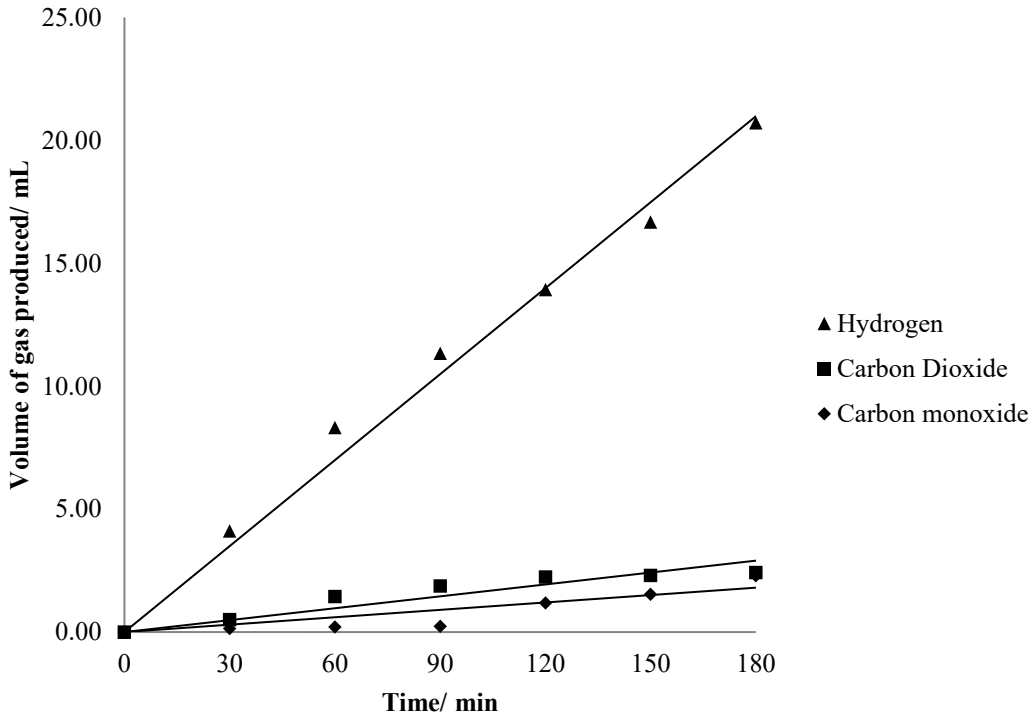

Figure 4.3. H_2 and CO_2 production over time for photocatalytic methanol reforming using 0.5%Pd/TiO_2 in the gas phase (10 mL water)

There is a higher rate of hydrogen production in the gas phase compared to the liquid phase with 20.72 mL of hydrogen produced in the gas phase and 10.7 mL in the liquid phase within 3 hours. It is possible that there is a higher ratio of methanol to water in gas phase reactions. Raoult's law allows the approximation of vapour pressure of water and methanol to be calculated at a particular temperature. Equation 4.1 shows how the vapour pressure of water and methanol can be calculated where P_i = vapour pressure, P_i^* = vapour pressure of pure component and x_i = mole fraction.

Equation 4.1. Raoult's law for calculation of vapour pressures

The approximate temperature of reaction is 40°C. At this temperature the vapour pressure of pure methanol is 229.1 mm Hg [33] and the vapour pressure of pure water is 55.3 mm

Hg.[34] Using equation 1 the vapour pressure during the gas phase reaction was calculated to be 1.02 mm Hg for methanol and 54.75 mm Hg for water. This gives a ratio of methanol to water of 1:53. In the liquid phase the molar ratio of methanol to water is 1:2227. This suggests that in the gas phase there would be less competition between methanol and water for the active sites on Pd, leading to a higher rate of methanol decomposition and therefore a higher rate of hydrogen production.

The presence of CO in the gas phase reaction and not in the liquid phase reaction is interesting. Adsorbed CO is an intermediate during photocatalytic methanol reforming according to the proposed mechanism. It is possible that desorption of CO happens more readily in the gas phase compared to the liquid phase. Another possibility is that the CO_2 produced during the reaction is reacting with the vacancies in the TiO_2 lattice. During photocatalytic methanol reforming, CO is oxidised by an excited O^- species. This leaves a vacancy in the lattice which is filled with water. It could be suggested that CO_2 fills the vacancy and is reduced to CO. As mentioned earlier, the ratio of methanol to water is higher in the gas phase which suggests that there would be less competition with water for the vacancy, which is why this might occur in the gas phase and not in the liquid phase.

In the gas phase reaction using 10 ml water 20.72 mL of H_2, 2.42 mL CO_2 and 0.96 mL CO were produced in 3 hours. This is a H_2:CO_2 ratio of 8.35:1. Incorporating CO into the ratio (H_2:C) calculation gives 5.64:1 which is closer to the expected 3:1 ratio. The volume of water used during photocatalytic methanol reforming was reduced to 1 mL which gave a H_2:CO_2 ratio of 5.4:1 and H_2:C ratio of 3.8:1 (Figure 4.4). Therefore this suggests that with less water present, a better stoichiometric relationship is achieved. The optimum stoichiometric relationship is 3 moles of hydrogen to one mole of carbon dioxide. This would be significant evidence to support the proposed mechanism.

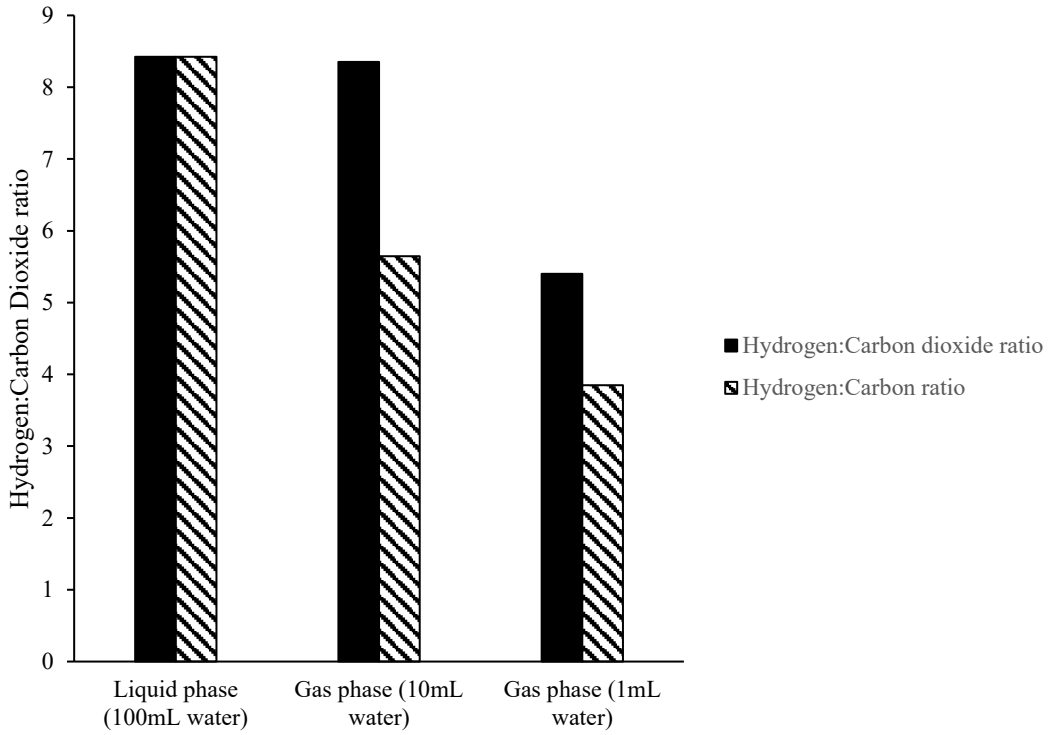

Figure 4.4. Ratio of Hydrogen:Carbon dioxide and Hydrogen:Carbon for photocatalytic methanol reforming in liquid phase and gas phase

The pH of the water was recorded before and after reaction and it was noted that the pH decreased. CO_2 dissolves in water and can react with water to produce carbonic acid reaction (4.13).

$$CO_2 + H_2O \quad H_2CO_3 \qquad (4.13)$$

The observed decrease in pH suggested that the CO_2 produced during the reaction could be dissolved in the reaction solution. To establish whether this was happening the reaction solution (gas phase, 10 mL water) was heated after the reaction and the level of CO_2 was measured (Figure 4.5).

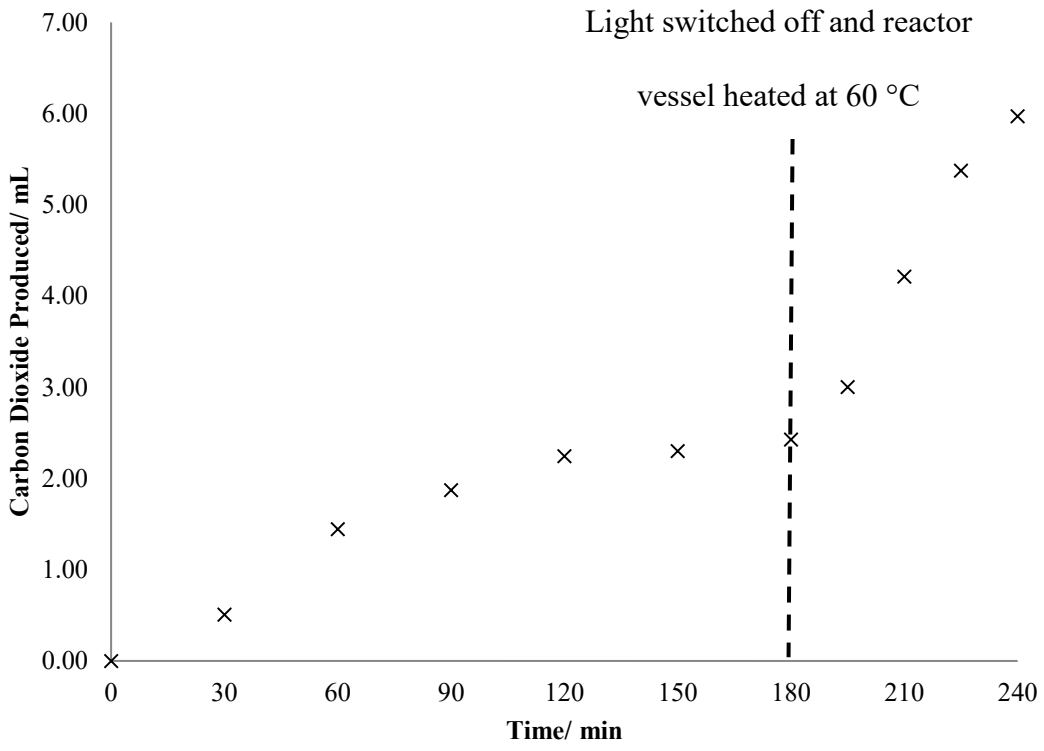

Figure 4.5. CO_2 level throughout photocatalytic methanol reforming and after reaction during heating at 60 °C (light switched off and heating began at 180 min)

Figure 4.5 shows that heating the reaction solution after the reaction evolves CO_2. This is evidence that the CO_2 produced during the reaction was dissolving in the reaction solution. After heating at 60 °C for 1 hour, the level of CO_2 had risen to 5.96 mL. The ratio of H_2:CO_2 after heating was found to be 3.47:1. Therefore this has demonstrated that hydrogen and carbon dioxide are produced in a ~3:1 ratio which is strong evidence of the proposed mechanism.

4.2.2 Carbon Monoxide

It has been reported that methanol decomposes on Pd to form adsorbed CO at ambient temperatures.[36] The proposed mechanism for photocatalytic methanol reforming suggests that it is adsorbed CO that is oxidised by the active oxygen species (O^-) to produce a vacancy in TiO_2, allowing water to be split. Therefore, it is possible to use CO as the

sacrificial agent, also known as the water gas shift reaction. [37] So CO was employed as the hole scavenger to examine hydrogen evolution further.

4.2.2.1 Concentration

The volume of CO was varied and the rate of hydrogen production was recorded to establish at what point saturation of the catalyst actives sites occurs (Figure 4.6).

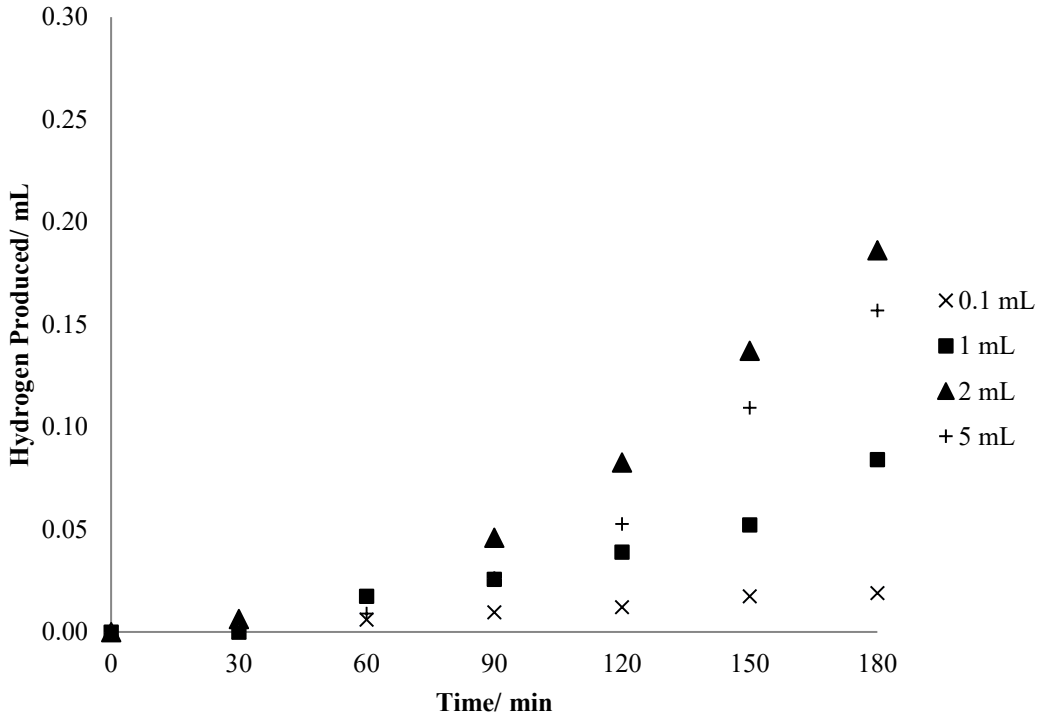

Figure 4.6. Hydrogen production using CO and 0.5%Pd/TiO_2

Figure 4.6 shows that hydrogen production increases with the amount of CO until 2 mL. Using 5 mL CO gives a slight reduction in hydrogen production. The trend is similar to work by Bowker *et al.* which also used varying amounts of CO but here the most hydrogen was produced using 1 mL of CO.[37]

4.2.2.2 Phase

The reaction using CO as a sacrificial agent was carried out in both the gas and liquid phases to establish whether the same trend is seen as for methanol, where higher hydrogen

yields were found for the gas phase reaction. The hydrogen produced from CO (2mL) is shown below for the liquid phase and gas phase reactions (Figure 4.7).

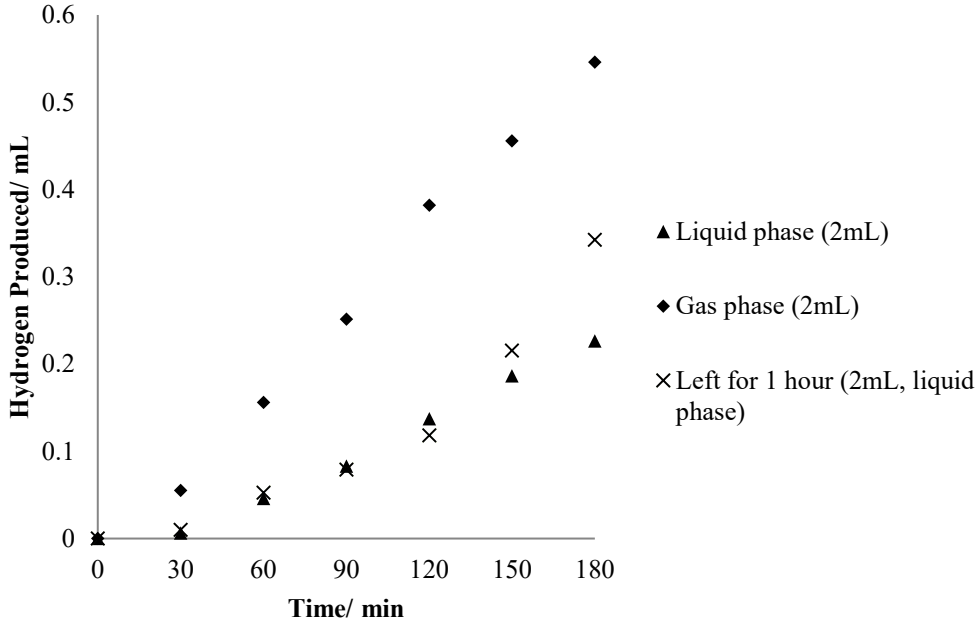

Figure 4.7. Hydrogen production using CO and 0.5%Pd/TiO_2 in liquid and gas phase

Figure 4.7 shows that 2 mL CO in the gas phase generates over double what is produced in the liquid phase. The solubility of CO in water is 27.6 mg L^{-1}. This means that the majority of the CO will be in the gas phase. Therefore in the gas phase there is likely to be a higher CO:H_2O ratio, meaning less competition with water, generating more hydrogen.

The liquid phase reaction with CO was repeated (crosses on Figure 4.7), however this time the reaction solution was left for one hour prior to turning on the lamp to allow the CO more time to dissolve into the water. Figure 7 shows that there is not a significant difference between the two.

The reactions using CO are further proof of the proposed mechanism and also highlight the effect of competition with water on the hydrogen yield. It is also important to note

that this is essentially the water gas shift reaction but at low temperatures. Normally very high temperatures are required but in this case light provides the additional energy.

4.2.3 Polyols

The use of polyols as sacrificial agents has been investigated. Polyols were chosen to investigate as they have alpha hydrogen adjacent to all the hydroxyl groups which should allow them to be dehydrogenated by Pd and they should therefore fully decompose to H_2 and CO_2, as methanol does, according to the rules proposed by Bahruji *et al.*[4] In addition Leung *et al.* reported high yields of hydrogen using glycerol.[6] It was suggested that only hydrogen atoms bonded to hydroxyl carbon would be evolved as hydrogen, thus implying that the more OH groups in a polyol, so the hydrogen yield might be higher.

4.2.3.1 Hydrogen Production

Methanol and C2-C5 polyols were used as sacrificial agents for photocatalytic hydrogen production using the same number of moles of each. This meant that a direct comparison could be achieved. Hydrogen production over time is shown below in Figure 4.8 for each polyol.

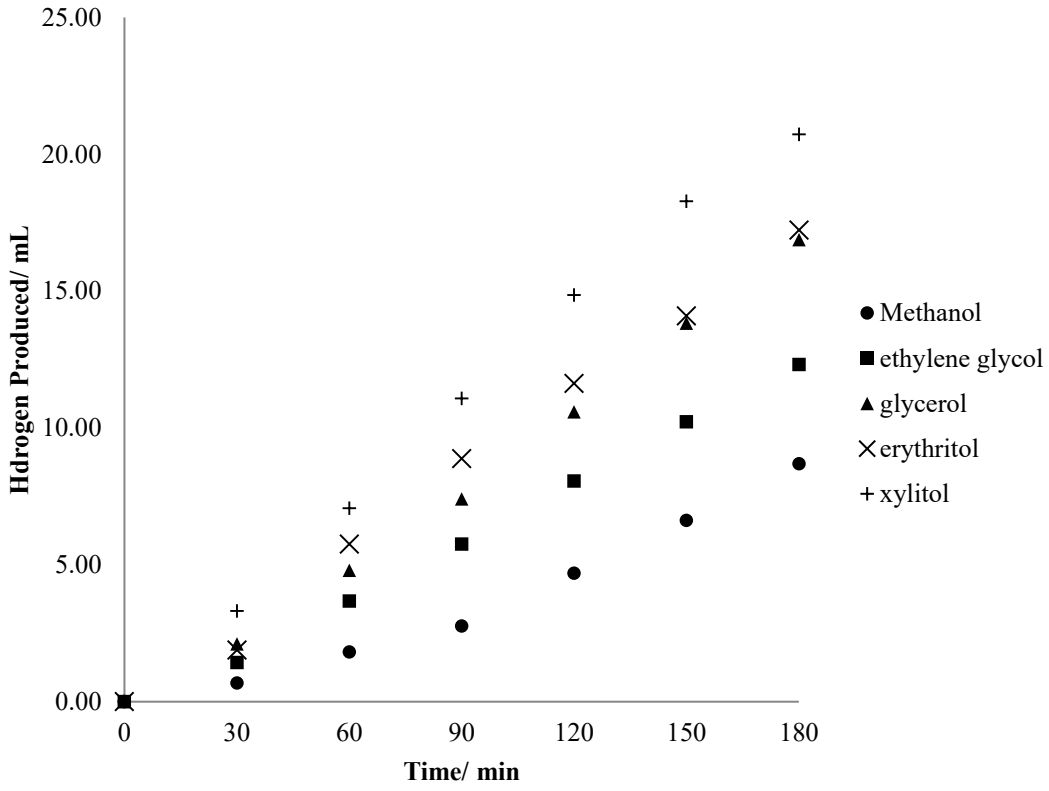

Figure 4.8. Hydrogen production using methanol and C2-C5 polyols with 0.5%Pd/TiO_2 catalyst

Figure 8 shows that hydrogen is produced at a steady rate, with no induction time observed for methanol through to xylitol. Hydrogen yield increases from methanol to xylitol indicating that with more OH groups in the alcohol, the higher the hydrogen yield.

If the polyols were following a similar reaction mechanism to the previously proposed mechanism and completely decomposing, the only by-product of this reaction should be CO_2. Gas chromatography analysis showed that this was true and CO_2 was the only other product. The volumes of CO_2 detected after 3 hours of reaction are shown in Figure 4.9.

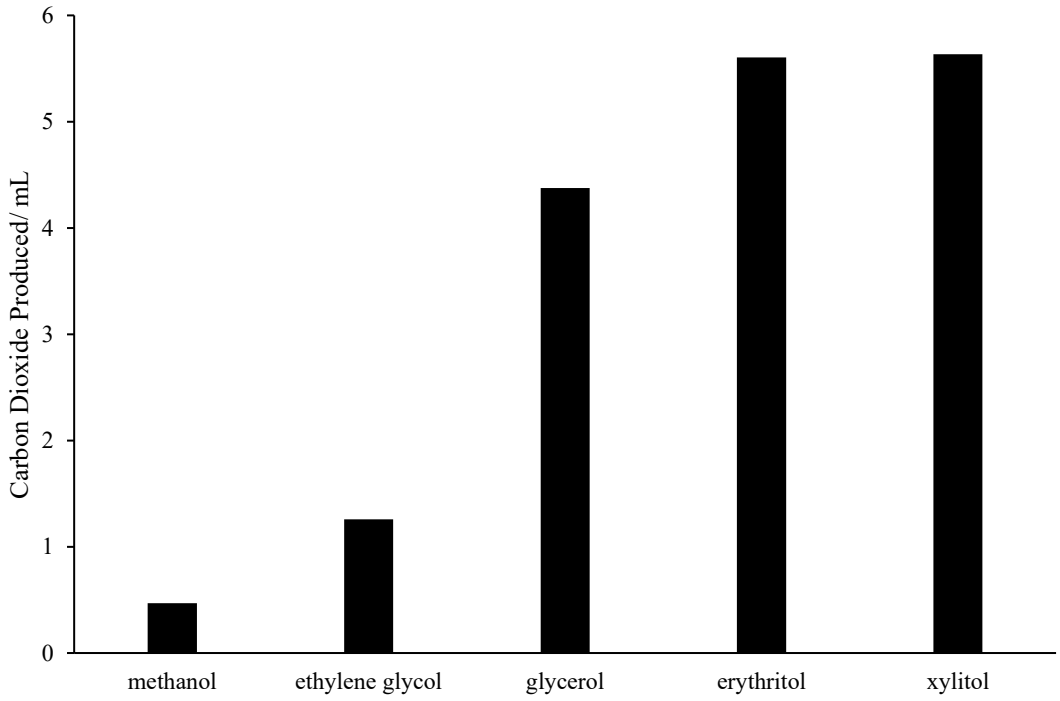

Figure 4.9. CO_2 production after 3 hours of reaction for methanol and C2-C5 polyols using 0.5%Pd/TiO_2 catalyst

Figure 4.9 shows that methanol and C2-C5 polyols all produce CO_2, however the ratio of H_2:CO_2 is not consistent with the proposed stoichiometry. This issue has been addressed previously in the chapter, where the low amount of CO_2 was attributed to it being dissolved in the reaction solution.

The proposed reaction schemes are shown below. The stoichiometries are derived from the rules proposed by Bahruji *et al*.[4] and the formula proposed by Klondarides (scheme (11)).[30]

$$CH_3OH + H_2O \rightarrow 3H_2 + CO_2 \quad (12)$$

$$C_2H_4(OH)_2 + 2H_2O \rightarrow 5H_2 + 2CO_2 \quad (15)$$

$$C_3H_5(OH)_3 + 3H_2O \rightarrow 7H_2 + 3CO_2 \quad (16)$$

$$C_4H_6(OH)_4 + 4H_2O \rightarrow 9H_2 + 4CO_2 \quad (17)$$

$C_5H_7(OH)_5 + 5H_2O \rightarrow 11H_2 + 5CO_2$ (18)

The above reaction schemes allow the prediction of the number of moles of hydrogen produces by each polyol per one mole of polyol used. A graph of the relationship between the number of OH groups and the expected hydrogen yield and the experimental hydrogen yield is shown below in Figure 4.10.

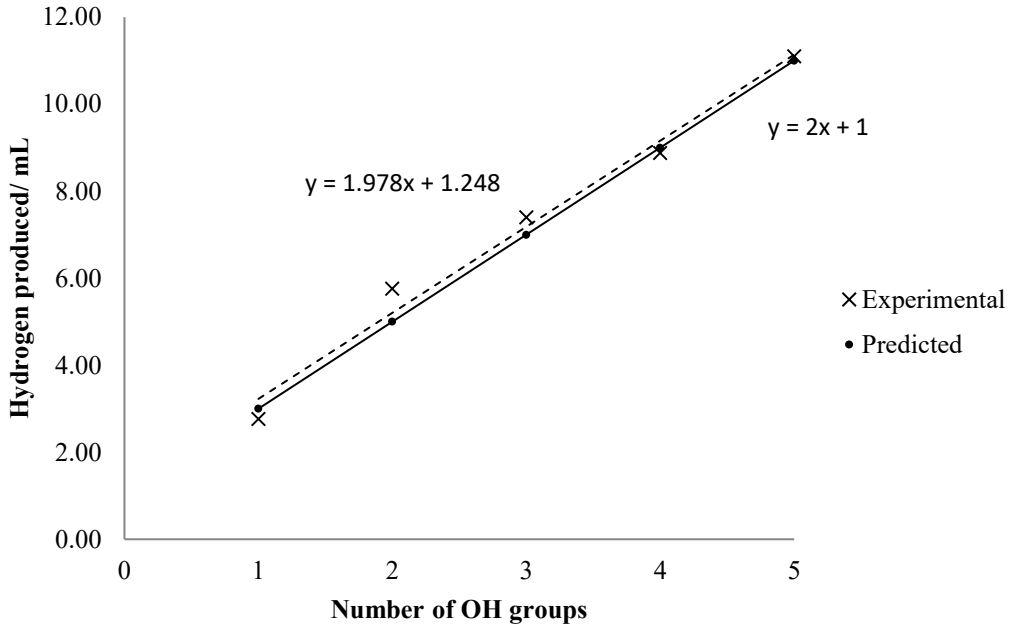

Figure 4.10. The relationship between the experimental hydrogen yield (dashed line, yield taken at 90 minutes) and the predicted hydrogen yield (solid line) and the number of OH groups

The plot for both the experimental and expected yield gives a straight line with the relationship y=1.978x+1.248 and y=2x+1 respectively. This suggests that the predicted reaction schemes are correct and is evidence that all the hydrogen atoms in the polyol are evolved as hydrogen.

In order to explain the equation for the straight line (y=2x+1) for the number of moles of hydrogen from polyol reforming, the relationship between the moles of hydrogen evolved

from the polyol and the moles of hydrogen from water was analysed. This is summarised in Table 4.2.

Polyol	Moles H_2 from polyol	Moles of H_2 from water
Methanol	2	1
Ethylene Glycol	3	2
Glycerol	4	3
Erythritol	5	4
Xylitol	6	5

Table 4.2. Number of moles of hydrogen evolved from polyol and water

The number of moles of hydrogen released from the polyol is equal to one mole per carbon/OH group and one additional mole of hydrogen from the terminal hydrogen on the terminal carbons of the polyol. This yields a formula of (n+1) where n = number of carbons/OH groups. Each carbon in the polyol requires one mole of water to oxidise adsorbed CO to CO_2. This process then also releases one additional mole of hydrogen per hydroxyl group. Therefore total number of moles of hydrogen = (n+1) + n. This equation can then be simplified to 2n+1, which is the relationship observed above in Figure 4.10.

Equation 4.2. Formula for prediction of number of moles hydrogen produced by polyol

Equation 4.2 can then be used to predict the moles of hydrogen from other polyols where n = the number of C-OH groups in the polyol.

Looking at the number of moles of hydrogen evolved from the polyol and the number of moles evolved from water led to another interesting observation. The proportion of

hydrogen from water splitting itself actually increases with an increase in OH groups. This is shown below in Table 4.3.

Polyol	% hydrogen from water splitting
Methanol	33
Ethylene Glycol	40
Glycerol	42
Erythritol	44
Xylitol	45

Table 4.3. Proportion of hydrogen from water splitting for methanol and C2-C5 polyols.

Table 4.3 suggests that using a sacrificial agent with more OH groups is a more efficient process than with methanol as more hydrogen is produced directly from water splitting. For example 33% of the hydrogen produced using methanol is from water splitting whereas when using xylitol the percentage of hydrogen from water splitting increases by over 10 %.

4.2.3.2 Mechanism

Using polyols with more OH groups has been shown to increase the volume of H_2 released. The number of moles of H_2 produced using the different polyols, is relative to the predicted reaction schemes as they are at the correct ratio to the amount of hydrogen produced by methanol. This suggests that the reaction mechanism is similar to that of methanol. Beginning with the adsorption of the polyol, followed by decomposition of the polyol and photo-activation of TiO_2 and finally water reduction.

The first step of the reaction is the adsorption of the polyol on the Pd. The adsorption of ethylene glycol on Pd(111) has been studied using TPR by Griffin *et al.* where dehydrogenation of both the O-H groups was observed indicating that the polyol adsorbs

via the oxygen, also yielding adsorbed hydrogen.[38] Other adsorption studies have found that only one of the oxygen atoms adsorbs, although these studies were based on Pt, Ni and Rh.[39, 40] A study conducted by Tereshchuk *et al*. used DFT to probe the adsorption of glycerol on Pt surfaces and found that glycerol also adsorbs via one oxygen of the glycerol molecule.[41] Therefore it is likely that the polyol adsorbs via a hydroxyl group (reaction 4.19). The O-H bond is dissociated, forming an alkoxy species and adsorbed hydrogen (reaction 4.20).

The only other product detected other than H_2 is CO_2 which suggests that complete dehydrogenation and decarbonylation occurs during the decomposition of the polyol. It has been reported by Greeley *et al.* that dehydrogenation and decarbonylation occurs at an energy comparable to that for O-H and C-H scission after the removal of several hydrogen atoms from glycerol.[42] It is possible that cascade dehydrogenation and decarbonylation of the polyol occurs, breaking the C-H and C-C bonds to produce adsorbed CO and adsorbed H (reaction 4.21). It is then suggested all adsorbed hydrogen is evolved as hydrogen gas (reaction 4.22).

Meanwhile UV light excites electrons in the TiO_2 to produce Ti^{3+} and O^- (reaction 4.23). The active oxygen species migrates to the interface between the TiO_2 and the Pd and oxidises the adsorbed CO to CO_2 (reaction 4.24). This leaves a vacancy in the TiO_2 which is filled with water. The O-H bonds in the water are broken which produces hydrogen and the oxygen restores the TiO_2 lattice (reaction 4.25).

Below is a summary of the suggested processes involved during photocatalytic polyol reforming using xylitol as an example.

1. Polyol adsorption

$C_5H_7(OH)_5$ (l) → $C_5H_7(OH)_5$ (a) (4.19)

$C_5H_7(OH)_5$ (a) → $C_5H_7(OH)_4O$ (a) + H (a) (4.20)

2. Polyol decomposition

$C_5H_7(OH)_4O$ (a) + H (a) → 5CO + 12H (a) (4.21)

3. Desorption of H (a)

12H (a) → $6H_2$ (4.22)

4. Photoactivation of TiO_2

$TiO_2 + h\nu \rightarrow Ti^{3+} + O^-$ (4.23)

5. CO oxidation

$5CO\ (a) + 5O^- \rightarrow 5CO_2\ (g) + 5V_0^{2-}$ (4.24)

6. Water reduction

$5H_2O\ (l) + 5V_0^{2-} \rightarrow 5H_2\ (g) + O^{2-}$ (4.25)

Overall

$C_5H_7(OH)_5\ (l) + 5H_2O\ (l) \rightarrow 11H_2\ (g) + 5CO_2\ (g)$ (4.26)

As is shown in reaction (4.26), the suggested mechanism fits with the stoichiometry seen from the experimental data which is further evidence of the processes involved.

There are a few aspects of this reaction that are interesting and pose questions. The first is that, if the proposed mechanism is correct, using longer chain polyols will require more O^- species to oxidise CO to CO_2 (reaction 24). The O^- is produced photocatalytically from TiO_2 (Reaction 23). This suggests that the quantum efficiency of the reaction using longer chain polyols increases. It has been reported by Schrob *et al.* that the scavenging efficiency was better with polyols with more OH groups[27] which could be the case here.

The reaction using methanol has been suggested to be near zero order with respect to methanol and therefore adheres to saturation type kinetics.[10] This means that the active sites on the catalyst are saturated with CO/methoxy and increasing the amount of methanol has little effect on the amount of hydrogen produced. The mechanism suggests that the polyols decompose fully to CO as with methanol. Using xylitol as the sacrificial agent is effectively increasing the concentration of CO as it decomposes to five CO, however using xylitol produces more hydrogen than methanol. This poses the question; how do the polyols produce more hydrogen than methanol in the same amount of time if all of the active sites are saturated with CO? Evaluating the rate determining step could answer this question. If the rate determining step was the oxidation of CO to CO_2 then it would be likely that the polyols and methanol would produce hydrogen at the same rate. If the rate determining step during the photocatalytic reaction was the adsorption of the polyol/methanol and the rate of methanol adsorption was slower than the polyols then this would explain how polyols exhibit faster hydrogen production.

4.2.4 Sugars

The experiments with linear polyols previously in the chapter have shown that using molecules with more OH groups increases hydrogen production. Sugars are a renewable resource and are naturally high in hydroxyl groups. Because of this, it was thought likely that sugars would produce high hydrogen yields. Glucose, fructose and sucrose (all 0.00247 mol) were tested for photocatalytic hydrogen production from reforming with water under the same conditions as the linear polyols. Glucose and fructose have 5 hydroxyl groups and sucrose has 8. The hydrogen produced by the sugars is shown below in Figure 4.11.

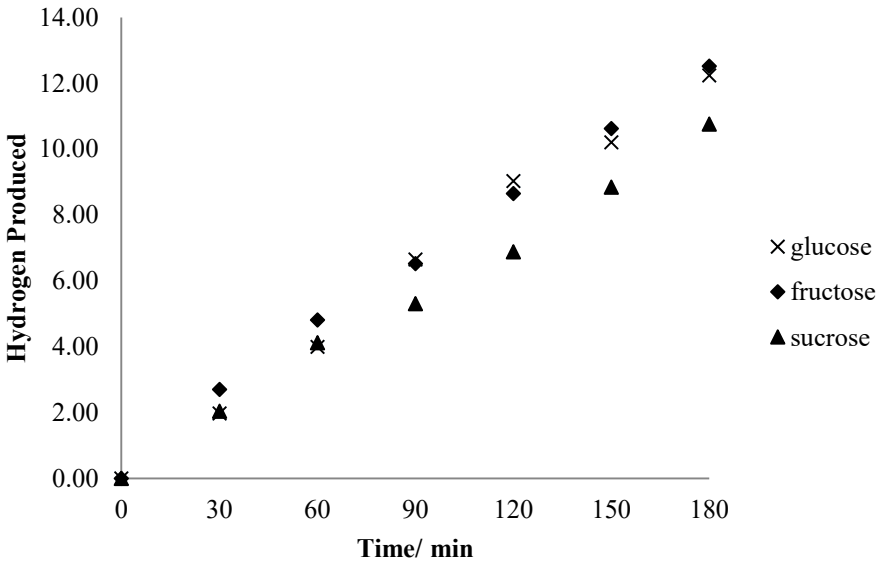

Figure 4.11. Hydrogen production from photocatalytic sugar reforming using glucose, fructose and sucrose

Figure 11 shows that the three sugars; glucose, fructose and sucrose are all active molecules for photocatalytic hydrogen production by reforming with water. Despite the molecules having different numbers of OH groups, the hydrogen yield for all three is similar; ~11 ml and is not very much higher than for methanol. This is disappointing as it was expected that due to the number of hydroxyl groups present, the hydrogen yield would be high. If the formula proposed earlier in the chapter was applied here (2n +1 = number of moles of hydrogen produced) then the +1 would be omitted as there are no terminal carbons as it is a ring structure. Therefore the formula would become 2n = number of moles of hydrogen produced, where n = number of carbon with oxygen containing group. The predicted stoichiometries for the sugars are shown below in reaction 4.27 and 4.28.

Glucose

$C_6H_{12}O_6 + 6H_2O \rightarrow 12H_2 + 6CO_2$ (4.27)

Fructose

$C_6H_{12}O_6 + 6H_2O \rightarrow 12H_2 + 6CO_2$ (4.28)

For glucose and fructose the stoichiometries predicted using the formula proposed in this chapter is in agreement with the formula proposed by Kondarides *et al*.[30] Deriving the reaction scheme for sucrose using the proposed formula is difficult as there is one carbon left over which is not attached to an oxygen containing group. It is possible that it forms CO_2 by using more water or it forms methane using hydrogen. The two possible reaction schemes are shown below in reaction 4.29 and 4.30.

Sucrose

$C_{12}H_{22}O_{11} + 13H_2O \rightarrow 24H_2 + 12\ CO_2$ (4.29)

$C_{12}H_{22}O_{11} + 11H_2O \rightarrow 20H_2 + 11\ CO_2 + CH_4$ (4.30)

No traces of methane were detected by the GC so the more likely reaction is the production of CO_2 reaction (4.29).

The amount of hydrogen produced in 3 hours using the sugars was ~11 mL. This is low considering xylitol produced ~21 mL in 3 hours. This suggests that the rate of hydrogen production when using the sugars is lower than with the linear polyols. It has been suggested that the higher the molecular the mass of the sugar, the slower the reaction due to slow movement through the reaction solution.[7] Glucose and fructose have similar molecular weights to xylitol however xylitol produces more hydrogen so it is unlikely the cause of lower yields. The sugars used are bulkier structures compared to the linear polyols. This could mean that sites on the catalyst are being blocked which is slowing

down the reaction. Another difference between the sugars and linear polyols is that some the OH groups on the sugars are bonded to a ring (Figure 4.12). It is possible that the C-C scission is slower for ring structures than linear structures. This could mean that there is a difference in the activity of OH groups directly attached to the ring and the ones attached to the ring via a methyl group.

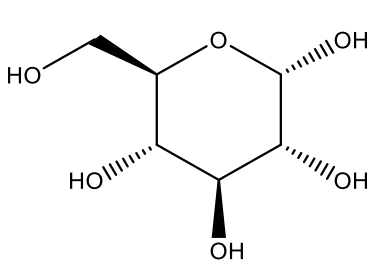

Glucose

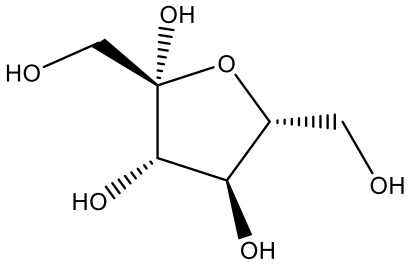

Fructose

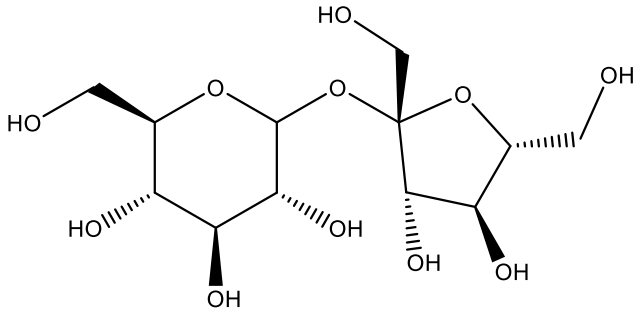

Sucrose

Figure 4.12. Structures of glucose, fructose and sucrose

To investigate whether there was a difference between OH groups directly attached to a ring and those indirectly attached, cyclohexanol and cyclohexane methanol were used for photocatalytic hydrogen production. The structures are shown below (Figure 4.13).

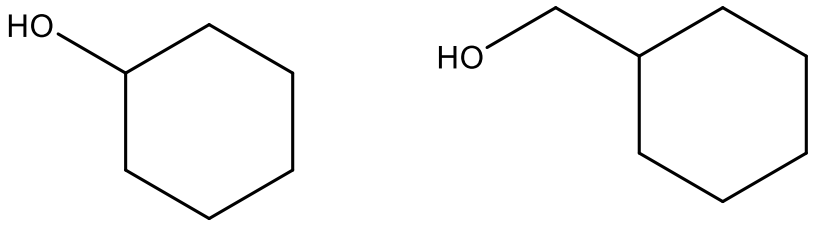

Figure 4.13. Cyclohexanol (left) and cyclohexane methanol (right)

The hydrogen produced by cyclohexanol and cyclohexylmethanol is shown below in Figure 4.14.

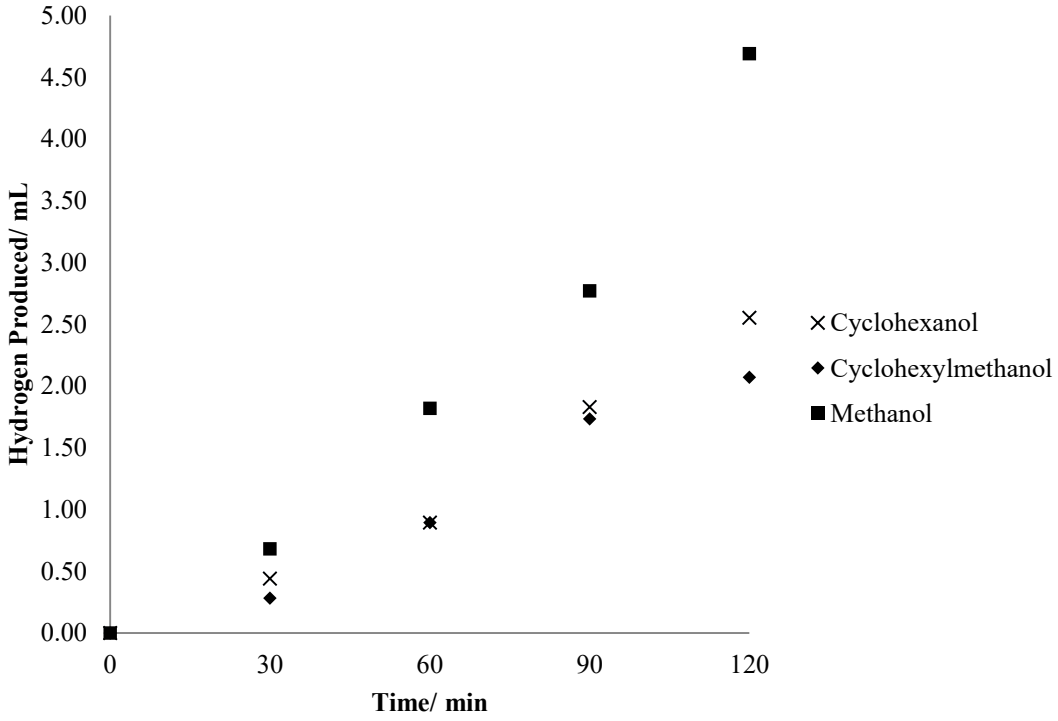

Figure 4.14. Hydrogen production from photocatalytic reforming with water using methanol, cyclohexanol and cyclohexyl methanol (0.00247 mol of each used in reaction)

Figure 4.14 shows that cyclohexanol and cyclohexyl methanol produce ~2.5 and 2 mL respectively in 2 hours. There is no significant difference between the activity of cyclohexanol and cyclohexyl methanol. This suggests that the activity is not affected by the OH group being directly attached to ring or the OH group being attached to a linear

alkyl. For the molecule to react, the C-C adjacent to the OH group must break. Therefore this implies that C-C scission of linear and ring carbon happens at similar rates. The experiment with cyclohexanol is evidence that a ring opening reaction has taken place. This experiment was undertaken in order to explain why the rates of hydrogen production from sugars is so low and whether it is the only the OH groups indirectly attached to the sugar ring that is reacting. The rings in the sugars: glucose, fructose and sucrose are oxygen containing rings so a direct comparison is difficult however the reaction with cyclohexanol and cyclohexyl methanol show that ring opening is possible. As there was no significant difference between cyclohexanol and cyclohexyl methanol, it is likely that this is not the cause of the lower activity in the case of the sugars.

Figure 4.14 shows that methanol produces ~4.5 mL hydrogen in 2 hours. This is almost double the yield of hydrogen produced from cyclohexanol and cyclohexyl methanol. The hexyl ring of cyclohexanol and cyclohexyl methanol is significantly more bulky than the methyl of methanol. This suggests that the ring is causing steric hindrance, blocking the active sites on the Pd, slowing the reaction which results in lower hydrogen yields. This could be evidence that the size of the sugar molecules is slowing the reaction and this is the reason for the lower hydrogen yields seen when using glucose, fructose and sucrose.

4.2.5 Position on ring with cyclohexanediols

Cyclohexane diols with OH groups at different positions have been used to explore whether their position affects hydrogen yield. The structures of those used are shown in Figure 4.15.

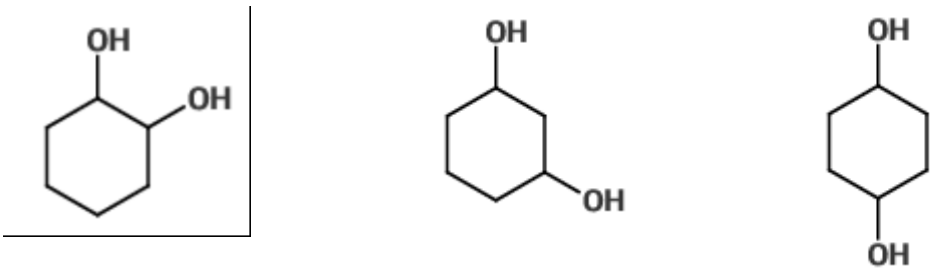

Figure 4.15. 1,2-cyclohexanediol, 1,3-cyclohexanediol and 1,4-cyclohexanediol (from left to right)

1,2-cyclohexanediol, 1,3-cyclohexanediol and 1,4-cyclohexanediol (all 0.00247 mol) were used for photocatalytic hydrogen production from reforming with water under the same reactions conditions as the linear polyols and sugars. The hydrogen produced using the cyclohexanediols is shown in Figure 4.16.

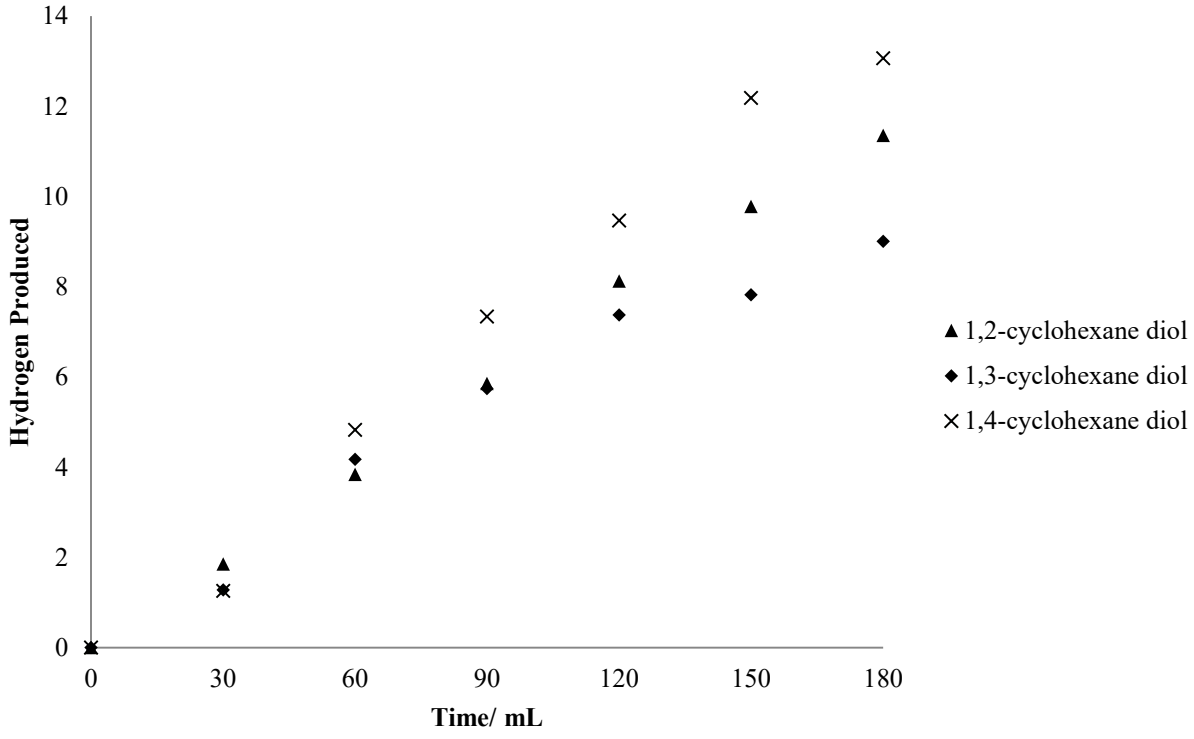

Figure 4.16. Hydrogen production from photocatalytic reforming with water using 1,2-cyclohexanediol, 1,3-cyclohexanediol and 1,4-cyclohexanediol

Figure 16 shows that all three cyclohexane diols are active for photocatalytic hydrogen production with 1,4-cyclohexanediol producing the most hydrogen at ~13 mL in 3 hours. 1,3-cyclohexanediol produces the least at 9 mL in 3 hours. The fact that the cyclohexanediols are active for photocatalytic hydrogen production from reforming using water is not surprising as they all have alpha hydrogens on the carbons with the hydroxyl groups. The gas phase products were analysed using mass spectrometry (MS). The

products detected are shown in Table 4.4 are evidence of ring opening reactions taking place.

Cyclohexane diol	Gas products
1,2-cyclohexane diol	H_2, CO_2 and C_4H_{10}
1,3-cyclohexane diol	H_2, CO_2 and C_3H_8
1,4-cyclohexane diol	H_2, CO_2

Table 4.4. Gaseous products from photocatalytic cyclohexane diol reforming using MS

Previous work by Bowker *et al.* suggests a set rules applying to sacrificial agents dictating whether hydrogen will be produced and how much.[4] These are summarised in the introduction of this chapter in section. Using these rules and what has been established earlier in the chapter; reaction schemes can be suggested (reaction 4.31, 4.32 and 4.33).

1,2-cyclohexanediol

$$C_6H_{12}O_2 + 2H_2O \rightarrow 3H_2 + 2CO_2 + C_4H_{10} \qquad (4.31)$$

Reaction 31 with 1,2-cyclohexanediol proposes both hydroxyl carbons being oxidised to CO_2, releasing H_2 and the alkyl group from the ring (butyl) using one mole of the H_2 released to yield butane as suggested by Bowker *et al.*[4] Butane was present in the MS analysis of the gaseous product which indicates that reaction 31 is likely.

1,3-cyclohexanediol

$$C_6H_{12}O_2 + 4H_2O \rightarrow 6H_2 + 3CO_2 + C_3H_8 \qquad (4.32)$$

The products seen in the MS of the gaseous products from 1,3-cyclohexane diol were H_2, CO_2 and propane. 1,3-cyclohexane diol has a methylene group between the two hydroxyl groups. Bowker *et al.* reported that methylene groups between alcohols are fully oxidised

to CO_2.[4] Methane was not seen in the MS, suggesting that the methylene group was fully oxidised to CO_2, hence the proposed reaction (4.32).

1,4-cyclohexanediol has two ethylene groups in between the carbons with the OH groups. The MS for the reaction using 1,4-cyclohexanediol saw only H_2 and CO_2. This suggests that the ethylene groups completely oxidise to CO_2 which would yield reaction (4.33) as seen below.

$$C_6H_{12}O_2 + 10H_2O \rightarrow 16H_2 + 6CO_2 \qquad (4.33)$$

Looking at the proposed reactions for the cyclohexanediols, one would expect 1,4-cyclohexanediol to produce ~4 times more hydrogen than 1,2-cyclohexanediol and 1,3-cyclohexanediol to produce double. Figure 4.16 however shows that this is not the case with 1,4-cyclohexanediol producing only slightly more hydrogen and 1,3-cyclohexanediol producing less. It is possible that the complete oxidation of ethylene and methylene to CO_2 is a slow process, which is why substantially higher hydrogen yields are not seen. The rate of hydrogen production could also be limited by the size of the molecules (as seen with cyclohexanol). If these reactions were continued to completion, it is likely considering the proposed reactions that 1,4-cyclohexanediol and 1,3-cyclohexanediol would produce more hydrogen based on the stoichiometry above (reaction 31, 32 and 33).

4.2.6 Lactic acid

Lactic acid contains one hydroxyl with an alpha hydrogen and a carboxylic acid group without an alpha hydrogen as seen in Figure 4.17. It has been reported that only OH groups with an alpha hydrogen will produce hydrogen. To see whether the organic acid would react further, lactic acid (0.00247 mol) was tested for photocatalytic hydrogen production from reforming with water under the same conditions as the linear polyols.

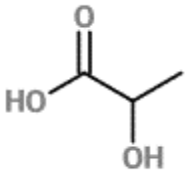

Figure 4.17. Structure of lactic acid

The hydrogen produced by lactic acid and a comparison with methanol is shown below in Figure 4.18.

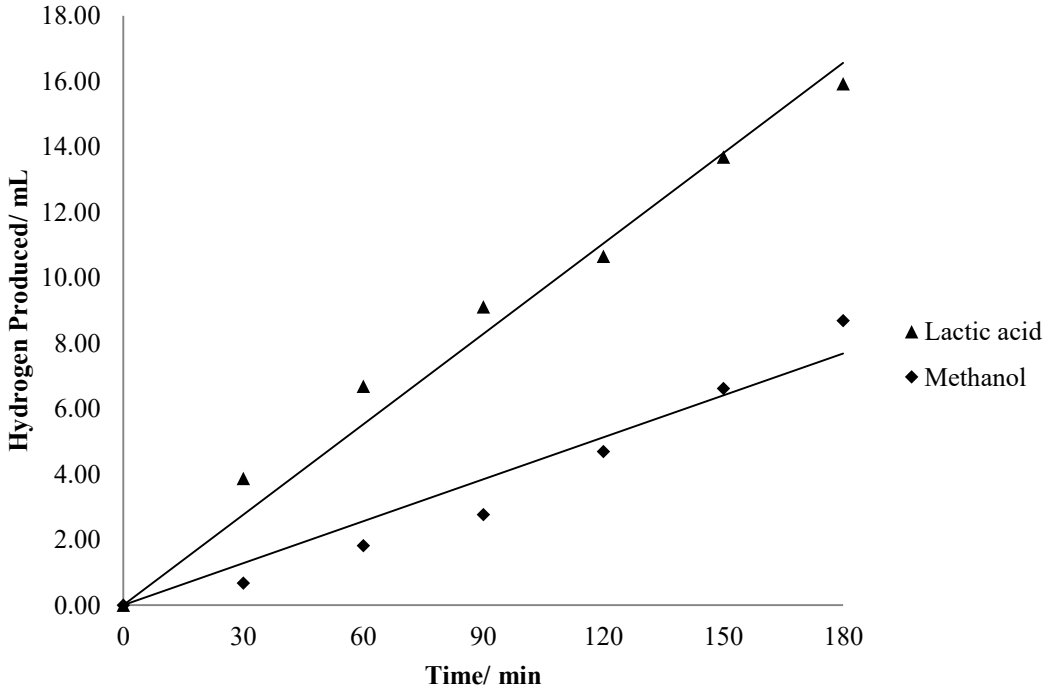

Figure 4.18. Hydrogen production from photocatalytic reforming with water using lactic acid and methanol

Figure 4.18 shows that lactic acid is very active for photocatalytic hydrogen production from reforming using water producing ~16 mL in three hours. This is unsurprising as it possesses an alpha hydrogen on the hydroxyl carbon. What is interesting, however, is the amount of hydrogen produced by lactic acid compared to methanol. If only the one hydroxyl group on the lactic acid was reacting to form hydrogen, the amount of hydrogen

produced would be similar to methanol. In this case, however, lactic acid produced significantly more hydrogen than methanol. This suggests that lactic acid is fully decomposing even though the acid group does not have an alpha hydrogen. It has been reported that acetic acid is not active for photocatalytic hydrogen production from reforming using water,[4] however studies have shown that formic acid readily decomposes on Pd.[43-45] Acetic acid does not have an alpha hydrogen but formic acid does. It is possible that an intermediate in the reaction using lactic acid is formic acid, which then decomposes fully to hydrogen and carbon dioxide. The methyl group attached to hydroxyl carbon will be competing for a hydrogen with formate. It is possible that the methyl group will, instead, decompose to hydrogen and carbon dioxide. This could explain why lactic acid produces almost double the hydrogen compared to methanol. The proposed reaction scheme for lactic acid is shown below in reaction 4.34, 4.35 and 4.36.

$$C_3H_6O_3 + 3H_2O \rightarrow 5H_2 + 2CO_2 + CH_2O_2 \quad (4.34)$$

$$CH_2O_2 \rightarrow H_2 + CO_2 \quad (4.35)$$

$$\text{Overall - } C_3H_6O_3 + 3H_2O \rightarrow 6H_2 + 3CO_2 \quad (4.36)$$

The high hydrogen yield achieved with lactic acid is evidence of the rule proposed that "competing" methyl groups will further decompose to carbon dioxide and hydrogen.

4.3 Conclusions

This chapter has focussed on using different sacrificial agents, on what aspects of the reaction dictate the hydrogen yield and on exploring the mechanism by which they react. The first part involved establishing a stoichiometric relationship between hydrogen and carbon dioxide when using methanol. This was found to be 3:1 hydrogen to carbon dioxide which is evidence of the proposed mechanism by Bowker and co-workers.[10] This ratio was only observed when the reaction mixture was heated as the carbon dioxide was

found to be dissolved in the reaction mixture. More evidence for the proposed mechanism by Bowker *et al.* [10] was the fact that CO could be used as the sacrificial agent. It was suggested that CO is an intermediate in the reaction with methanol. Using different concentrations of CO showed that the reaction with respect to CO followed near zero order kinetics after the 'saturation' point. This was also observed for methanol in previous work. The mechanism for methanol suggests that molecules with a C-O-H group will be active for photocatalytic hydrogen production from reforming using water. It was then postulated that molecules with more of these groups could produce more hydrogen. A range of molecules containing C-O-H groups were tested for photocatalytic hydrogen production including linear polyols, sugars, cyclo-alcohols and lactic acid. The relationship observed between the number of oxygenate groups and hydrogen production is shown in Figure 4.19.

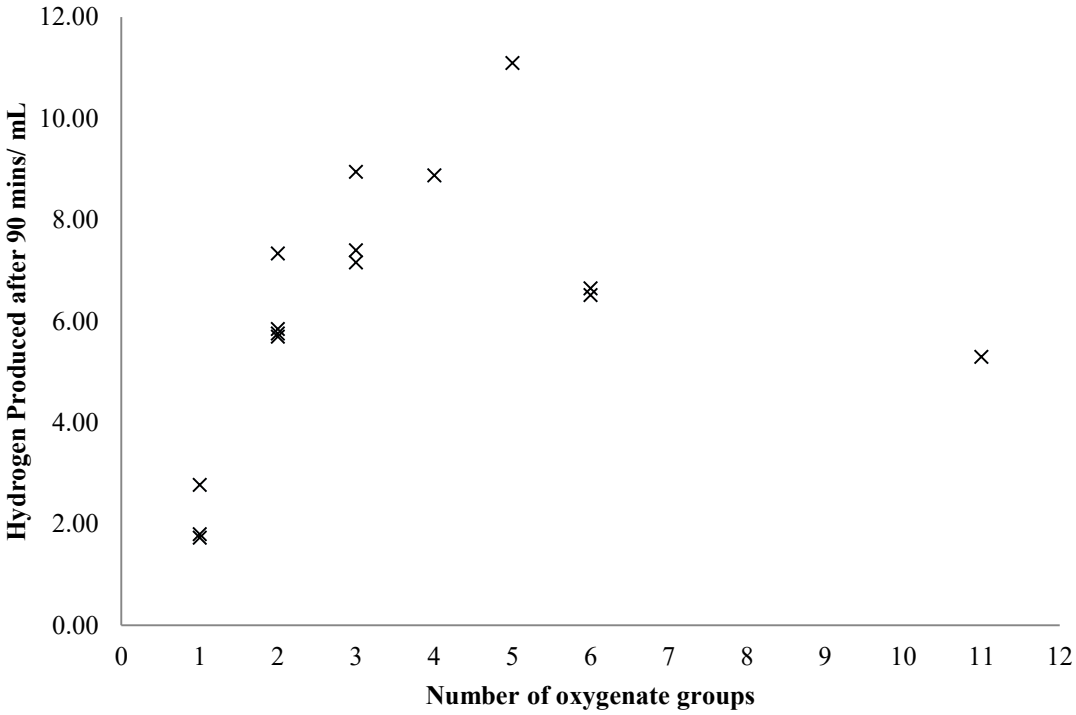

Figure 4.19. The relationship between number of oxygenate groups in a molecule and hydrogen production

Figure 4.19 shows that with more oxygenate groups, generally more hydrogen is produced, however it is clear that there are other factors influencing the rate of hydrogen production. The linear polyols showed a direct relationship between the number of OH groups and hydrogen production and a formula of 2n + 1 = moles of hydrogen produced where n = number of C-O-H groups was proposed. Sugars were considerably less active than predicted, this was attributed to the size of the molecules causing blocking of the active sites. Using cyclohexane diols with OH groups at different positions on the ring provided evidence for "competing" alkyls groups fully decomposing to carbon dioxide and hydrogen, and that molecules that fully decompose to carbon dioxide and hydrogen produce more hydrogen as was also seen with lactic acid. In conclusion, a sacrificial agent that has a high number of OH groups, and is linear, will fully decomposes to carbon dioxide and hydrogen and will produce more hydrogen. Xylitol was found to have the highest rate of hydrogen production because it has five OH groups, is linear and it fully decomposes to carbon dioxide and hydrogen.

1.1 References

1. P. Tans, *NOAA/ESRL* www.esrl.noaa.gov/gmd/ccgg/trends/.
2. W. Grochala and P. P. Edwards, *Chemical Reviews*, 2004, 104, 1283.
3. Y. Z. Yang, C. H. Chang and H. Idriss, *Applied Catalysis B-Environmental*, 2006, 67, 217.
4. H. Bahruji, M. Bowker, P. R. Davies and F. Pedrono, *Applied Catalysis B-Environmental*, 2011, 107.
5. M. Bowker, P. R. Davies and L. S. Al-Mazroai, *Catalysis Letters*, 2009, 128.
6. X. Fu, X. Wang, D. Y. C. Leung, Q. Gu, S. Chen and H. Huang, *Applied Catalysis B-Environmental*, 2011, 106, 681.
7. X. Fu, J. Long, X. Wang, D. Y. C. Leung, Z. Ding, L. Wu, Z. Zhang, Z. Li and X. Fu, *International Journal of Hydrogen Energy*, 2008, 33, 6484.
8. T. Kawai and T. Sakata, *Journal of the Chemical Society-Chemical Communications*, 1980.
9. M. Kawai, S. Naito, K. Tamaru and T. Kawai, *Chemical Physics Letters*, 1983, 98, 377.
10. A. Dickinson, D. James, N. Perkins, T. Cassidy and M. Bowker, *Journal of Molecular Catalysis a-Chemical*, 1999, 146.
11. J. M. Herrmann, *Catalysis Today*, 1999, 53, 115.
12. A. V. Emeline, A. V. Rudakova, V. K. Ryabchuk and N. Serpone, *Journal of Physical Chemistry B*, 1998, 102, 10906.
13. M. Bowker, L. Millard, J. Greaves, D. James and J. Soares, *Gold Bulletin*, 2004, 37.
14. G. N. Nomikos, P. Panagiotopoulou, D. I. Kondarides and X. E. Verykios, *Applied Catalysis B-Environmental*, 2014, 146, 249.

15. S. S. Akarmazyan, P. Panagiotopoulou, A. Kambolis, C. Papadopoulou and D. I. Kondarides, *Applied Catalysis B-Environmental*, 2014, 145, 136.

16. F. Chojnowski, P. Clechet, J. R. Martin, J. M. Herrmann and P. Pichat, *Chemical Physics Letters*, 1981, 84, 555.

17. P. Pichat, M. N. Mozzanega, J. Disdier and J. M. Herrmann, *Nouveau Journal De Chimie-New Journal of Chemistry*, 1982, 6, 559.

18. T. Chen, Z. Feng, G. Wu, J. Shi, G. Ma, P. Ying and C. Li, *Journal of Physical Chemistry C*, 2007, 111, 8005.

19. X.-J. Zheng, L.-F. Wei, Z.-H. Zhang, Q.-J. Jiang, Y.-J. Wei, B. Xie and M.-B. Wei, *International Journal of Hydrogen Energy*, 2009, 34, 9033.

20. Y. Nosaka, K. Koenuma, K. Ushida and A. Kira, *Langmuir*, 1996, 12, 736.

21. G. L. Chiarello, L. Forni and E. Selli, *Catalysis Today*, 2009, 144.

22. T. A. Kandiel, R. Dillert, L. Robben and D. W. Bahnemann, *Catalysis Today*, 2011, 161, 196.

23. H. Bahruji, M. Bowker, C. Brookes, P. R. Davies and I. Wawata, *Applied Catalysis a-General*, 2013, 454, 66.

24. H. Bahruji, M. Bowker, P. R. Davies, L. S. Al-Mazroai, A. Dickinson, J. Greaves, D. James, L. Millard and F. Pedrono, *Journal of Photochemistry and Photobiology a-Chemistry*, 2010, 216.

25. P. Panagiotopoulou, E. E. Karamerou and D. I. Kondarides, *Catalysis Today*, 2013, 209, 91.

26. V. Gombac, L. Sordelli, T. Montini, J. J. Delgado, A. Adamski, G. Adami, M. Cargnello, S. Bernal and P. Fornasiero, *Journal of Physical Chemistry A*, 2010, 114.

27. I. A. Shkrob, M. C. Sauer and D. Gosztola, *Journal of Physical Chemistry B*, 2004, 108, 12512.

28. R. D. Cortright, R. R. Davda and J. A. Dumesic, *Nature*, 2002, 418, 964.

29. A. Demirbas, *Progress in Energy and Combustion Science*, 2007, 33, 1.

30. D. I. Kondarides, V. M. Daskalaki, A. Patsoura and X. E. Verykios, *Catalysis Letters*, 2008, 122.

31. L. Saeed Al-Mazroai, M. Bowker, P. Davies, A. Dickinson, J. Greaves, D. James and L. Millard, *Catalysis Today*, 2007, 122.

32. A. Naldoni, M. D'Arienzo, M. Altomare, M. Marelli, R. Scotti, F. Morazzoni, E. Selli and V. Dal Santo, *Applied Catalysis B-Environmental*, 2013, 130, 239.

33. J. A. Dean, *Lange's Handbook of Chemistry*, McGraw Hill, Inc, 15th edn., 1999.

34. *CRC Handbook of Chemistry and Physics*, CRC Press, Cleaveland, Ohio, 55th edn., 1974.

35. W. E. Kaden, W. A. Kunkel, F. S. Roberts, M. Kane and S. L. Anderson, *Journal of Chemical Physics*, 2012, 136.

36. K. Christmann and J. E. Demuth, *Journal of Chemical Physics*, 1982, 76, 6318.

37. L. Millard and M. Bowker, *Journal of Photochemistry and Photobiology a-Chemistry*, 2002, 148.

38. M. B. Griffin, E. L. Jorgensen and J. W. Medlin, *Surface Science*, 2010, 604, 1558.

39. M. M. M. Jansen, B. E. Nieuwenhuys and H. Niemantsverdriet, *Chemsuschem*, 2009, 2, 883.

40. O. Skoplyak, M. A. Barteau and J. G. G. Chen, *Journal of Physical Chemistry B*, 2006, 110, 1686.

41. P. Tereshchuk, A. S. Chaves and J. L. F. Da Silva, *Journal of Physical Chemistry C*, 2014, 118, 15251.

42. B. Liu and J. Greeley, *Journal of Physical Chemistry C*, 2011, 115, 19702.

43. G. Q. Lu, A. Crown and A. Wieckowski, *Journal of Physical Chemistry B*, 1999, 103, 9700.

44. D. A. Bulushev, S. Beloshapkin and J. R. H. Ross, *Catalysis Today*, 2010, 154, 7.

45. K. Tedsree, T. Li, S. Jones, C. W. A. Chan, K. M. K. Yu, P. A. J. Bagot, E. A. Marquis, G. D. W. Smith and S. C. E. Tsang, *Nature Nanotechnology*, 2011, 6, 302.

Chapter 5

5.1 Introduction

Since the discovery of photochemical water splitting over a TiO_2 electrode by Fujishima and Honda,[1] many studies have focused on using TiO_2 as catalyst for photocatalytic water splitting. It has been reported many times that loading TiO_2 with metal nanoparticles *e.g.* Pd,[2] Au,[3] Pt [4] has shown to increase yields of hydrogen greatly. The work in the previous two chapters has been conducted using TiO_2-P25 as the photoactive support loaded with metal nanoparticles via incipient wetness. This chapter explores the effect of synthesising TiO_2 using sol-gel methods and also the effect of using different nanoparticles synthesis methods with the aim of producing more active catalysts and also establishing what makes a good photocatalyst for photocatalytic methanol reforming.

5.1.1 TiO_2 preparation

The are several ways to prepare TiO_2; chemical precipitation,[5] microemulsion,[6] hydrothermal,[7, 8] ultrasonic irradiation [9] and sol-gel.[10-12] The most promising of these is sol-gel synthesis, which has been reported to have high photocatalytic activity for water splitting.[13] Some have reported better hydrogen yields using sol-gel TiO_2 than with TiO_2-P25.[14] The performance of the sol-gel TiO_2 is affected by the calcination conditions. There is a trade-off between surface area and crystallinity.[15] At lower calcination temperatures, higher surface areas are seen however crystallinity is low. This means there are more defects and therefore more sites of recombination of e^-/h^+ pairs leading to lower activity.[16] Addition of metals during the sol-gel synthesis is possible.[17, 18] It is reported that the metal nanoparticles are better dispersed when added during the sol-gel synthesis of TiO_2 than nanoparticles on catalysts prepared via wet impregnation.

5.1.2 Nanoparticle synthesis

The preparation method of nanoparticles for loading on TiO_2 can greatly affect the photocatalyst activity. The incipient wetness technique is a simple method of adsorbing

metal nanoparticles on TiO_2 and can produce very active catalysts for photocatalytic methanol reforming.[19, 20] Varying the weight loading can have a significant effect on activity.[19] Another method to produce metal loaded TiO_2 is to synthesise the nanoparticles first and then adsorb them onto the TiO_2 surface. The Turkevich method of synthesising Au nanoparticles uses sodium citrate as both the reducing and capping agent.[21] Citrate stabilised Au/TiO_2 has been reported to produce active photocatalysts for methanol reforming. Kmetyko *et al.* synthesised Au/TiO_2 using different concentrations of citrate to produce catalysts with different sized Au nanoparticles.[22] The higher the concentration of citrate, the smaller the nanoparticles and the more homogeneous. With increasing loading of nanoparticles, hydrogen production increased until a maximum of around 6 nm after which point hydrogen yield decreased. The method of synthesis of the catalyst has been reported to change the oxidation state of the metal. Xu *et al.* produced a range of Cu/TiO_2 catalysts for photcatalytic methanol reforming using sol-gel, wet impregnation, chemical reduction using $NaBH_4$ and photodeposition.[23] The method and Cu species are shown in Table 5.1. Chemical reduction was found to produce the most active catalyst.

Preparation method	Cu species
Sol-gel	CuO
Wet-impregnation	CuO
Chemical reduction with $NaBH_4$	Cu_2O
Photodeposition	Cu metal

Table 5.1. Preparation method of Cu/TiO_2 and Cu species

Metal nanoparticle size can depend on the type of TiO_2 used.[24] Anatase has a higher Fermi level than rutile which results in greater interaction with the metal nanoparticles loaded on the surface. This can limit growth or agglomeration, producing smaller nanoparticles.[25]

The preparation method of a catalyst can significantly change its properties and therefore its activity towards a particular reaction. In this chapter the effects of preparation method on metal/TiO_2 catalysts for photocatalytic methanol reforming have been investigated. Photocatalysts using anatase, rutile, brookite and sol-gel TiO_2 have been investigated. Metal nanoparticles have be synthesised using a variety of methods where particle size and distribution have controlled.

5.2 Results and discussion

5.2.1 TiO_2 phase and activity

1%Pd/TiO_2 catalysts were prepared via incipient wetness on P25, anatase and rutile. The catalysts were tested for photocatalytic methanol reforming in the liquid phase to establish how much better TiO_2-P25 is compared to other TiO_2 types. The reaction profiles are shown in Figure 5.1. It is clear that P25 provides the best semi-conductor

support for this reaction having almost double the hydrogen yield of TiO_2-anatase. P25 is made up from a mixture of rutile and anatase at a ratio of 20:80. The increased activity of P25 is possibly due to the difference in Fermi levels of anatase and rutile. When electrons are produced in either phase they can flow into the other. This is said to elongate the e^-/h^+ separation time, leading to a more active catalyst.[26] 1%Pd/TiO_2-rutile shows negligible activity compared to anatase and P25 which is possibly due to the combination of quick e^-/h^+ recombination and low flat band energy in rutile reducing the catalysts ability to reduce water as reported by Katoh *et al.* and Sreethawong *et al*.[27, 28]

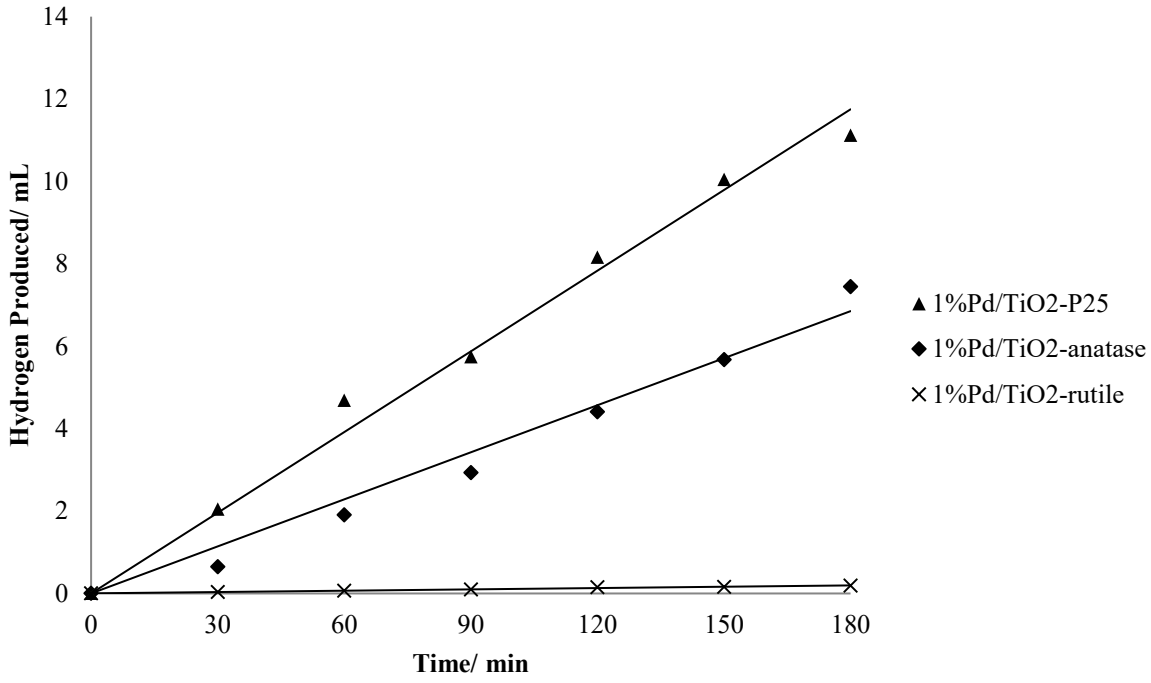

Figure 5.1. Hydrogen produced from photocatalytic methanol reforming using 1%Pd supported on P25, anatase and rutile in liquid phase

The reactions were repeated in the gas phase to establish whether this would improve the activity of anatase and rutile as well as TiO_2-P25, the results are shown in Figure 5.2. Again the most active catalyst is Pd/TiO_2-P25 but exhibits significantly higher activity than in the liquid phase with ~12 mL in the liquid phase and ~27 mL in the gas phase.

Interestingly, Pd/TiO_2-rutile which was inactive in the liquid phase, shows significant increase in activity in the gas phase. A possible explanation for this is that during gas phase reactions there will be a higher concentration of methanol adsorbed to the catalyst surface due to higher concentration of methanol in the gas compared to solution.[29] Another factor to consider is temperature. Usually temperature would not affect the rate of a photocatalytic reaction but, as discussed in chapter 1, it is likely that the rate determining step for this reaction is a catalytic step. Therefore for this process, temperature could have an effect on the overall rate of hydrogen production. Although the reaction set up does not directly apply heat to the reaction vessel, the lamp gets hot during the reaction. Liquid will heat up more slowly than gas, therefore it is likely that the temperature of the gas phase reaction is hotter than the liquid phase reaction which could increase the rate and therefore the yield.

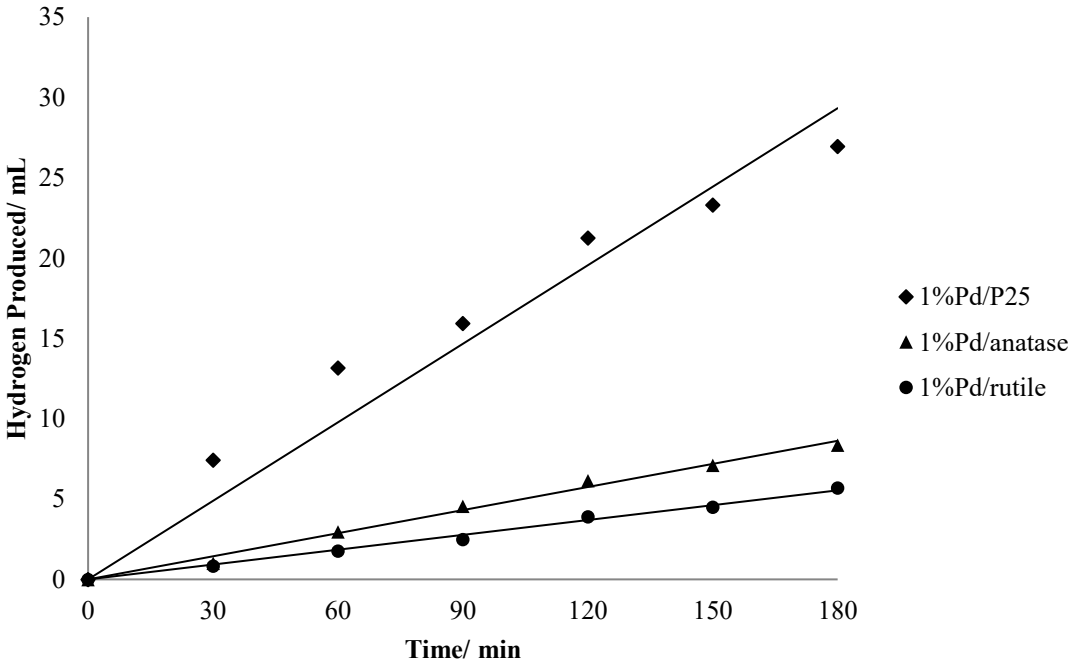

Figure 5.2. Hydrogen produced from photocatalytic methanol reforming using 1%Pd supported on P25, anatase and rutile in gas phase

As TiO_2-P25 is a mixture of anatase and rutile, anatase and rutile were physically mixed in a crucible and tested for photocatalytic hydrogen production from methanol reforming. The purpose of this was to establish whether the location of the metal nanoparticle i.e. either on the anatase or on the rutile, affected the activity. 1%Pd/TiO_2-anatase was mixed with TiO_2-rutile and 1%Pd/TiO_2-rutile was mixed with TiO_2-anatase. The effects of this are shown below in Figure 5.3.

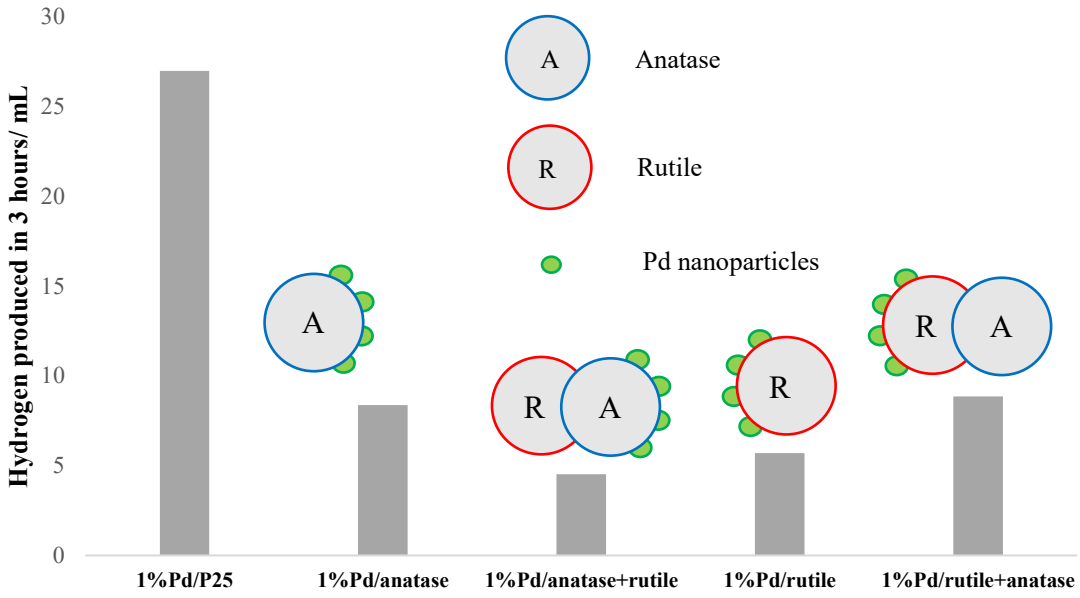

Figure 5.3. Hydrogen produced by 1%Pd supported on different phases on TiO_2

The activity of 1%Pd/anatase alone was found to be significantly better than when mixed with rutile. On the other hand, the activity of 1%Pd/rutile was increased when mixed with anatase. Electron paramagnetic resonance (EPR) studies have shown that electrons move from rutile to anatase and holes move from anatase to rutile.[30-32] The movement of charge is shown below in Figure 5.4 from the work of Scanlon *et al.*[33]

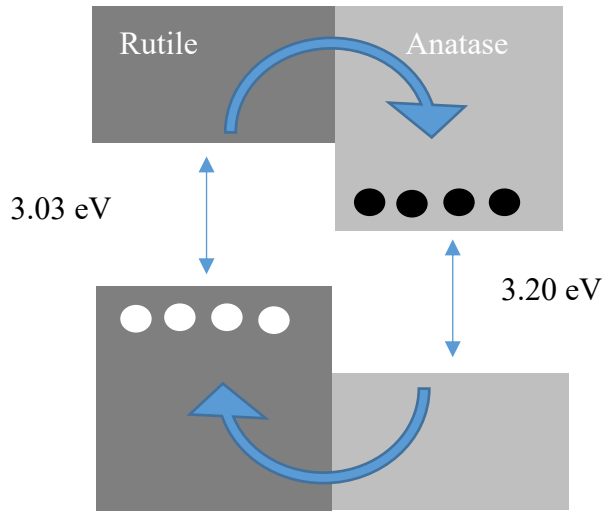

Figure 5.4. Electron (black) and hole (white) movement in rutile/anatase mixes

The active site for water splitting is suggested to be a hole at the interface between the TiO_2 and Pd.[34] When anatase is added to 1%Pd/rutile, holes move into the rutile, providing more active sites close to the interface between Pd and rutile which could explain the increase in activity. On the other hand when rutile is added to 1%Pd/anatase, holes move into the rutile away from the interface between Pd and anatase, decreasing the activity. This has shown that the location of the metal is important and can affect activity.

5.2.2 Sol-gel preparation of TiO_2

The sol-gel technique for synthesising TiO_2 is promising. To explore further whether the location of Pd can affect activity, 1%Pd/TiO_2 using a sol-gel technique with one catalyst incorporating Pd into the bulk and was adsorbing Pd onto the surface via incipient wetness. TiO_2 was prepared using a sol-gel method from titanium (IV) tetraisopropoxide and isopropyl alcohol.[35] Palladium was deposited on to the TiO_2 surface using incipient

wetness (1%Pd/TiO_2-sol-gel (IW)) and also incorporated into the sol-gel prep (1%Pd/TiO_2-sol-gel). The catalysts were tested for photocatalytic methanol reforming.

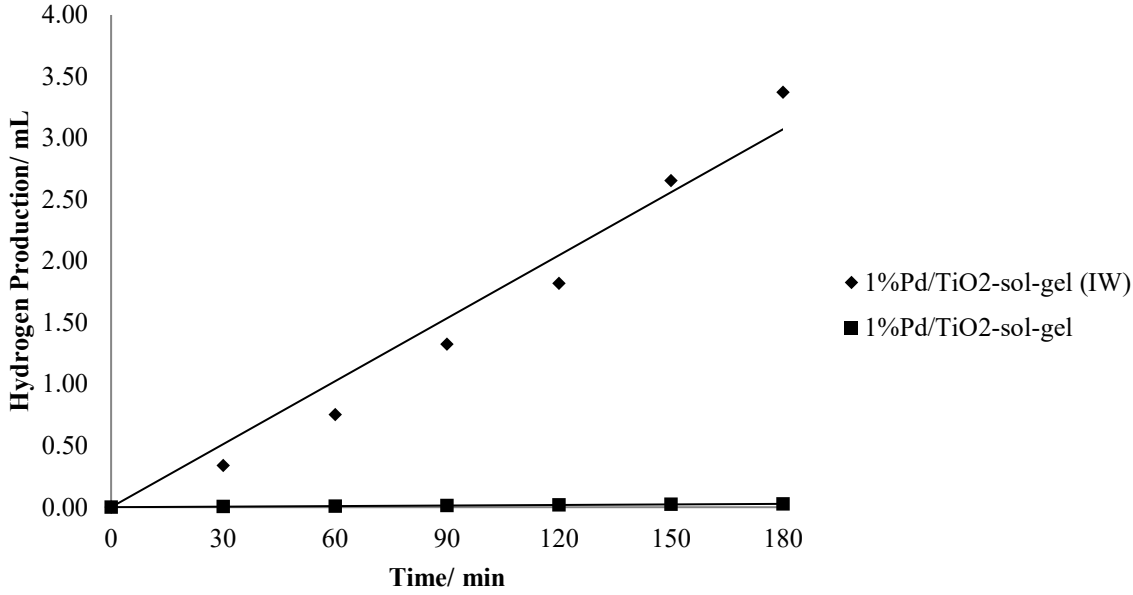

Figure 5.5. Hydrogen produced from photocatalytic methanol reforming using 1%Pd/TiO_2-sol-gel (IW) and 1%Pd/TiO_2-sol-gel

Figure 5.5 shows that incorporating Pd into the sol-gel synthesis of TiO_2 produces an inactive catalyst for this reaction however adsorbing Pd to the sol-gel titania using incipient wetness produces an active catalyst for this reaction. This contradicts the work of Tseng *et al*. somewhat where the addition of Cu into the sol-gel preparation improved the activity for CO2 reduction.[18] A possible reason for the low activity of 1%Pd/TiO_2-sol gel is that the majority of the palladium was in the bulk of the TiO_2, reducing the number of active sites. The two catalysts were characterised using XRD to probe whether the catalysts contained different phases, crystallinity or crystallite sizes which could cause the difference in activity. XRD was also carried out as a comparison for phase composition and crystallinity.

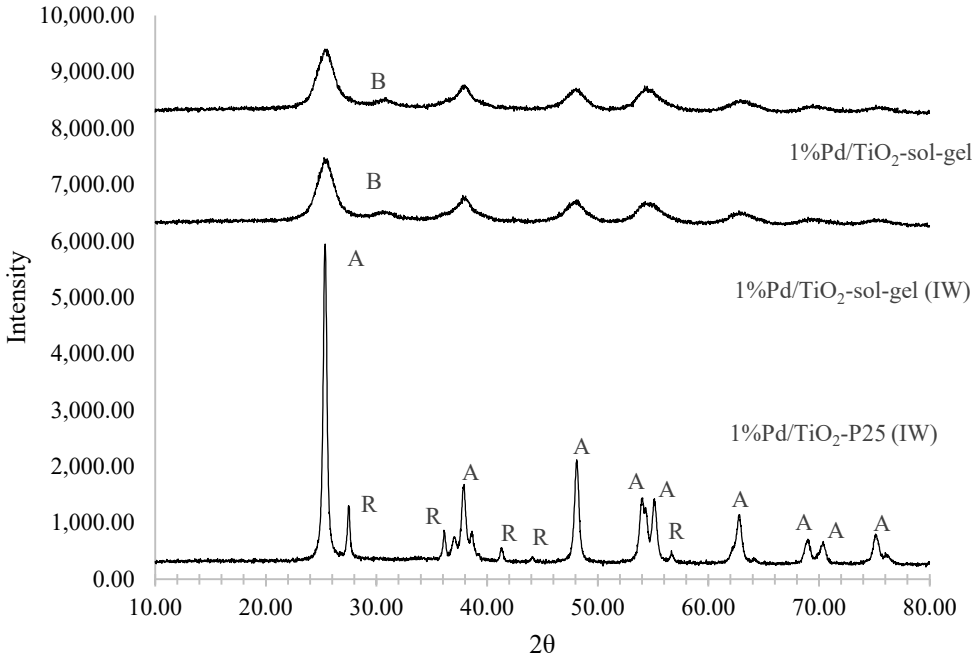

Figure 5.6. XRD pattern of 1%Pd/TiO_2 catalysts where A = anatase, R = rutile and B = brookite

Figure 5.6 shows the XRD pattern for 1%Pd/TiO_2-P25 (IW), 1%Pd/TiO_2-sol-gel (IW) and 1%Pd/TiO_2-sol gel. From the XRD it is clear that 1%Pd/TiO_2-P25 (IW) is a mixture of anatase and rutile.[36] There is no Pd peak is observed suggesting high dispersion and low loading of Pd on the support.[37] It is possible estimate the relative amounts of anatase and rutile in the sample using Equation 5.1where is ratio of rutile to anatase, I_A is the intensity of anatase peak and I_R is the intensity of rutile peak.[38]

Equation 5.1. Equation for ratio of rutile to anatase

The ratio given by this equation is 0.19 which equates to ~20:80 rutile to anatase which is in agreement with literature.[30] The peaks are well defined suggesting high crystallinity. The XRD pattern for 1%Pd/TiO_2-sol-gel (IW) and 1%Pd/TiO_2-sol-gel are almost

identical which indicates that there no difference in phase composition when Pd is added during the sol-gel preparation of TiO_2. The peak at 31° matches with brookite,[39] this is not seen in the TiO_2-P25 sample. The other peaks correspond to anatase and there appears to be no rutile in the sample. Anatase-brookite mixtures have been reported to give higher hydrogen yields than P25,[40] however the results in this experiment contradict this. The peaks are not well defined which suggests that the sol-gel sample has some amorphous impurities and that the particles are very small.

BET analysis was used to determine the surface area of 1%Pd/TiO_2-P25 (IW), 1%Pd/TiO_2-sol-gel (IW) and 1%Pd/TiO_2-sol-gel (Table 5.2).

Catalyst	Surface area/ m^2 g^{-1}	XRD crystallite size/ Å
1%Pd/TiO_2-P25 (IW)	56.41	28.3
1%Pd/TiO_2-sol-gel (IW)	181.21	6.3
1%Pd/TiO_2-sol-gel	179.43	6.4

Table 5.2. BET surface areas for 1%Pd/TiO_2 catalysts

From Table 5.2 it is clear that sol-gel preparation produces very high surface area TiO_2 which is consistent with literature.[28] The Scherrer equation was used to determine the crystallite size [41] which is also shown in Table 5.2. The BET surface areas appear to correlate with the crystallite sizes. Although in catalysis more surface area usually means better activity, for this photocatalytic process, crystallinity appears to play a bigger role as the catalyst prepared using TiO_2-P25 has a surface area 56.41 m^2 g^{-1} and the sol-gel catalysts exhibiting a surface area of around 180 m^2 g^{-1}. As the two sol-gel catalysts appear to be very similar in phase composition and surface area, it seems likely that the low activity of 1%Pd/TiO_2-sol-gel is possibly caused by the Pd nanoparticles being present in the bulk of the TiO_2. The Pd nanoparticles on 1%Pd/TiO_2-sol-gel (IW) are

likely to be on the catalyst surface allowing methanol to easily adsorb, hence the higher activity. Again this experiment has highlighted the importance of the location of the Pd. The comparison with TiO_2-P25 has also suggested that crystallinity of the titania is another factor that needs to be considered.

5.2.3 Modifying the Sol-gel Technique

From the XRD seen from the sol-gel catalysts, it appears that they have very poor crystallinity. Poor crystallinity has shown to increase electron recombination. Therefore in attempt to increase crystallinity the sol-gel technique was modified. The preparation of 1%Pd/TiO_2-sol-gel (IW) was modified by altering the calcination temperature and also the pH. Pd was not added during the sol-gel synthesis as this was found to produce an inactive catalyst.

5.2.4 Effect of calcination temperature on sol-gel synthesis

Calcination temperature has been shown to affect the crystallinity of TiO_2. The calcination temperature was increased to try to improve the crystallinity of the sol-gel TiO_2 in an attempt to improve activity. The temperature was increased only up to 500°C because after this temperature it is possible that it will convert anatase to rutile.[42]

5.2.4.1 Hydrogen Production

1%Pd/TiO_2-sol-gel prepared at pH 3.5 was calcined at different temperatures (120°C, 300°C, 500°C) to probe whether it can affect phase composition but mainly the crystallinity of TiO_2. The effect of calcination temperature on activity towards photocatalytic methanol reforming is shown below in Figure 5.7.

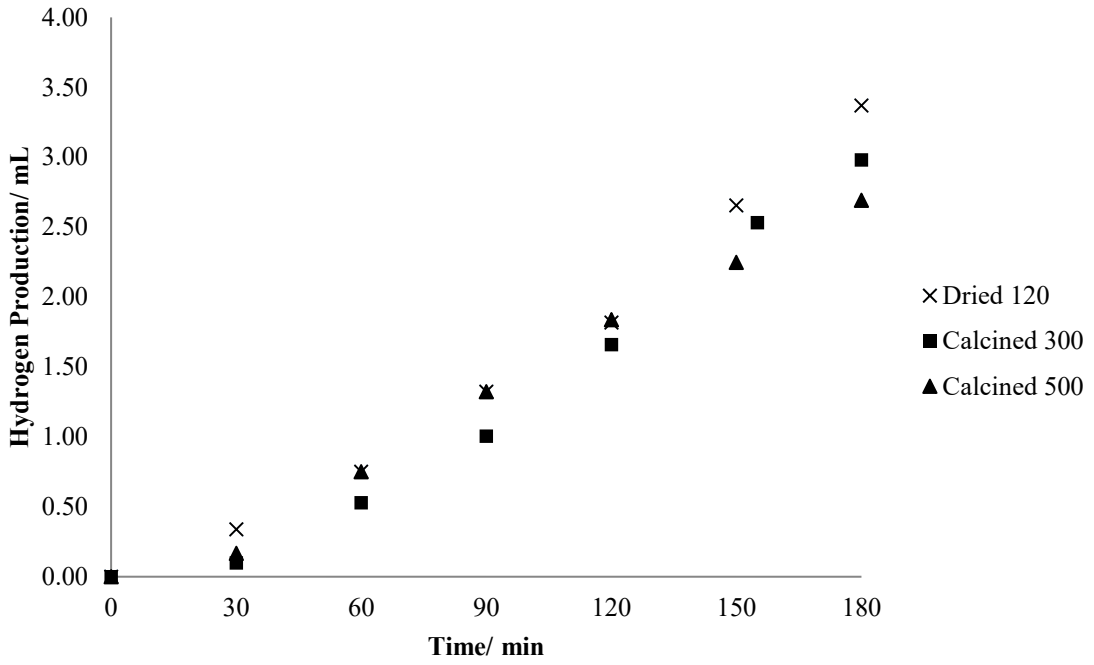

Figure 5.7. Hydrogen production for 1%Pd/TiO_2 sol-gel catalysts calcined at different temperatures

Figure 5.7 shows that the temperature of calcination has very little effect on the activity of the catalyst. The catalysts were characterised using XRD, RAMAN and BET to investigate the reason for this.

5.2.4.2 Characterisation

XRD was used to determine the phases present and the crystallite size of the sol-gel catalysts calcined at different temperatures. The XRD pattern for 1%Pd/TiO_2-sol-gel catalysts calcined at different temperatures are shown in Figure 5.8.

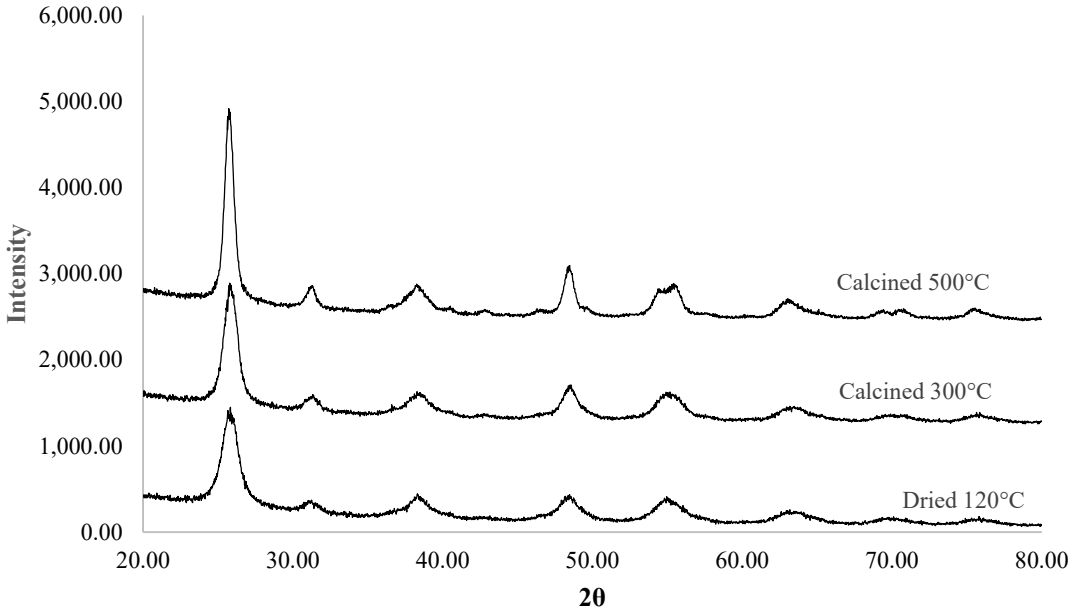

Figure 5.8. XRD pattern for 1%Pd/TiO_2 sol-gel catalysts calcined at different temperatures

Figure 13 shows that the phases present are anatase [36] and brookite.[39] The crystallite size was calculated using the Scherrer equation (also shown in Table 5.3). The peaks get more defined with higher calcination temperature indicating higher crystallinity and larger particles.

RAMAN was used to provide further confirmation that the catalyst was composed of anatase and brookite.

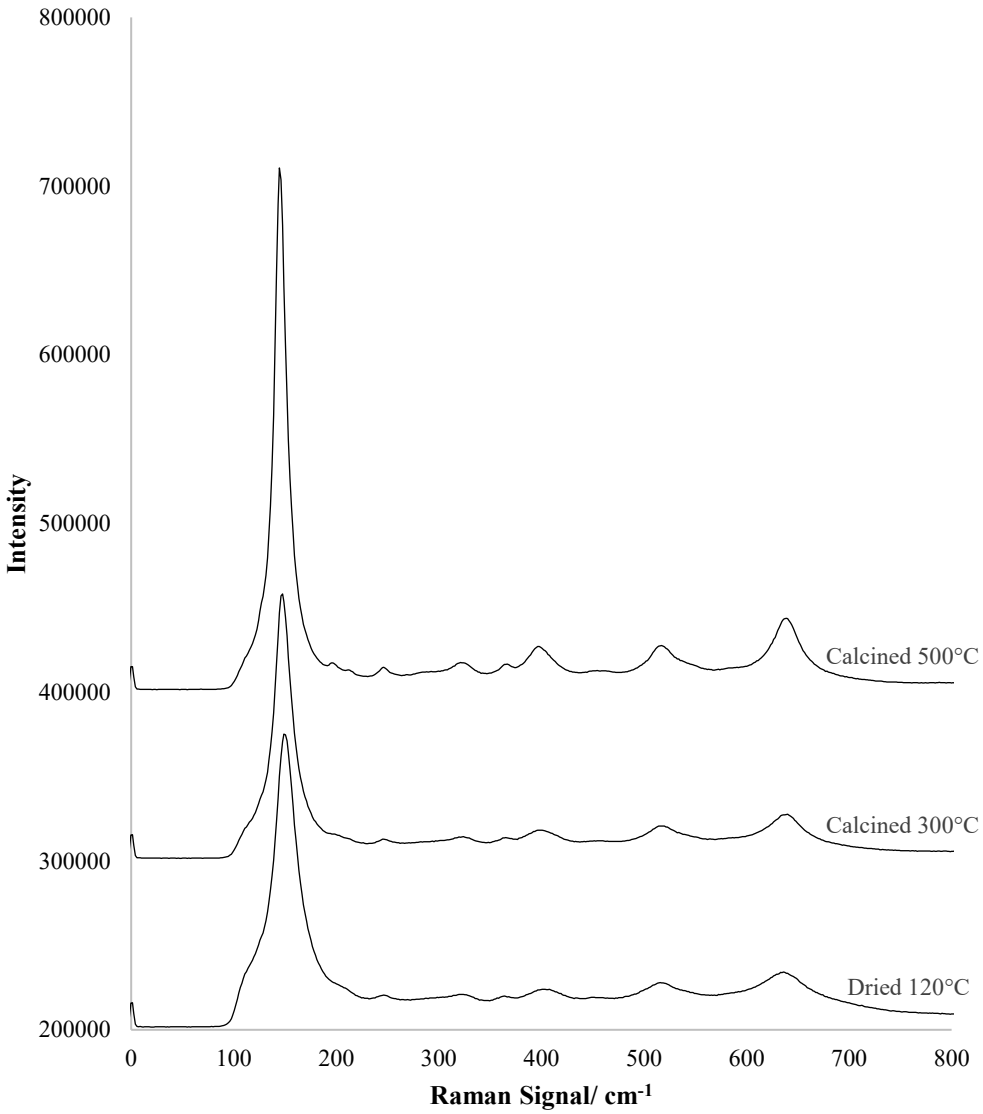

Figure 5.9. RAMAN shift for 1%Pd/TiO_2 sol-gel catalysts calcined at different temperatures

Although the peaks get more defined at higher calcination temperatures the same peaks are present for each sample. The peaks correspond to anatase and brookite with peaks at around 399, 513 and 639 cm^{-1} for anatase and 246, 324, 412 cm^{-1} for brookite.[42, 43]

BET was used to determine the surface area of the 1%Pd/TiO_2-sol-gel catalysts. These are shown in Table 5.3.

Calcination temperature/ °C	BET surface area/ $m^2 g^{-1}$	Crystallite size/ Å
120	181	63
300	104	93
500	49	117

Table 5.3. BET surface area, crystallite size and anatase brookite composition for 1%Pd/TiO_2 sol-gel catalysts calcined at different temperatures

BET analysis shows that with higher calcination temperature the surface area of the catalyst decreases. This is in agreement with the crystallite size calculated from XRD.

This has shown that increasing calcination temperature improves crystallinity however this did not affect the activity. It is possible that although crystallinity has been improved, the decrease in surface area affects the activity. Therefore the activity per unit area was plotted against the calcination temperature. (Figure 5.10).

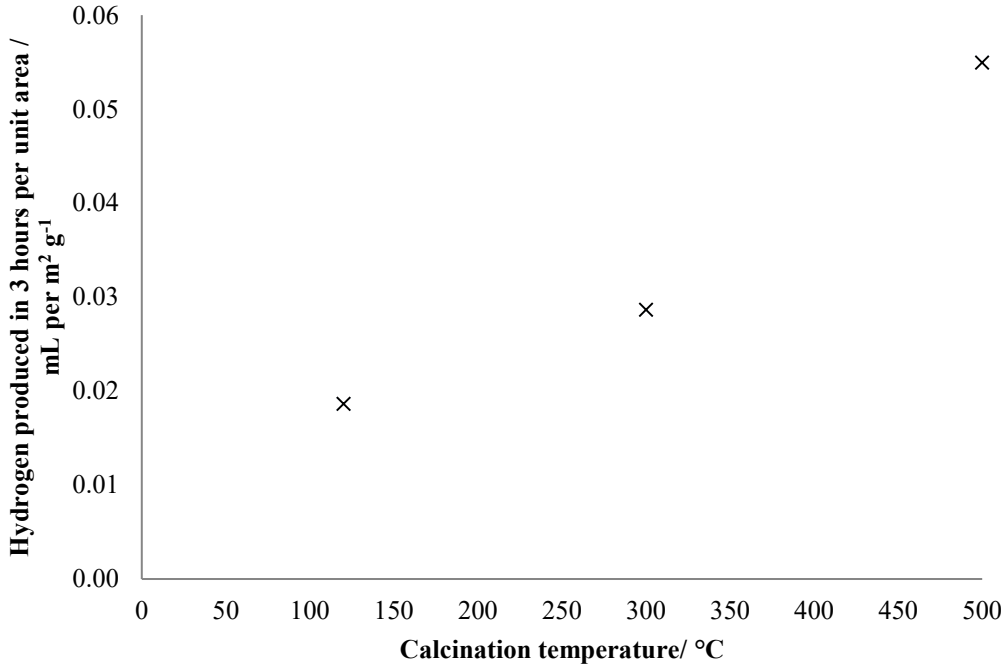

Figure 5.10. Activity towards photocatalytic hydrogen production from methanol reforming per unit area against calcination temperature of sol-gel TiO_2

Figure 5.10 shows that increasing the calcination temperature, increases the activity of the photocatalyst per unit area. This suggests that with increasing calcination temperature, crystallinity is improved and if the surface area of the catalysts were the same, the hydrogen yield would be higher for the sol-gel TiO_2 calcined at 500°C. This indicates that there is a trade-off between crystallinity and surface area with regards to activity.

5.2.5 Effect of pH on sol-gel synthesis

5.2.5.1 Hydrogen Production

The effect of pH on the sol-gel preparation of TiO_2 was probed. The hydrolysis of titanium tetraisopoxide (sol-gel synthesis of TiO_2) has been shown to be affected by pH which in turn has been shown to have an effect on the size and morphology of TiO_2 crystal produced. More anatase rich TiO_2 (sol-gel) has been reported to be synthesised with higher concentrations of acid.[44] With lower acid concentration, smaller crystallite sizes of TiO_2 were produced. The sol-gel preparation is conducted in acidified water. The pH of the water was lowered to 2.5 and increased to 5. The pH of the standard sol-gel procedure was 3.5. The hydrogen produced from photocatalytic methanol reforming is shown below in Figure 5.11.

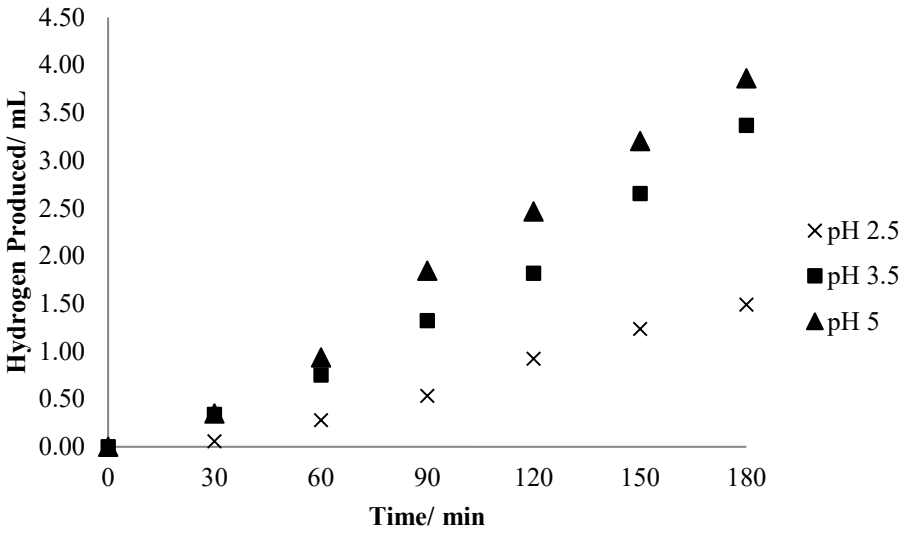

Figure 5.11. Hydrogen production for 1%Pd/TiO_2 sol-gel catalysts prepared at different pH

Altering the pH of the water during sol-gel synthesis affects the activity of the catalyst produced as seen in Figure 5.11. When the pH is increased to 5 the activity of the catalyst is slightly better. Lowering the pH to 2.5 reduced hydrogen production to less than half that of the hydrogen produced by the photocatalyst synthesised using pH 3.5. The catalysts were characterised using XRD, RAMAN and BET to investigate the cause of change in activity.

5.2.5.2 Characterisation

The XRD spectra for 1%Pd/TiO_2-sol-gel catalysts prepared at different pH is shown below in Figure 5.12.

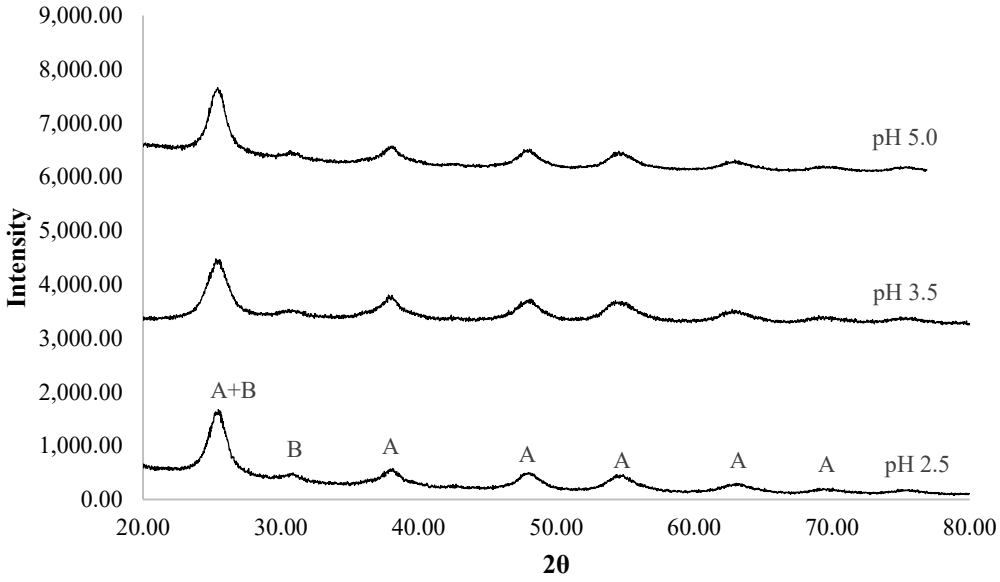

Figure 5.12. XRD pattern for 1%Pd/TiO_2 sol-gel catalysts prepared at different pH

The phases present in all three samples are anatase [36] and brookite.[39] All three patterns have similar peak widths suggesting similar crystallite size. The Scherrer equation was used to estimate crystallite size. The values obtained are shown in Table 5.4. The XRD pattern does not show a clear difference in phase composition or crystallinity. To try and gain a better idea of phase composition RAMAN was used. RAMAN shift for 1%Pd/TiO_2-solgel catalysts prepared at different pH is shown in Figure 5.13.

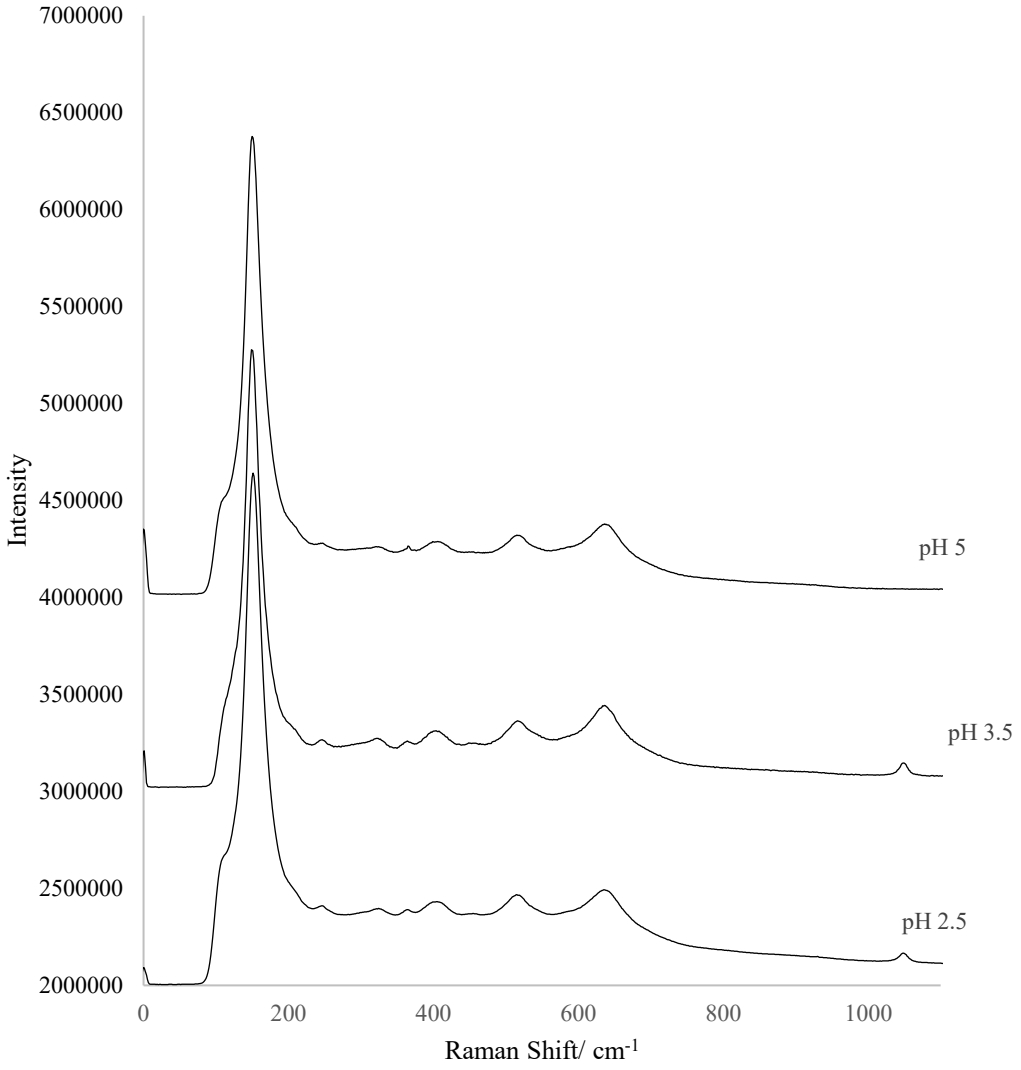

Figure 5.13. RAMAN spectra for 1%Pd/TiO_2 sol-gel catalysts prepared at different pH

The peaks correspond to anatase and brookite only. Brookite has peaks at 246, 324 and 412 cm^{-1}.[43] Anatase has peaks at 399, 513 and 639 cm^{-1}.[45] This is further evidence that the sol-gel TiO_2 is a mixture of anatase and brookite.

BET was used to determine the surface area of the catalyst (Table 5.4). All three catalysts exhibit relatively high surface areas compared to TiO_2-P25. The pH during sol-gel synthesis does not appear to affect the surface area of the catalyst significantly.

Having established that the sol-gel catalysts are very similar in crystallite size/surface area, it is unlikely the cause for the difference in activity between the TiO_2 prepared at pH 3.5 and 5, and pH 2.5. Therefore the XRD pattern was revisited and the proportion of brookite and anatase in the sample was analysed using Reitveld refinement on Maud software.[46] This is shown in Table 5.4.

pH during sol-gel preparation	BET surface area/ $m^2 g^{-1}$	Crystallite size/ Å	Proportion anatase/%	Proportion brookite/%
2.5	162	8.2	65	35
3.5	181	6.4	39	61
5	220	5.1	44	56

Table 5.4. BET surface area, crystallite size and anatase brookite composition for 1%Pd/TiO_2 sol-gel catalysts prepared at different pH

Rietveld analysis of the XRD patterns show that the TiO_2 prepared using pH 3.5 and 5 have a higher proportion of brookite than the TiO_2 prepared at pH 2. The TiO_2 prepared using pH 3.5 and 5 are composed of 61% and 56% brookite, respectively. The TiO_2 prepared at pH 2 contains only 35% brookite.

A change in brookite content in the TiO_2 appears to be the main difference between the TiO_2-sol-gel catalysts prepared at different pH. The activity of 1%Pd/TiO_2-sol-gel prepared at pH 2.5 is considerably lower than the other two catalysts. At pH 2.5 there is a much lower brookite content compared to pH 3.5 and pH 5. This could explain the lower activity as brookite has been reported to be an active photocatalyst.[47]

Modifying the sol-gel procedure has not generated a more active catalyst than Pd/TiO_2-P25 however it has shown the importance of crystallinity and also phase composition and

that these properties can be affected by altering the calcination temperature and the pH at which the sol-gel method takes place.

5.2.6 Au/TiO_2 preparation methods

The previous section of the chapter has focussed on the TiO_2 support. The next section will explore using different preparation methods for producing Au nanoparticles for catalysts for photocatalytic hydrogen production using methanol. The previous work in this thesis has used incipient wetness to produce and adsorb the nanoparticles onto the TiO_2. Here surfactant methods and impregnation have been used to attempt to control particle size and distribution and to explore whether this can have an effect on activity.

5.2.6.1 Turkevich Method

The Turkevich method involves using sodium citrate as the reductant and capping agent to produce gold nanoparticles.[21] The gold nanoparticles can be adsorbed onto TiO_2 (in this case TiO_2-P25) to produce Au/TiO_2 photocatalyst. Au/TiO_2 has been reported to be an effective catalyst for photocatalytic methanol reforming.[19] The effect of Au loading and citrate concentration has been investigated in an attempt to find the optimum conditions.

0.25, 0.5, 1 and 2 Wt% Au/TiO_2 was prepared using the Turkevich method with the concentration of citrate kept at 1% w/v. The catalysts were dried at 120°C. The rate of hydrogen production from methanol by each catalyst is shown below in Figure 5.14.

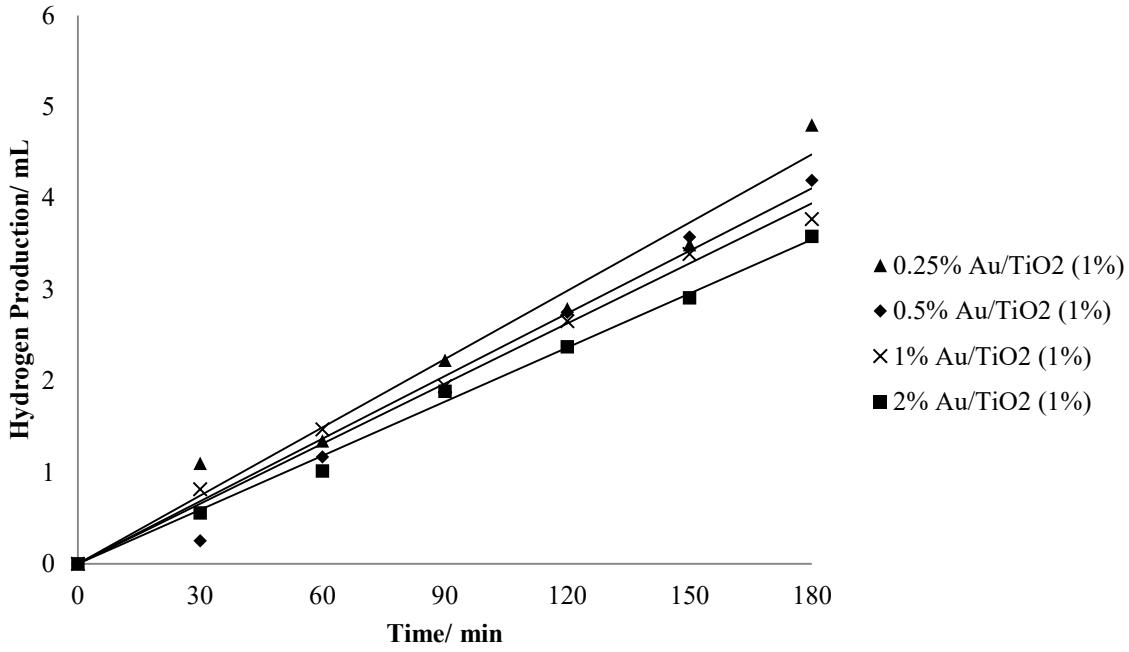

Figure 5.14. Hydrogen production using Au/TiO_2 prepared using the Turkevich method at different weight loadings

Figure 5.14 shows that there isn't a significant difference between the activities of the Au/TiO_2 catalysts prepared at different weight loadings. It is possible that the active site for the reaction is being blocked by the citrate as drying at 120°C would not remove the citrate from the surface of the catalyst. There also appears to be no induction time suggesting that the citrate is not being removed during the reaction. Calcination is a possible way of removing the capping agent. The effect of calcining the Au/TiO_2 catalysts at 400°C is shown in Figure 5.15.

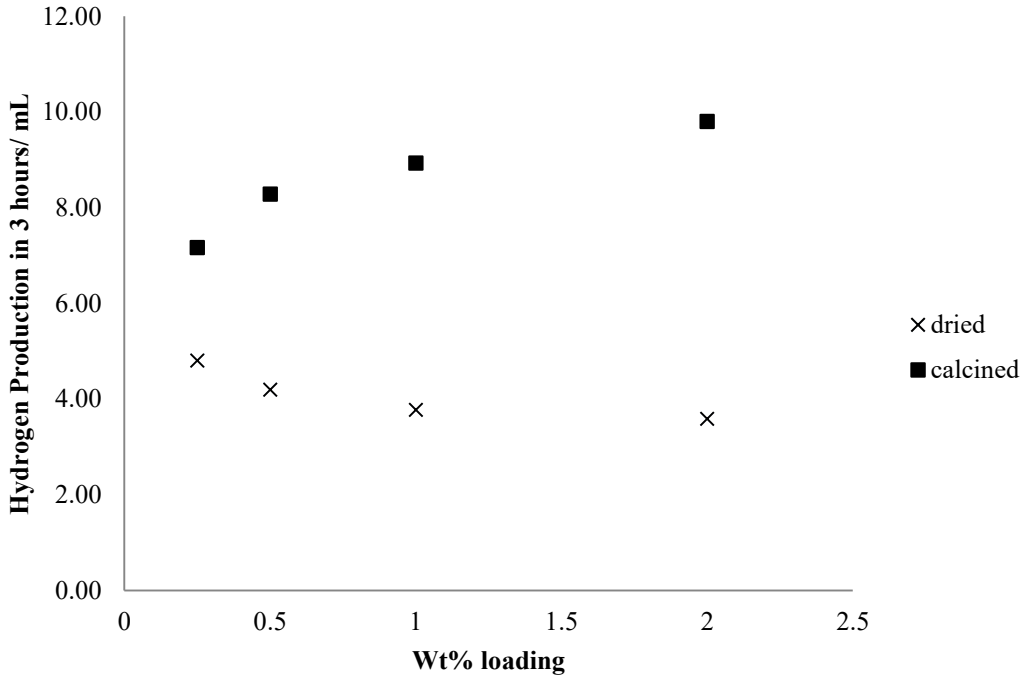

Figure 5.15. Hydrogen production using Au/TiO_2 prepared using the Turkevich method at different weight loadings, dried and calcined

Calcining at 400°C has increased the activity of all of the citrate stabilised Au/TiO_2 catalysts (Figure 5.15). This suggests that the calcination step has removed the citrate and exposed the actives sites. However the activity of $2\%Au/TiO_2$ has increased much more than the activity for $0.25\%Au/TiO_2$. This suggests that the $2\%Au/TiO_2$ catalyst has more active sites which indicates that higher Au loadings prepared using Turkevich method are more active catalysts. This is interesting as with the Au/TiO_2 catalysts prepared via incipient wetness in Chapter 3 with varied loadings, the most active catalyst was $0.5\%Au/TiO_2$. A comparison with $0.5\%Au/TiO_2$ prepared using incipient wetness and $2\%Au/TiO_2$ prepared using citrate is shown in Figure 5.16.

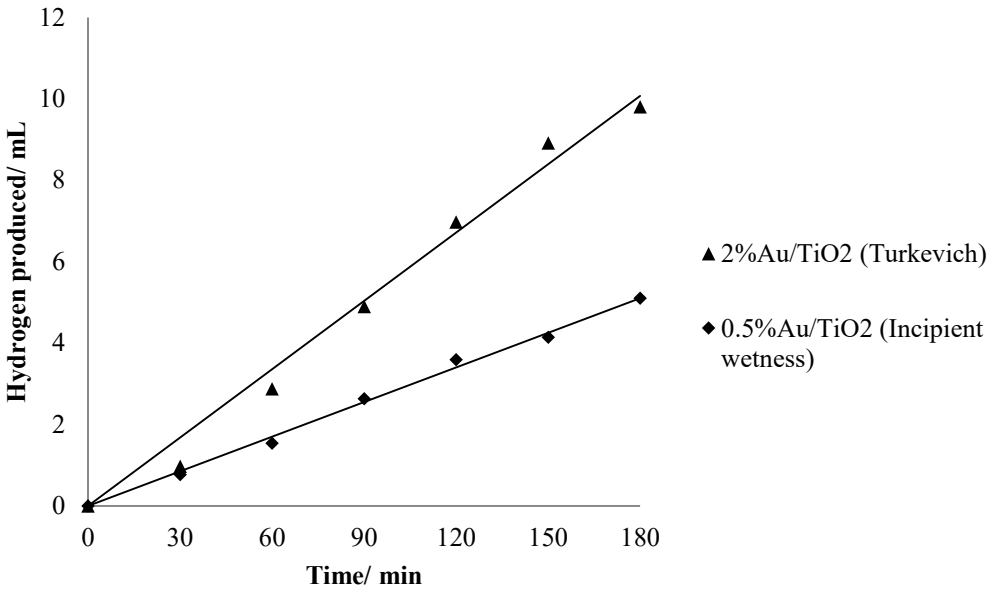

Figure 5.16. Hydrogen production using 0.5%Au/TiO_2 prepared via incipient wetness and 2%Au/TiO_2 using citrate

Figure 5.16 shows that the Turkevich method has produced a more active catalyst than the incipient wetness catalyst. It is possible that the nanoparticles produced via the Turkevich method are smaller and more dispersed than those produced via incipient wetness. This result also highlights the importance of removing the citrate, as without removing the citrate, the activity of 2%Au/TiO_2 was poor.

Hutchings and co-workers reported a facile method of removing stabiliser ligands from supported gold nanoparticles using a reflux method.[48] The reflux method is reported to stop sintering of the nanoparticles and thereby retaining their size and shape. Many reports in the literature have reported lower activity due to sintering when heat treating a catalyst at high temperatures therefore it is very important retain smaller nanoparticles.[49] As citrate is soluble in water and the solubility of citrate increases with temperature, it was thought that it was likely that refluxing the stabilised gold nanoparticles could help

to remove the citrate. The dried catalyst was refluxed using this method and the result is shown below in Figure 5.17.

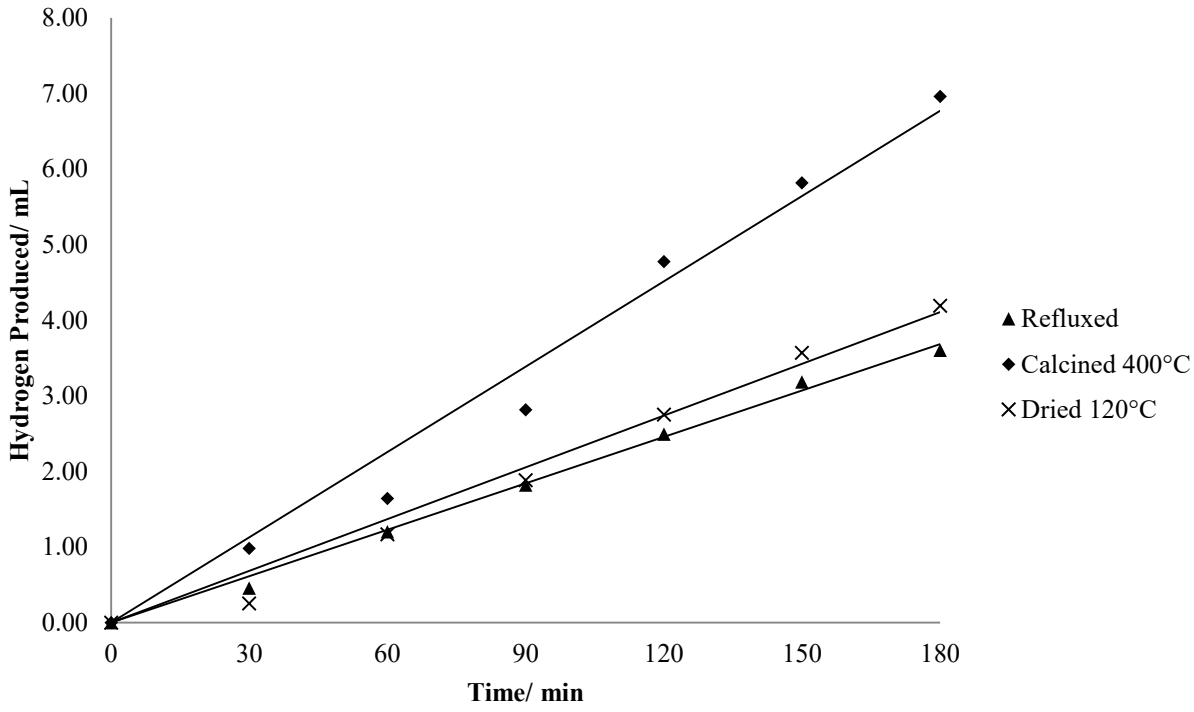

Figure 5.17. Citrate stabilised 0.5%Au/TiO_2 dried at 120°C, calcined at 400°C and refluxed

Refluxing the citrate stabilised Au/TiO_2 catalyst appears to decrease the activity when compared to the calcined catalyst as seen in Figure 5.17. In this experiment, refluxing does not improve the catalyst activity. It is possible that the reflux method does not work for citrate stabilised nanoparticles.

5.3 Conclusions

This chapter explored how different preparation methods could affect the activity of the catalyst for photocatalytic methanol reforming for hydrogen production. The first section involved attempting to improve the activity of TiO_2 and get better hydrogen yields than TiO_2-P25. Using different polymorphs of TiO_2, including anatase and rutile in the liquid and gas phase revealed that higher hydrogen yields are achieved in the gas phase. Even rutile which is has negligible activity in the liquid phase, had much higher activity in the gas phase. This was attributed to there being a higher concentration of methanol in the gas phase. An interesting finding was that the location of the metal played an important role in the activity of the catalyst. It was found that the catalyst was more active when the metal was on the rutile and it was concluded that this was due to the movement of holes into the rutile, closer the metal and closer to the active sites. It was also found that the metal needs to be on the surface of the catalyst and not in the bulk.

A sol-gel technique to synthesise TiO_2 was employed in an attempt to improve on TiO_2-P25. Although higher hydrogen yields were not achieved, these tests allowed for a development in the understanding of what properties of TiO_2 are important. Higher crystallinity was found to improve hydrogen yields. This was attributed to the longer charge separation times due to the presence of fewer recombination sites. Higher calcination temperatures produced TiO_2 with higher crystallinity however this reduced the surface area and it was concluded that there needs to be compromise between these two properties. The sol-gel synthesis produced TiO_2 with anatase and brookite phases. It was found that the higher the brookite content, the higher the activity. This property could be controlled using acidified water of higher pH.

The second part of the chapter involved using the Turkevich method to synthesise Au nanoparticles in an attempt to improve hydrogen yields when compared to catalysts

synthesised using incipient wetness. This method produced active catalysts for photocatalytic methanol reforming. It was found that the catalyst needed to be calcined. This highlighted the importance of removing the citrate as it was blocking the active sites. Using the Turkevich method to produce 2%Au/TiO_2, however, did achieve higher hydrogen yields when compared with 2%Au/TiO_2 prepared via incipient wetness. This was attributed to the Au nanoparticles being smaller and more dispersed.

In conclusion the factors that improve the activity of the catalyst are; the position of the metal, the crystallinity, surface area and phase of the TiO_2 and the size and dispersion of the metal. The aim was to produce catalysts with higher hydrogen yields than metal loaded TiO_2-P25 prepared via incipient wetness. Here no improvement was made on TiO_2-P25 however progress was made on understanding the factors that influence activity. Using the Turkevich method to produce Au/TiO_2 however did achieve higher hydrogen yields than Au/TiO_2 prepared via incipient wetness.

1.1 References

1. A. Fujishima and K. Honda, *Nature*, 1972, 238, 37.

2. A. Dickinson, D. James, N. Perkins, T. Cassidy and M. Bowker, *Journal of Molecular Catalysis a-Chemical*, 1999, 146.

3. G. R. Bamwenda, S. Tsubota, T. Nakamura and M. Haruta, *Journal of Photochemistry and Photobiology a-Chemistry*, 1995, 89.

4. A. Galinska and J. Walendziewski, *Energy & Fuels*, 2005, 19, 1143.

5. E. Scolan and C. Sanchez, *Chemistry of Materials*, 1998, 10, 3217.

6. M. Lal, V. Chhabra, P. Ayyub and A. Maitra, *Journal of Materials Research*, 1998, 13, 1249.

7. M. M. Wu, G. Lin, D. H. Chen, G. G. Wang, D. He, S. H. Feng and R. R. Xu, *Chemistry of Materials*, 2002, 14, 1974.

8. S. Kambe, K. Murakoshi, T. Kitamura, Y. Wada, S. Yanagida, H. Kominami and Y. Kera, *Solar Energy Materials and Solar Cells*, 2000, 61, 427.

9. J. C. Yu, J. G. Yu, L. Z. Zhang and W. K. Ho, *Journal of Photochemistry and Photobiology a-Chemistry*, 2002, 148, 263.

10. T. Khalil, F. Abou El-Nour, B. El-Gammal and A. R. Boccaccini, *Powder Technology*, 2001, 114, 106.

11. C. C. Wang and J. Y. Ying, *Chemistry of Materials*, 1999, 11, 3113.

12. C. Su, B. Y. Hong and C. M. Tseng, *Catalysis Today*, 2004, 96, 119.

13. J. Jitputti, S. Pavasupree, Y. Suzuki and S. Yoshikawa, *Journal of Solid State Chemistry*, 2007, 180, 1743.

14. H. Yi, T. Peng, D. Ke, D. Ke, L. Zan and C. Yan, *International Journal of Hydrogen Energy*, 2008, 33, 672.

15. V. F. Stone and R. J. Davis, *Chemistry of Materials*, 1998, 10, 1468.

16. B. Ohtani, Y. Ogawa and S. Nishimoto, *Journal of Physical Chemistry B*, 1997, 101, 3746.

17. T. Sreethawong, Y. Suzuki and S. Yoshikawa, *International Journal of Hydrogen Energy*, 2005, 30, 1053.

18. I. H. Tseng, J. C. S. Wu and H. Y. Chou, *Journal of Catalysis*, 2004, 221, 432.

19. M. Bowker, L. Millard, J. Greaves, D. James and J. Soares, *Gold Bulletin*, 2004, 37.

20. L. Saeed Al-Mazroai, M. Bowker, P. Davies, A. Dickinson, J. Greaves, D. James and L. Millard, *Catalysis Today*, 2007, 122.

21. J. Turkevich, P. C. Stevenson and J. Hillier, Discuss. Faraday. Soc, 1951, vol. 85, p. 3317.

22. A. Kmetyko, K. Mogyorosi, P. Pusztai, T. Radu, Z. Konya, A. Dombi and K. Hernadi, *Materials*, 2014, 7, 7615.

23. S. Xu, J. Ng, X. Zhang, H. Bai and D. D. Sun, *International Journal of Hydrogen Energy*, 2010, 35, 5254.

24. M. Murdoch, G. I. N. Waterhouse, M. A. Nadeem, J. B. Metson, M. A. Keane, R. F. Howe, J. Llorca and H. Idriss, *Nature Chemistry*, 2011, 3, 489.

25. F. Cardenas-Lizana, S. Gomez-Quero, H. Idriss and M. A. Keane, *Journal of Catalysis*, 2009, 268, 223.

26. B. Sun and P. G. Smirniotis, *Catalysis Today*, 2003, 88, 49.

27. R. Katoh, M. Murai and A. Furube, *Chemical Physics Letters*, 2008, 461, 238.

28. T. Sreethawong, Y. Suzuki and S. Yoshikawa, *Journal of Solid State Chemistry*, 2005, 178, 329.

29. H. Bahruji, M. Bowker, P. R. Davies, D. J. Morgan, C. A. Morton, T. A. Egerton, J. Kennedy and W. Jones, *Topics in Catalysis*, 2015, 58, 70.

30. D. C. Hurum, A. G. Agrios, K. A. Gray, T. Rajh and M. C. Thurnauer, *Journal of Physical Chemistry B*, 2003, 107, 4545.

31. D. C. Hurum, A. G. Agrios, S. E. Crist, K. A. Gray, T. Rajh and M. C. Thurnauer, *Journal of Electron Spectroscopy and Related Phenomena*, 2006, 150, 155.

32. S. Leytner and J. T. Hupp, *Chemical Physics Letters*, 2000, 330, 231.

33. D. O. Scanlon, C. W. Dunnill, J. Buckeridge, S. A. Shevlin, A. J. Logsdail, S. M. Woodley, C. R. A. Catlow, M. J. Powell, R. G. Palgrave, I. P. Parkin, G. W. Watson, T. W. Keal, P. Sherwood, A. Walsh and A. A. Sokol, *Nature Materials*, 2013, 12, 798.

34. M. Bowker, D. James, P. Stone, R. Bennett, N. Perkins, L. Millard, J. Greaves and A. Dickinson, *Journal of Catalysis*, 2003, 217.

35. M. Addamo, V. Augugliaro, A. Di Paola, E. Garcia-Lopez, V. Loddo, G. Marci and L. Palmisano, *Thin Solid Films*, 2008, 516, 3802.

36. D. T. Cromer and K. Herrington, *Journal of the American Chemical Society*, 1955, 77, 4708.

37. J. B. Zhong, Y. Lu, W. D. Jiang, Q. M. Meng, X. Y. He, J. Z. Li and Y. Q. Chen, *Journal of Hazardous Materials*, 2009, 168, 1632.

38. R. A. Spurr and H. Myers, *Analytical Chemistry*, 1957, 29, 760.

39. X. S. Ye, J. Sha, Z. K. Jiao and L. D. Zhang, *Nanostructured Materials*, 1997, 8, 919.

40. A. A. Ismail, T. A. Kandiel and D. W. Bahnemann, *Journal of Photochemistry and Photobiology a-Chemistry*, 2010, 216, 183.

41. A. L. Patterson, *Physical Review*, 1939, 56, 978.

42. R. D. Shannon, *Journal of Applied Physics*, 1964, 35, 3414.

43. G. A. Tompsett, G. A. Bowmaker, R. P. Cooney, J. B. Metson, K. A. Rodgers and J. M. Seakins, *Journal of Raman Spectroscopy*, 1995, 26, 57.

44. C. S. Lim, J. H. Ryu, D. H. Kim, S. Y. Cho and W. C. Oh, *Journal of Ceramic Processing Research*, 2010, 11, 736.

45. T. Ohsaka, F. Izumi and Y. Fujiki, *Journal of Raman Spectroscopy*, 1978, 7, 321.

46. M. Rezaee, S. M. M. Khoie and K. H. Liu, *Crystengcomm*, 2011, 13, 5055.

47. B. Ohtani, J. Handa, S. Nishimoto and T. Kagiya, *Chemical Physics Letters*, 1985, 120, 292.

48. J. A. Lopez-Sanchez, N. Dimitratos, C. Hammond, G. L. Brett, L. Kesavan, S. White, P. Miedziak, R. Tiruvalam, R. L. Jenkins, A. F. Carley, D. Knight, C. J. Kiely and G. J. Hutchings, *Nature Chemistry*, 2011, 3, 551.

49. H. Yin, C. Wang, H. Zhu, S. H. Overbury, S. Sun and S. Dai, *Chemical Communications*, 2008, 4357.

6.1 Conclusions and further work

This study investigated the effect of three variables for photocatalytic reforming for hydrogen production using metal loaded TiO_2; the effect of using different metals, the use of different sacrificial agents and using different preparation techniques for metal loaded TiO_2.

The first body of work in Chapter 3 involved an investigation into the activity of a range of different metals loaded on to TiO_2 for photocatalytic methanol reforming to produce hydrogen. The study highlighted two main factors that influence the activity of the catalyst; ease of reducibility of the metal oxide and the work function of the metal.

XPS analysis showed that in general the metals were present as metal oxides prior to reaction and were reduced during the reaction. The first step of the reaction involves the decomposition of methanol[1] which is known to readily decompose to CO and H_2 on many of the metals.[2-4] The kinetics of this however are significantly faster on metals in the metallic state compared to the oxides due to increased site availability. A relationship between ease of reducibility and activity was observed where the more easily reduced metal oxides exhibited higher activities.

The factor which correlates best with photocatalytic activity was found to be the work function of the metal. This was briefly suggested in work conducted by Chiarello *et al*.[5] however this study used a limited number of metals (Pt, Pd and Au). The work in this chapter assessed the activity of many metals, giving more strength to the argument. The higher the work function of the metal, the greater the Schottky barrier between the metal and the TiO_2, suggesting that more of the photo-induced electrons will be trapped in the metal,[6] not only increasing the electron-hole lifetime but also facilitating the reduction the methanol, increasing the activity of the catalyst. In order to pursue this work further,

an investigation using other metals with high work functions such as osmium could be used for photocatalytic methanol reforming. It also important to consider the support. It is the difference between the metal and support that produces the Schottky barrier. Therefore it would be interesting to use semi-conductors with different work functions and assess how this affects the rate of photocatalytic methanol reforming. The effect of particle size should also be addressed as this has been reported to have an effect on the position of the Fermi level.[7] Therefore TEM images of the photocatalysts would be useful to assess the particle size of the metals and whether there is a correlation with activity.

In Chapter 4, a model predicting hydrogen production from sacrificial agents with varying OH groups was proposed. The sacrificial agents chosen to examine adhered to the rules suggested by Bahruji et al.[8] which dictate whether a sacrificial agent will be active for photocatalytic reforming reactions. Straight chain polyols were found to fit the model, exhibiting a direct relationship between the number of C-OH groups and the number of moles of hydrogen produced as seen in Equation 6.1.

Equation 6.1. Model for number of moles of hydrogen produced from polyols where n = number of C-OH groups

The model was only found to be applicable to straight chain polyols as they fully decompose into carbon dioxide and hydrogen. Sacrificial agents with larger more bulky structures, such as sugars, were found to suffer from steric interference which has been known to decrease the rate of catalytic reactions.[9] Similar work has been conducted where models have been proposed to predict hydrogen production from photocatalytic reforming reactions,[10] however longer straight chain polyols such as erythritol and xylitol have not been examined in this way before. In order to progress with this work, testing

the model using a straight chain polyol with ten C-OH groups would be beneficial as it would be interesting to see whether there still a linear trend with even longer chains. The mechanism for the photo-reforming of methanol has already been investigated, [1, 8] however the mechanism for the photo-reforming of longer chain polyols such as xylitol and also larger structures such as fructose has not. Therefore analysis of the liquid phase and gas phase products from these reactions using GC-MS and NMR could identify intermediates in the reactions and possibly further the understanding of the mechanism.

In the final results chapter preparation methods and the effect of these on activity towards photocatalytic methanol reforming in an attempt to produce more active catalysts. There is a great deal of work using TiO_2 for photocatalytic hydrogen production and the vast majority uses TiO_2-P25 which is very much seen as a bench mark material for photocatalytic methanol reforming for hydrogen production.[11-13] In an attempt to improve on this activity, TiO_2 was prepared using a sol-gel method [14] which has been reported to be more active than TiO_2-P25. [15] Unfortunately, higher hydrogen yields than TiO_2-P25 were not achieved, however the process revealed what factors are important in producing active TiO_2 for photocatalytic methanol reforming for hydrogen production. The first of which is the trade-off between crystallinity and surface area which has been identified for other photocatalytic reactions[12] but not for methanol reforming. Crystallinity is known to affect photocatalytic activity[16] as the more crystalline a material, the fewer defects and therefore fewer electron/hole recombination sites, increasing the activity. As a general catalytic principle, the higher the surface area, the higher the catalytic activity.[17] In this study calcination temperature was found to affect the crystallinity and the surface area where the higher the calcination temperature, the higher the crystallinity and the lower the surface area. The three catalysts prepared at different calcination temperatures showed very little variation in activity however when analysing the activity per unit area

it was clear that the TiO_2 prepared at a higher calcination temperature exhibited higher activity. This confirmed that TiO_2 with a higher crystallinity is more active but it also highlighted that there is a compromise between the two properties. Therefore to further this work it would be helpful to establish an optimum between crystallinity and surface area. The second factor found to influence TiO_2 activity was the phase composition. This has been well documented for anatase/rutile mixtures.[18] In this study, the solgel TiO_2 was found to contain anatase and brookite. Anatase/brookite nanorods produced *via* other synthesis methods have been reported to have high activities.[19, 20] The pH during the sol-gel synthesis was found to affect the anatase/brookite ratio. At less acidic pH, the level of brookite was found to be higher, along with the activity. It is possible that the higher activity of the catalysts with higher brookite content could be due to the lower flat band of brookite. The flat band of brookite is more cathodic than anatase which promotes interfacial electron transfer, giving better charge separation and therefore better photoactivity.[21] It is difficult however to assign a single reason for the enhanced photocatalytic activity as there are many factors that could also affect the activity. Therefore it in order to gain a better understanding, it would be beneficial to do a more comprehensive study of anatase/brookite mixtures. This could include using a wider range of pH and possibly EPR studies to investigate electron/hole lifetimes.

The second part of the chapter involved using the Turkevich method to synthesise Au nanoparticles in an attempt to improve hydrogen yields when compared to catalysts synthesised using incipient wetness. The most active Au/TiO_2 prepared using the Turkevich method was $2\%Au/TiO_2$. This catalyst found to be more active than the most active Au/TiO_2 prepared using incipient wetness. This was attributed to the Au nanoparticles being smaller and more dispersed. Smaller nanoparticle size has been shown to increase activity in many areas of catalysis[22] due to a higher number of active

sites. To support this theory, images of the catalysts achieved using TEM before and after the calcination/reflux to assess particle size and how this affected activity would be very beneficial.

The aim of this research was to develop and progress photocatalysts and to increase hydrogen yields from reforming reactions. Although the photocatalysts produced may not have greatly improved on previous hydrogen yields, the work has advanced the understanding of the process. The most important outcomes of the research are; the correlation found between activity and work function of the metal and the use of longer straight chain polyols for higher hydrogen yields.

6.2 References

1. A. Dickinson, D. James, N. Perkins, T. Cassidy and M. Bowker, *Journal of Molecular Catalysis a-Chemical*, 1999, **146**.

2. M. Kawai, S. Naito, K. Tamaru and T. Kawai, *Chemical Physics Letters*, 1983, **98**, 377.

3. W.-C. Lin, W.-D. Yang, I. L. Huang, T.-S. Wu and Z.-J. Chung, *Energy & Fuels*, 2009, **23**, 2192.

4. M. Rebholz and N. Kruse, *Journal of Chemical Physics*, 1991, **95**, 7745.

5. G. L. Chiarello, M. H. Aguirre and E. Selli, *Journal of Catalysis*, 2010, **273**.

6. M. Jakob, H. Levanon and P. V. Kamat, *Nano Letters*, 2003, **3**, 353.

7. V. Subramanian, E. E. Wolf and P. V. Kamat, *Journal of the American Chemical Society*, 2004, **126**, 4943.

8. H. Bahruji, M. Bowker, P. R. Davies and F. Pedrono, *Applied Catalysis B-Environmental*, 2011, **107**.

9. Y. Liu, E. Lotero and J. G. Goodwin, Jr., *Journal of Catalysis*, 2006, **243**, 221.

10. D. I. Kondarides, V. M. Daskalaki, A. Patsoura and X. E. Verykios, *Catalysis Letters*, 2008, **122**.

11. G. L. Chiarello, A. Di Paola, L. Palmisano and E. Selli, *Photochemical & Photobiological Sciences*, 2011, **10**, 355.

12. H. Yi, T. Peng, D. Ke, D. Ke, L. Zan and C. Yan, *International Journal of Hydrogen Energy*, 2008, **33**, 672.

13. M. Bowker, *Green Chemistry*, 2011, **13**.

14. M. Addamo, V. Augugliaro, A. Di Paola, E. Garcia-Lopez, V. Loddo, G. Marci and L. Palmisano, *Thin Solid Films*, 2008, **516**, 3802.

15. J. Jitputti, S. Pavasupree, Y. Suzuki and S. Yoshikawa, *Journal of Solid State Chemistry*, 2007, **180**, 1743.

16. V. F. Stone and R. J. Davis, *Chemistry of Materials*, 1998, **10**, 1468.

17. M. Bowker, *The Basics and Applications of Heterogeneous Catalysis*, Oxford University Press, 1998.

18. R. Abe, K. Sayama, K. Domen and H. Arakawa, *Chemical Physics Letters*, 2001, **344**, 339.

19. T. A. Kandiel, A. Feldhoff, L. Robben, R. Dillert and D. W. Bahnemann, *Chemistry of Materials*, 2010, **22**, 2050.

20. Q. Tay, X. Liu, Y. Tang, Z. Jiang, T. C. Sum and Z. Chen, *Journal of Physical Chemistry C*, 2013, **117**, 14973.

21. A. Zachariah, K. V. Baiju, S. Shukla, K. S. Deepa, J. James and K. G. K. Warrier, *Journal of Physical Chemistry C*, 2008, **112**, 11345.

22. G. C. Bond and D. T. Thompson, *Catalysis Reviews-Science and Engineering*, 1999, **41**, 319.